REPORT DOCUMENTATION PAGE

Form Approved OMB No. 0704-0188

1. REPORT DATE *(DD-MM-YYYY)*	2. REPORT TYPE	3. DATES COVERED *(From – To)*
02-03-2005	Final Report	1 January 2003 - 01-Jan-05

4. TITLE AND SUBTITLE

HCF + LCF Interactions at Elevated Temperature

5a. CONTRACT NUMBER
F61775-02-C4050

5b. GRANT NUMBER

5c. PROGRAM ELEMENT NUMBER

6. AUTHOR(S)

Professor James Byrne

5d. PROJECT NUMBER

5d. TASK NUMBER

5e. WORK UNIT NUMBER

7. PERFORMING ORGANIZATION NAME(S) AND ADDRESS(ES)

University of Portsmouth
Anglesea Building, Anglesea Road
Portsmouth PO1 3DJ
United Kingdom

8. PERFORMING ORGANIZATION REPORT NUMBER

N/A

9. SPONSORING/MONITORING AGENCY NAME(S) AND ADDRESS(ES)

EOARD
PSC 821 BOX 14
FPO 09421-0014

10. SPONSOR/MONITOR'S ACRONYM(S)

11. SPONSOR/MONITOR'S REPORT NUMBER(S)
SPC 02-4050

12. DISTRIBUTION/AVAILABILITY STATEMENT

Approved for public release; distribution is unlimited.

13. SUPPLEMENTARY NOTES

14. ABSTRACT

This report results from a contract tasking University of Portsmouth as follows: The onset of high cycle fatigue (HCF) crack propagation in Ti-6Al-4V will be studied under combined HCF/low cycle fatigue (LCF) loading conditions at elevated temperatures up to 350°C, where creep, stress ratcheting and environmental effects may arise. The study will be applied to a simulated mission-loading spectrum. SEM fractography, metallography, and crack closure measurements will be used to assess the mechanisms contributing to fatigue crack growth. The study will be carried out on corner crack (CN) square cross-section specimens of forged Ti-6Al-4V and on single edge cracked rolled plate specimens of the same alloy. Information previously obtained for this alloy at room temperature will provide a baseline for comparison.

15. SUBJECT TERMS

EOARD, Materials, Fracture mechanics, Fatigue, Metallic Materials

16. SECURITY CLASSIFICATION OF:			17. LIMITATION OF ABSTRACT	18, NUMBER OF PAGES	19a. NAME OF RESPONSIBLE PERSON
a. REPORT	b. ABSTRACT	c. THIS PAGE			JOAN FULLER
UNCLAS	UNCLAS	UNCLAS	UL	80	19b. TELEPHONE NUMBER *(Include area code)* +44 (0)20 7514 3154

UNIVERSITY OF PORTSMOUTH

I.R.I. Research Report
Contract No. F61775-02-C4050

HCF+LCF INTERACTIONS
at
ELEVATED TEMPERATURE

Final
Report
(F579)

January 2002 to December 2004

Submitted by :

R.F. Hall, J. Ding & J. Byrne

Mechanical Behaviour of Materials Laboratory
Department of Mechanical and Design Engineering

Anglesea Building, Anglesea Road
Portsmouth PO1 3DJ

Phone: +44 (0)23 92 842325 e-mail : rod.hall@port.ac.uk
Phone: +44 (0)23 92 842323 e-mail : jian.ding@port.ac.uk
Phone: +44 (0)23 92 842370 e-mail : jim.byrne@port.ac.uk
Fax: +44 (0)23 92 842351

Contents

Summary

This final report covers all aspects of the HCF/LCF crack propagation study at elevated temperature, including overload effects and variations in stress ratio R, for Ti6Al4V alloy at 350°C. The results are compared with those earlier obtained for room temperature and trends and differences discussed. The crack grwoth prediction codes FASTRAN and AFGROW are used for both room temperature and elevated temperature and compared with the experimental results. Reasonable, conservative predictions of pure HCF and combined HCF/LCF crack growth rates and of the onset for HCF activity, ΔK_{onset}, are obtained for room temperature. However, for 350C much less accurate predictions are obtained and an alternative two parameter (ΔK and K_{max}) approach is suggested. A preliminary finite element study has been carried out on crack closure in support of the necessary inputs to the predictive codes. Detailed conclusions are drawn and recommondations made for future work.

Declaration

The Contractor, University of Portsmouth, hereby declares that, to the best of its knowledge and belief, the technical data delivered herewith under Contract No. F61775-02-C4050 is complete, accurate, and complies with all requirements of the contract.

27thJanuary 2005

Professor J Byrne

I certify that there were no subject inventions to declare as defined in FAR 52.227-13, during the performance of this contract.

27th January 2005

Professor J Byrne

HCF+LCF Interactions at Elevated Temperature

REPORT FOR THE PERIOD January 2002 to December 2004

REPORT No F 579

NOTATION

DCPD	direct current potential difference
FCG	fatigue crack growth
HCF	high cycle fatigue
LCF	low cycle fatigue
da/dN_{HCF}	crack growth increment resulting from the application of a HCF cycle
da/dN_{LCF}	crack growth increment resulting from the application of a LCF cycle
da/dB	crack growth increment resulting from the application of a HCF + LCF loading block
da/dB_{HCF}	crack growth increment resulting from the application of the HCF cycles within a loading block
da/dB_{LCF}	crack growth increment resulting from the application of the LCF cycles within a loading block
ΔK, DK	stress intensity range
ΔK_{HCF}	stress intensity range associated with a HCF cycle
ΔK_{LCF}	stress intensity range associated with a LCF cycle, i.e. the peak-to-peak load cycle
$\Delta K_{HCF.onset}$	the value of ΔK_{HCF} associated with the onset of HCF crack growth
$\Delta K_{LCF,onset}$	the value of ΔK_{LCF} associated with the onset of HCF crack growth
ΔK_{th}	threshold value of stress intensity range
ΔK^{+}	the positive part of the applied stress intensity range
$\Delta K_{eff(ARC)}$	effective stress intensity range with an adjusted compliance ratio
$K_{max,th}$	threshold value of maximum stress intensity
$\sigma_{max,HCF}$	maximum HCF stress
$\sigma_{min,HCF}$	minimum HCF stress
$\sigma_{max,LCF}$	maximum LCF stress
$\sigma_{min,LCF}$	minimum LCF stress
N_{HCF}	number of HCF cycles in a loading block
N_{LCF}	number of LCF cycles in a loading block
n	cycle ratio N_{HCF} : N_{LCF}
R_{HCF}	stress ratio of the HCF cycles
R_{LCF}	stress ratio of the LCF cycles
s	seconds
T	overload ratio; i.e. the maximum LCF stress / maximum HCF stress.
W	Wheeler constant

1. Introduction

Ti-6Al-4V alloy is a material typically selected for the construction of the front, low-temperature, stages of aero-engines because this alloy shows high specific strength and toughness combined with light weight and excellent corrosion resistance. With increasing concern about high cycle fatigue (HCF) as one of the prime failure modes in aeroengine rotating components, room and elevated temperature fatigue crack growth (FCG) behaviour of Ti-6Al-4V alloy has been re-evaluated in many recent studies [1-7]. These studies focused mainly on the near-threshold regime of crack growth, since a major percentage of component life is consumed in nucleation and growth of a crack to a detectable size.

However, the typical load history experienced by rotating aerofoils includes both high cycle fatigue and low cycle fatigue (LCF). In such components, the LCF or major cycle loading, arises from the large cyclic variation of the conjoint centrifugal and thermal stresses, normally occurring once per flight, while the HCF or minor cycle loading, arises from small-amplitude vibrations. During the flight these high-frequency minor cycles are always superimposed on each major cycle, so that the fatigue integrity assessment must consider the behaviour of aero-engine materials under combined LCF and HCF loadings.

Powell et al [8] showed that the fatigue crack growth curve for a simplified loading combining major and minor cycles is characterised by two regimes of behaviour, as shown in Fig. **1**, where the growth increment per loading block (d*a*/d*block*) is plotted as a function of the total stress intensity factor range (ΔK_{total}). At the lower values of ΔK_{total} the individual minor cycles do not contribute to the advance of the crack. When ΔK_{total} exceeds an onset point (ΔK_{onset}), each minor cycle commences to contribute to the growth, which causes the growth rate to increase rapidly, deviating from the response to the application of a separate LCF loading. With a larger number of HCF cycles compared to LCF cycles, this onset point usually signifies the end of useful life.

The influence of LCF overload on FCG under combined HCF/LCF cycles at room temperature (RT) was reported recently for Ti-6Al-4V [9]. It was found that systematic increases in the overload, applied prior to the commencement of the HCF cycles, retards the contribution of the HCF cycles to crack growth rates, and meanwhile enhances the stress intensity range (ΔK_{onset}) at which the HCF cycles begin to contribute to crack growth rate.

The purpose of the present work is to extend the investigation to the effect of temperature on FCG rates under the same HCF and LCF conditions. Testing temperature is 350 °C, since this temperature is approximately the maximum working temperature to which Ti-6Al-4V is commonly subjected in compressor applications. The test results are compared with those at room temperature reported previously [9]. Furthermore, two fatigue crack growth predictive codes, FASTAN and AFGROW, are used to rationalize both effects of stress ratio and temperature on FCG rates.

2. Material and experimental procedure

The material studied was forged Ti-6Al-4V alloy, cut from disc forgings that have been solution treated and overaged. The microstructure consists of 47% primary alpha phase and 53% transformed beta phase with an average colony size of 15 μm, Fig. **2**. Typical values of material properties for room temperature and 350 °C are given in Table 1. Minimum 0.2% proof stress for the material reduces from 830MPa at room temperature to 500MPa at 350^0C, i.e. a reduction of about 1/3 [10]**.** The change of Young's Modulus in forged Ti-6Al-4V from RT to 350°C is less than 10%.

Table 1 Material properties of Ti-6Al-4V at room temperature and 350 °C

Material properties	RT	350 °C
Young's Modulus (GPa)	103	96.6
Yield Stress (MPa)	860	570
Tensile strength (MPa)	980	713

Corner notched specimens were used, which had a gauge length with a square cross-section of 7.0 × 7.0 mm or 10.0 × 10.0 mm and a 0.25 mm depth notch located on one corner, Fig. **3**. The specimens were firstly precracked to a minimum length of 0.6 mm. Precracked specimens were then cyclically loaded in a special test facility which combines an electromagnetic vibrator with a servo-hydraulic fatigue machine. This hybrid machine can therefore apply HCF cycles and LCF cycles either separately or conjointly.

Fig. **4** schematically illustrates loading patterns used in the test programme. A single overload cycle was followed by 1,000 HCF cycles in each loading block. Such a combination made the cycle ratio (n) between minor cycles and major cycle equal to 1000. The HCF cycles were sinusoidal stress waves with a frequency of 157 Hz, stress ratios R being 0.7, 0.8 and 0.9. During testing the maximum stress of the HCF cycles was kept constant at 187 MPa (25% less than the value at room temperature), whilst the minimum stress varied according to the stress ratio. The LCF cycle was a trapezoidal stress wave at R = 0.01, where the rise and fall times were 1s while the times at maximum and minimum loads were 6.8s and 1.2s, respectively. The magnitude of the overload was indicated by the overload ratio (T), which is defined as

$$T = \frac{\sigma_{\max,LCF}}{\sigma_{\max,HCF}} \tag{1}$$

where $\sigma_{max,\ LCF}$ and $\sigma_{max,\ HCF}$ are the maximum LCF and HCF stresses, respectively.

During testing crack growth was monitored by a pulsed direct current potential difference (DCPD) system. Analysis of the test results was presented as diagrams of FCG rate, log(da/dN), against log(ΔK) calculated using Pickard's [11] solution for CN type specimens.

Fatigue thresholds at the HCF load only were determined by the "jump-in" method suggested by Marci et al [12]. The crack was first grown under a LCF loading with stress ratio of 0.01, and then the HCF loading with the required stress ratio of 0.7, 0.8 or 0.9 was applied, Fig. **5**. The maximum applied LCF stress was equal to the maximum applied HCF stress. The crack growth rate was calculated over 1 million HCF cycles and then compared with the accepted threshold FCG rate of 1×10^{-11} m/cycle. If the threshold value had not been exceeded, further LCF cycles at R = 0.01 were applied to extend the crack and consequently increase ΔK, before returning to cycles at the same HCF loads as before. If the crack growth rate exceeded the accepted threshold value, the threshold test was terminated. A jump-in ΔK_{th} for a given high stress ratio was defined by the mean of the last two ΔK values calculated in terms of the HCF loading.

Two experiments have been undertaken applying loads (flight simulations) typical of those which could be experienced in service. A schematic diagram of the loading pattern is given in Fig. **6**, where for convenience, the climb stage instead of gradual reduction in stress has been divided into three stages. The stresses induced in the material and the number of cycles applied at each stage are stated along with the resultant stress ratio and the effective overload ratio consequent upon the reduction in maximum load on progression from one stage to the next.

3. Experimental results

The experiments which have been completed during the course of the current contract are presented in Table 2. The results of most having been reported previously [13-15]**.**

In the following diagrams, experimental data has been replaced by a polynomial curve visually fitted through the data plots. This has been found to greatly simplify the presentation of the results and determination of trends occurring from the changes in the loads applied to the specimens. It is these polynomial curves which have been used in the construction of Figs. **7** to **11**. The background to these diagrams can be found in previous reports [13-15].

Table 2 Summary of LCF only, HCF only, combined HCF+LCF experiments undertaken at 350^0C (maximum HCF stress = 187.5MPa), HCF jump-in thresholds and flight simulations.

Experiment type	**Stress ratio, R**	**Overload ratio Max LCF/ Max HCF**	**Cycle ratio HCF cycles: LCF cycles**	**Number of experiments**
LCF cycles only	0.01			3
HCF cycles only	0.7			2
	0.8			2
	0.9			2
HCF+LCF cycles	0.7	1.0	1000:1	2
	0.7	1.3	1000:1	2
	0.7	1.45	1000:1	1
	0.7	2.0	1000:1	2
	0.8	1.3	1000:1	2
	0.9	1.0	1000:1	2
	0.9	1.3	1000:1	1
	0.9	2.0	1000:1	2
HCF threshold	0.7			3
	0.8			2
	0.9			2
Flight simulation				2

3.1 Fatigue crack growth under LCF or HCF only

Room and elevated temperature fatigue crack growth curves for LCF only (R = 0.01) are compared in Fig. **7**. The increase in temperature reduces the gradient of the data. In the present case, the gradient at 350^0C is approximately 1.5 and at room temperature 5.0 the intersection of the two curves being at ΔK of approximately 14.3MPa$\sqrt{m}$.

Fig. **8** shows HCF growth rates with R = 0.7, 0.8 and 0.9 at 350 °C. FCG rates at 350 °C are obviously greater than the rates at room temperature. At both 350^0C and room temperature an obvious R-ratio effect on the fatigue crack growth rate was observed in the near-threshold regime even at such high ratios. At low values of ΔK, FCG rates appear to increase as stress ratios decrease but this effect is caused by the smaller values of $\Delta K_{threshold}$ at the larger stress ratios. However, as ΔK increased, the influence of R on da/dN decreased.

3.2 Fatigue crack growth under combined LCF overload + HCF loadings

Experiments with prior LCF overloads were undertaken at stress ratios of 0.7, 0.8 and 0.9 at both 350^0C and room temperature. Fig. **9** illustrates the curves from experiments at a stress ratio of 0.7 both for 350^0C and room temperature. Only overload ratios common to both 350^0C and room temperature **[16]** have been included in the diagram. The FCG rates are plotted as crack length increment per combined HCF+LCF block (da/db) i.e. every LCF cycle with superimposed 1000 HCF cycles. The reduction in FCG rates with increasing prior LCF overload (increasing value of T) is consistent at both 350^0C and room temperature. Generally, all the curves are approximately parallel to each other, following the accepted profile of accelerated crack growth rates directly after onset, later curving to become parallel to the LCF only curve at an enhanced FCG rate. FCG rates in general are greater at 350^0C than at room temperature, this results in the HCF cycles at this stress ratio not being fully suppressed at an overload ratio of

2.0, whereas at room temperature the HCF cycles were very nearly suppressed at this overload ratio. This is partly due to the increased FCG rates at 350^0C and partly due to the rotation of LCF only data to a lower slope (Fig. 7) as described in a previous report [14]. Considering the curves in detail it is seen that FCG rate reductions with increasing T are unevenly spaced in the diagram, the difference between T = 1.3 and T = 1.45 appearing wide at 350^0C but with little difference at room temperature. The reasonable deduction is that these are extremes and actual differences are less at 350^0C and greater at room temperature, more in line with the difference in overload ratio

The increase in the value of ΔK_{onset} with increasing overload ratio is also evident in Fig. **9**. The range in onset between T = 1.0 and 2.0 being greater at 350^0C than at room temperature, 11.7 to 9.1 MPa√m. The cause of this difference again appears to be largely due to the rotation of the LCF only curve between 350^0C and room temperature (Fig. 7). Values of ΔK_{onset} determined during the construction of Fig. **9** are presented in Table 3, together with those determined likewise at a stress ratio of 0.8 and 0.9.

Table 3 Values of ΔK_{onset} determined for both 350^0C and room temperature. Values are in MPa√m

350^0C

Stress Ratio	**Overload Ratio**			
	T = 1.0	**T = 1.3**	**T = 1.45**	**T = 2.0**
0.7	8.4	12.4	12.8	17.5
0.8		12.7		
0.9	13.2	13.2		16.9

Room Temperature

Stress Ratio	**Overload Ratio**			
	T = 1.0	**T = 1.30**	**T = 1.45**	**T = 2.0**
0.7	9.7	12.2	13.0	21.4
0.8	12.6	14.2	15.3	
0.9	15.1	18.2		

The same trends evident at a stress ratio of 0.7 may be seen at R=0.9 in Fig. **10**. Most noticeable is the closeness of the HCF+LCF data to the LCF only data. The effect of prior LCF overloads being much less at this HCF stress ratio. At 350^0C although clearly having different onset values, at ΔK values of 25MPa√m and above, there appears to be little difference in FCG rates whatever the prior LCF overload. Consequently there appears to be little suppression in FCG rates with increasing overload. This contrasts with the situation at room temperature, where the data curves are approximately parallel and the HCF constituent of the HCF+LCF cycles is suppressed by an overload ratio of 1.3.

Values of onset (Table 3) again follow the trend observed with a stress ratio of 0.7. The reduced effectiveness of the prior LCF overloads is evident in that there is marginal difference in ΔK_{onset} between overload ratios of 1.0 and 1.3 especially, compared with the values for room temperature.

It would be expected that at a stress ratio of 0.8 the effects of prior LCF overloads would be intermediate between the effects observed at 0.7 and 0.9, In Figure **11** this is observed to be, so consequently reinforcing the statements made when considering the effect of overload ratio and temperature at those stress ratios.

3.3 Threshold

Table 4 shows the comparison of jump-in fatigue threshold under HCF loads between room temperature and 350 °C. It is found that this temperature presents little influence on ΔK_{th} for the same *R*. At both temperatures, ΔK_{th} decreases with increasing *R* and is approximately close to 2.1 MPa√m at $R = 0.9$.

Table 4 Threshold values determined by Jump-in method

R	ΔK_{th} (MPa√m)	
	RT	350 °C
0.7	3.0	3.1
0.8	2.5	2.7
0.9	2.1	2.1

3.4 Flight simulation

Data for crack length increase for each stage of the simulation, from the last 15 cycles from one of the experiments is presented in Fig. **12**. The diagram contains the last complete cycle before the test was stopped when the crack exceeded the acceptable length. The contribution of each stage (see Fig. 6) of the flight to the overall crack growth may be seen, the crack extension increasing with each flight. The major contribution to crack growth is the first stage of climb (Climb 1) indicating as expected the influence of both load range and number of cycles. The last stage of climb and the cruise stage do not contribute to crack growth.

Fig. **13** shows the data from an equivalent flight simulation experiment at room temperature. The same trends can be seen but in the last flight a major contribution to crack growth by the cruise stage is evident. From the concept of an onset value of ΔK for HCF cycles before they contribute to crack growth, the premise is that in the experiment in Fig. **12** the onset value for the cruise stage had not been reached. Once the onset value has been exceeded, because of their greater number, the cycles in the cruise stage then provide the major contribution to crack growth.

4. Fatigue crack growth prediction

In the literature, retardation in FCG rates caused by overload is frequently interpreted by such mechanisms as crack tip blunting [17], crack deflection or bifurcation [18], residual compressive stresses ahead of the crack tip [19] and plasticity induced crack closure [20, 21]. Several predictive models have been proposed based on the concept of the increased levels of residual compressive stresses ahead of a fatigue crack due to overloads, such as the Wheeler model [22]. In the Wheeler model, retardation due to overload is evaluated by a retardation parameter, Cp, which is assumed to be a power function of the ratio between the current plastic zone and the distance from the crack tip to the border of the overload plastic zone, as follows:

$$C_p = \begin{cases} [\phi/(a_p - a_i)]^W & \text{for } a_i + \phi_p < a_p \\ 1 & \text{for } a_i + \phi_p \geq a_p \end{cases} \qquad (2)$$

where ϕ_p is the diameter of the monotonic plastic zone due to the current cycles, a_p is the sum of the crack length at overload, the diameter of the monotonic plastic zone at overload, a_i is the current crack length and W is a shaping exponent. The empirical constant W is determined by curve fitting to experimental HCF+LCF overload influenced FCG rate data, using constant amplitude HCF only FCG rate data at the appropriate stress ratio, factored by C_p. This model has been employed in previous work [9] to determine the fatigue growth life under the interaction of LCF overload and HCF loadings. However, the Wheeler model has a significant deficiency in that the existence of delayed retardation of the onset of HCF contribution to crack growth cannot be explained. In addition, since the retardation parameter varies with the load spectrum and specimen geometry, the model's application is limited.

The plasticity-induced closure mechanism suggests that crack growth retardation following an overload is the result of residual plastic deformation behind the crack

tip. The level of plasticity-induced crack closure is enhanced in the post-overload regime, which, in turn, promotes a retardation of FCG rate. Thus delayed retardation is naturally expected since some crack growth is needed before the overload plastic zone moves to the crack wake from the tip. On the basis of the closure concept, many analytical and numerical methods have been developed to calculate crack-opening stress and subsequently the crack growth rate under variable loading, such as FASTRAN and AFGROW. FASTRAN is a code developed by Newman [23-25], which has been widely used to analyse the fatigue crack growth behaviour of aerospace materials under aircraft spectrum loadings. AFGROW was developed by J. Harter and Analytical Services and Materials at the US Air Force Research Laboratory, Wright-Patterson AFB, OH [26]. In the following sections both codes will be used to correlate crack growth data under combined HCF and LCF loading with the effect of single LCF overloads.

4.1 FASTRAN work

Newman's closure model is based on the Dugdale strip-yield model [27] but modified to leave plastically deformed material in the wake of a crack as described in detail in [23-25]. Fig. **14** shows a schematic diagram of the model and a flow chart for implementation.

According to the closure model, the crack-opening stress, S_o is first calculated. The details of the calculation under this constant-amplitude loading condition can be found in ref. [23]. For variable-amplitude loading conditions or spectrum loading, FASTRAN executes the calculation of the crack opening behaviour in terms of load history and crack length. Once the crack-opening stress is determined, the effective cyclic plastic zone corrected effective stress-intensity factor is given by

$$(\Delta K_p)_{eff} = (S_{\max} - S_0)\sqrt{(\pi d)}F(d/W) \qquad (3)$$

where d is the sum of the crack length and the size of a quarter of the cyclic plastic zone.

Consequently, the crack growth rate is calculated as follows:

$$da/dN = C((\Delta K_p)_{eff})^n G/H \qquad (4)$$

where $G = 1-(\Delta K_{eff,th}/\Delta K_{eff})^p$ and $H = 1-(K_{max}/C_5)^q$. The function G accounts for threshold variation with stress ratio and the function H accounts for the rapid crack-growth rates approaching fast fracture. The parameter C_5 is the cyclic fracture toughness. A discussion of the fast fracture behaviour is beyond the scope of the present paper, so H is set to unity. Note that the calculations herein are performed with FASTRAN Version 4.3.

To make a life prediction using FASTRAN, the effective threshold $(\Delta K_{eff})_{th}$ as a function of stress ratio R is required as input. The measured threshold values for the material have been reported before [9] and are shown here in Figure **15**, together with data from Powell and Duggan [28]. It indicates that ΔK_{th} decreases with increasing R and is close to 2.0 MPa$\sqrt{m}$ at R = 0.9. The ΔK_{th} value of 2.0 MPa$\sqrt{m}$ at R = 0.9 was considered to represent a practical lower bound of threshold for large cracks in the currently studied Ti-6Al-4V alloy. This value is a little lower than the value of 2.1 reported by Ritchie et al [29], who studied a Ti-6Al-4V alloy with a higher yield stress of 926 - 935 MPa and measured the threshold under constant K_{max}/increasing K_{min} cycling at R = 0.92. However, the variation of the effective threshold $(\Delta K_{eff})_{th}$ with R ratio is not investigated in the present study and no other relevant data were found in the literature. By trial and error, the solid line in Fig. **15** is chosen to represent the relationship between $(\Delta K_{eff})_{th}$ and R at room temperature. For the cases studied in this report, it was found that the $(\Delta K_{eff})_{th}$ against R curve has a dramatic effect on the prediction of the onset of HCF contribution, ΔK_{onset}. The current input gives an overall best fitted estimation under various stress ratios and overload ratios.

The curve of FCG rate (da/dN) versus effective stress intensity factor range ΔK_{eff} is also required as input. In the present study, this curve is estimated from experimentally determined FCG rate against stress intensity factor range (ΔK) data under constant-amplitude HCF loadings, as shown in Fig. **16**. For FCG rates greater than 1×10^{-10} m/cycle, the test data are obviously collapsed into a narrow band. It suggests that for such growth rates the plasticity-induced closure effect is negligible and therefore ΔK can be approximately regarded as ΔK_{eff}. A difference is observed however in the threshold regime, where the FCG rates at R = 0.9 are higher than those at R ratios of 0.7 and 0.8, corresponding with a lower threshold value at R = 0.9. The plasticity-induced closure model gives little interpretation for this difference at and near the threshold regime. Arguably, it is often explained by the influence of other closure effects in this regime, such as roughness- and oxide- induced closure [30], or an intrinsic mean (or maximum) stress intensity effect [31]. As a result, the da/dN and ΔK_{eff} relationship for the near-threshold regime is assumed to be close to the data at R = 0.9. The solid line in Fig. **16** is finally used to represent the estimated relationship between FCG rate and ΔK_{eff} at room temperature.

Fig. **17** shows a comparison between the predicted da/dblock versus ΔK_{LCF} curves and the experimental results at room temperature for overload ratios T of 1.0 (no overload) and 1.45 (45% overload) for R_{HCF} = 0.8. Both simulated and experimental results indicate that, as the overload ratio increases, the contribution of the HCF cycles to the overall FCG rate is reduced; at the same time, the commencement (ΔK_{onset}) of the HCF contribution is elevated to a larger stress intensity range. For both overload ratios, the predicted FCG rates agree well with the experimental data. The predicted ΔK_{onset} can also be found from Fig. **17**. They are 10.1 and 16.8 MPa$\sqrt{m}$ for T = 1.0 and T = 1.45, respectively. The comparison between predicted and experimental ΔK_{onset} values is shown in Table 5. The errors are within 15%

.

Table 5 Comparison between experimental and FASTRAN-predicted ΔK_{onset} under combined LCF + HCF loadings

HCF stress ratio R_{HCF}	Overload ratio T	Experimental ΔK_{onset} MPa√m	Predicted ΔK_{onset} MPa√m
0.8	1.0	12.6	10.1
0.8	1.45	15.3	16.8
0.7	1.0	9.7	7.1
0.7	1.45	13.0	10.8

Fig. **18** shows the comparison for the overload ratios of 1.0 and 1.45 for R_{HCF} = 0.7 at room temperature. The predictions are reasonably in agreement with the experimental results for FCG rates above 3×10^{-7} m/cycle for both overload ratios. However, ΔK_{onset} is underestimated by 27% and 17% for T = 1.0 and T = 1.45, respectively. The correspondingly FCG rates near ΔK_{onset} are obviously overestimated.

4.2 AFGROW work

In this study the NASGRO equation, developed by Newman and others [32] and already implemented in AFGROW, is used to describe crack growth. The equation is expressed as

$$da / dN = C\left(\Delta K_{eff}\right)^n G / H \qquad (4)$$

where $G = \left(1 - \Delta K_{th} / \Delta K\right)^p$ and $H = 1 - (K_{max} / K_c)^q$. The function G accounts for near-threshold FCG rates and the function H accounts for the rapid crack-growth rates approaching fast fracture. The parameter K_c is the cyclic fracture toughness. C, n, p, q are empirically obtained through best fits of the da/dN – ΔK data. ΔK_{eff} is calculated by

$$\Delta K_{eff} = \left[\left(\frac{1-f}{1-R} \right) \Delta K \right] \tag{5}$$

where f is the Newman closure function that accounts for plasticity-induced closure effects. f is empirically given as a function of stress ratio R:

$$f = \frac{K_{op}}{K_{\max}} = \max(R, A_0 + A_1 R + A_2 R^2 + A_3 R^3) \quad R \geq 0 \tag{6}$$

The calculation of coefficients A_0, A_1, A_2, A_3 is given in reference [26]. The Newman closure function is also used to determine ΔK_{th}, according to the following empirical equation:

$$\Delta K_{th} = \Delta K_{th,R=0} \Big/ \left(\frac{1-f}{1-A_0(1-R)} \right)^{(1+C_{th}R)} \tag{7}$$

where $\Delta K_{th,R=0}$ is the threshold stress intensity factor range at $R = 0$ and C_{th} is an empirical constant.

The empirical values of C, n, p, q, A_0, A_1, A_2, $A3$ and C_{th} for forged Ti-6Al-4V are given by NASGRO databases. NASGRO predicted FCG rates at constant-amplitude loadings are shown in Fig. **19**. For all three R ratios, the predicted FCG rates agree well with experimental results for the Paris regime. However, for two HCF stress ratios (R = 0.7 and 0.8), the ΔK_{th} values are less than the experimentally established data and the FCG rates near the threshold regime are correspondingly over-predicted.

In AFGROW, the load interaction, or overload effect, is accounted for by a closure factor, C_f [26]. The use of C_f is independent of what causes the load interaction effects, but is simply referred to as the ratio of the stress intensity value required to 'open' the crack (K_{op}) to the maximum stress intensity factor (K_{max}) for a given cycle. The relationship between C_f and R is given by

$$C_f = 1.0 - [(1 - C_{f0})(1 + 0.6R)(1 - R)] \quad (8)$$

The material parameter, C_{f0}, is the value of C_f at R = 0, and is used to adjust the curve for a given material. Once K_{op} and ΔK_{eff} are determined, a conversion back to apparent ΔK is required to calculate the crack growth rates. It is achieved according to the following equation:

$$\Delta K = \Delta K_{eff} (1 - R)(1 - C_f) \quad (9)$$

Fig. **20** shows a comparison between the predicted FCG rates and experimental results for combined HCF and LCF loadings, with overload ratios of 1.0 (no overload) and 1.45 (45% overload). The stress ratio of HCF cycles, R_{HCF}, is 0.7. It is seen that, for both cases, AFGROW gives a reasonable prediction of FCG rates above ΔK_{onset}, whilst ΔK_{onset} is underestimated and the FCG rates near ΔK_{onset} are overestimated.

Obviously, the capability of AFGROW to predict ΔK_{onset} and the FCG rates near ΔK_{onset} is not entirely satisfactory but is conservative. This corresponds with the inaccuracy of threshold prediction by AFGROW under HCF loadings only, Fig. **19**. These conclusions are in agreement with the earlier predictions by FASTRAN.

4.3 Elevated-temperature fatigue crack growth predicted by FASTRAN

FASTRAN was used in this study to attempt to predict combined LCF+HCF fatigue crack growth rates at 350 °C. Two inputs are required: one is the curve of effective threshold $(\Delta K_{eff})_{th}$ versus stress ratio R; the other is the curve of FCG rate (da/dN) versus effective stress intensity factor range ΔK_{eff}. Since the experimental results shows that fatigue thresholds at 350 °C are little difference to those at room-temperature, the room temperature curve in Fig. **15** is still used to represent the relationship between $(\Delta K_{eff})_{th}$ and stress ratio R. The experimentally

obtained da/dN - ΔK curve at R = 0.9 for 350 °C, Fig. **8**, is taken as the da/dN - ΔK_{eff} curve.

The comparison between the FASTRAN-predicted FCG rates and experimental data under LCF loading only (R = 0.01) at 350 °C is made in Fig. **21**, showing an obvious underestimation by FASTRAN.

Fig. **22** and **23** show comparisons between predictions and experiments under typical combined LCF+HCF loading conditions. For R_{HCF} = 0.7 (Fig. **22**), FASTRAN is conservative in that it underestimates the value of ΔK_{onset} and predicts higher FCG rates after onset when compared with the experimental results. However greater divergence is seen at R_{HCF} = 0.9, Fig. **23**. FASTRAN predicts a retarded FCG rate with the application of overload, together with an increase in the value of ΔK_{onset}. However, the test results indicate that the application of overload has not suppressed the contribution of HCF cycles

4.4 Current Status of Predictive Modelling

The capabilities of FASTRAN and AFGROW to facilitate the estimation of fatigue crack growth in the Ti-6Al-4V alloy under conjoint major and minor cycle loadings with and without the overload effect were first examined for room temperature. As illustrated in Figs.**18**-**21**, the predicted FCG rates beyond the ΔK_{onset} regime are reasonably good. Both codes also predicted the transition of onset point due to the effect of overload, however, the accuracy is not entirely satisfactory. Since the commencement of minor cycle growth is related to the minor cycle threshold value, inaccuracy of ΔK_{onset} prediction by FASTRAN and AFGROW can be directly attributed to the fact that the crack closure model cannot explain the variation of fatigue threshold at high R ratios as illustrated in Figs. **17** and **20**. Experimental work by Boyce and Ritchie [33] showed that although no global closure was detected above R = 0.5 based on compliance measurements, ΔK_{th} values did continue to decrease with increasing R, which corresponded with increasing $K_{max,th}$. Explanation of this phenomenon was

suggested to be a dependence on K_{max} of the intrinsic mechanism of fatigue-crack growth. It implies that, to accurately predict ΔK_{onset} and the early stage of fatigue growth, a further development of a mechanistic intrinsic threshold model is needed.

FASTRAN has also been used to correlate fatigue crack growth behaviour of Ti-6Al-4V at 350^0C. However the predictions significantly disagree with the experimental results. In the light of these differences, it is believed that crack closure cannot be the sole mechanism that dominates fatigue crack growth at elevated temperature.

More recently, the authors [34] have successfully used a two-parameter approach to account for both effects of stress ratio and temperature on fatigue threshold and crack growth in forged Ti-6Al-4V under purely LCF or HCF loadings. The two-parameter model, proposed by Vasudevan and Sadananda [35-38], suggests that the fatigue crack growth process is intrinsically a two-parameter controlled process that depends on the material deformation characteristics and on the crack-tip environment. Of these two parameters, ΔK, an amplitude term, governs the cyclic plasticity contribution to the damage, and K_{max} governs the fracture process required for crack growth. An increase in temperature leads to reduction in material strength due to increased ease of slip of dislocations, and thereby the K_{max} related environment-assisted propagation processes become more significant. As a result, elevated-temperature fatigue crack growth rate is normally increased. Further investigation is ongoing to quantitatively assess the effect of temperature on FCG rates under combined LCF overload + HCF loadings. A significant challenge of this work is to characterise the role of K_{max} and its changes under the influence of the overload plastic zone.

5. Finite Element Modelling of Fatigue Crack Growth, Crack Closure and Overload Effects

In addition to the work described in this report, an associated parallell FEM study was carried out within the MBM group. Two main aspects were considered: the role of residual stresses in plasticity-induced fatigue crack closure under cyclic loading with and without overloads; and, the role of plasticity-induced crack closure in the FCG of corner cracks. The detail of this work is contained in two papers submitted for journal publication and provided as Appendix 2.

For the essentially two-dimensional case of a centre-cracked specimen under plane stress conditions, it is shown that after the opening stress is stabilised, residual stresses ahead of the crack tip have a very small effect on the opening stress. However, after an overload, the residual stresses seem to have a more significant role in defining the opening/ closure stresses.

The much more complex (and time-consuming) task, of extending the FEM study to the three dimensional case of the corner crack growth considered in this report, has been commenced. The initial finding, using a 3-D elasto-perfect plastic model, is that on the crack front the stress state on the specimen sides is close to plane stress and significant closure is observed. Inside the specimen, the state of stress and strain is very close to axisymetric conditions and little closure is observed.

Clearly there is considerably more to be done using FEM to understand the crack closure and FCG behaviour under combined HCF/LCF and different R ratios of HCF, the main consideration of this report. This could be one the areas of focus for future work, providing better estimates for crack closure and effective ΔK inputs to the FASTRAN and AFGROW codes.

6. Conclusions

(i) Conclusions from the experimentation at 350^0C are :-

a) An increase in temperature generally increases FCG rates when compared with room temperature data.

b) This increase in temperature causes a rotation in the LCF only FCG rate data giving a lower slope of the da/dN versus ΔK plot.

c) Prior LCF overloads decrease the HCF+LCF FCG rates in a similar way as at room temperature

d) Prior LCF overloads the onset (ΔK_{onset}) level for HCF contribution to HCF+LCF FCG rates and this appears to be the chief benefit of the overloads.

e) The effectiveness of prior LCF overloads in suppressing the contribution of HCF cycles to combined HCF+LCF FCG rates is reduced at elevated temperature especially at high stress ratios.

f) An increase in temperature from room temperature to 350C has little effect on the value of ΔKthreshold.

g) The early stage of climb ("climb1") in the flight simulation study showed the greatest contribution to crack growth at elevated temperature, but the onset of the cruise stage contribution to crack growth may not have been reached.

(ii) FASTRAN and AFGROW, both of which use a plasticity-induced crack closure model to simulate the retardation phenomenon caused by overload, predicted reasonably well the crack growth rates on forged Ti-6Al-4V under combined LCF and HCF loading for a range of stress ratios and overload ratios at room temperature. Both models also predicted the transition of the ΔK_{onset} point due to the overload effect, however, the accuracy of this prediction, though conservative, is not entirely satisfactory. Elevated-temperature FCG rates under

LCF overload + HCF combination cannot be predicted entirely satisfactorily by FASTRAN and AFGROW, indicting that crack closure is not the sole mechanism affecting fatigue behaviour at 350 ^{0}C. There is a need to further develop a more accurate predictive model, probably based on a two parameter (ΔK and K_{max}) approach.

7. Recommended Future Work

The following items have been identified as worthy of investigation in the future.

a) Greater overload ratios (T) to establish the level for effective suppression of HCF activity.

b) Higher cycle ratios (n) to establish how the number of HCF cycles affects the suppression effects of overloads.

c) Higher temperature study of combined HCF+LCF under overload conditions for an alternative higher temperature material, e.g. Ti5331S (IMI829), nickel based superalloy or MMC.

d) Further development of the FCG predictive modelling using the two-parameter (ΔK and Kmax) approach.

e) Extension of the three-dimensional elasic-plastic FEM studies to consider combined HCF/LCF loading with variation of R for the HCF cycles.

8. References

[1] Goswami T. “Fatigue crack growth behaviour of Ti-6Al-4V alloy forging”. Materials and Design, 2003, 24, 423-433.

[2] Arakere NK, Goswami T, Krohn J and Ramachandran N. “High temperature fatigue crack growth behaviour” of Ti-6Al-4V. High Temperature Materials and Processes, 2002, 21, 229-236.

[3] Boyce BL and Ritchie RO. “Effect of load ratio and maximum stress intensity on the fatigue threshold in Ti-6Al-4V”. Engineering Fracture Mechanics, 2001, 68, 129-147.

[4] Peters JO and Ritchie RO. “Influence of foreign-object damage on crack initiation and early crack growth during high-cycle fatigue of Ti–6Al–4V”. Engineering Fracture Mechanics, 2000, 67, 193-207.

[5] Ritchie RO, Boyce BL, Campbell JP, Roder O, Thompson AW, Milligan WW. “Thresholds for high-cycle fatigue in a turbine engine Ti-6Al-4V alloy”. International Journal of Fatigue, 1999, 21, 653-662.

[6] Ritchie RO, Davidson DL, Boyce BL, Campbell JP and Roder O. “High-cycle fatigue of Ti-6Al-4V”. Fatigue Fracture Engineering Materials Structure, 1999, 22, 621-631.

[7] Evans WJ, Bache MR, McElhone M and Grabowski L. “Environmental interactions with fatigue crack growth in alpha/beta titanium alloys”. International Journal of Fatigue, 1997, 19, 177-182.

[8] Powell B. E., Duggan T. V. and Jeal R. H., “The influence of minor cycles on low cycle fatigue crack propagation”, International Journal of Fatigue, 4, 4-14, 1982.

[9] Byrne J., Hall R. F and Powell B. E., “Influence of LCF overloads on combined HCF-LCF crack growth”, International Journal of Fatigue, 25, 827-834, 2003.

[10] Personal communication from Rolls-Royce.

[11] Pickard AC. The application of 3-dimensional finite element methods to fracture mechanics and fatigue life predictions. EMAS, 1986.

[12] Marci G. Comparison of fatigue crack propagation threshold of two Ti turbine-disk materials. Fatigue, 1994, 16, 409-412.

[13] Hall R.F., Ding J. & Byrne J. US AFOSR Study Report; *Interim Report for F61775-02-C4050*, F574, June 2003.

[14] Hall R.F., Ding J. & Byrne J. US AFOSR Study Report; *Annual Report for F61775-02-C4050,* **F**576, January 2004.

[15] Hall R.F., Ding J. & Byrne J. US AFOSR Study Report; *Interim Report for F61775-02-C4050*, F577, June 2004.

[16] Hall R.F., Powell B.E. & Byrne J. US AFOSR Study Report; *Interim Report for Phase IV, F61775-02-WE007,* F570, May 2001.

[17] J. R. Rice, "Mechanics of crack tip deformation and extension by fatigue", in Fatigue Crack Propagation, ASTM STP 415, 1967, 247-309.

[18] S. Suresh, "Micromechanisms of fatigue crack growth retardation following overloads", Engineering Fracture Mechanics, 1983, 18, 577-593.

[19] S. Taira and K. Tanaka, "Local residual stress near fatigue crack tip", Transactions of the Iron and Steel Institute of Japan, 1979, 19, 411-418.

[20] W. Elber, "The significance of fatigue crack closure," Damage Tolerance in Aircraft Structures. ASTM STP 486, 1971, 230-242.

[21] K. Sadananda, A.K. Vasudevan, R. L. Holtz and E. U. Lee, "Analysis of overload effects and related phenomena", International Journal of Fatigue, 1999, 21, 233-246.

[22] O. E. Wheeler, "Spectrum loading and crack growth", Journal of Basic Engineering, 1972, 94, 181-186.

[23] J. C., Newman Jr., “A crack-closure model for predicting fatigue crack growth under aircraft spectrum loading,” Methods and Models for Predicting Fatigue Crack Growth under Random Loading, ASTM STP 748, 1981, 53-84.

[24] J. C., Newman Jr., “FASTRAN II - a fatigue crack growth structural analysis program,” NASA TM 104159, 1992.

[25] J. C., Newman Jr., “ Crack growth under variable amplitude and spectrum loading in 2024-T3 aluminum alloys”, Proceedings of the TMS Fall Meeting, 1997, 109-121.

[26] Harter, J. A., AFGROW Users Guide and Technical Manual, Version 4.0008.12.11, Air Force Research Laboratory, WPAFB OH 45433-7542, 2003.1.

[27] Dugdale D. S., “Yielding of steel sheets containing slits,” Journal of Mechanics and Physics of Solids, 8,100-104, 1960.

[28] B. E. Powell and T. V. Duggan, “Predicting the onset of high cycle fatigue damage: an application for long crack threshold data”, International Journal of Fatigue, 8, 1986, 187-194.

[29] R.O. Ritchie, B.L. Boyce, J.P. Campbell, O. Roder, A.W. Thompson, W.W. Milligan, “Thresholds for high-cycle fatigue in a turbine engine Ti-6Al-4V alloy,” International Journal of Fatigue, 1999, 21, 653-662.

[30] S. Suresh, Fatigue of Materials, Cambridge University Press, 1998.

[31] J. Byrne and T.V. Duggan, “Influence of crack geometry on the fatigue threshold condition”, in Fatigue Thresholds, ed. J. Backlund, AF Blom and CJ Beevers, EMAS, 1982, 759-775.

[32] Forman, R. G., and Mettu, S. R., “Behavior of Surface and Corner Cracks Subjected to Tensile and Bending Loads in Ti-6Al-4V Alloy,” In Fracture Mechanics: Twenty-second Symposium, Vol. 1, ASTM STP 1131, H. A. Ernst, A. Saxena, and D. L. McDowell, eds., American Society for Testing and Materials, Philadelphia, **1992**, 519-546.

[33] B. L. Boyce and R. O. Ritchie, “Effect of load ratio and maximum stress intensity on the fatigue threshold in Ti-6Al-4V”, Engineering Fracture Mechanics, 2001, 68, 129-147.

[34] J Ding, R Hall, J Byrne, “Effects of stress ratio and temperature on fatigue crack growth in a Ti-6Al-4V alloy,” International conference on fatigue damage of structure materials V, 18 - 24 September, 2004, Hyannis, MA, USA.

[35] Vasudevan AK and Sadanada K. “Classification of fatigue crack growth behaviour”. Met. Trans. A, 1995, 26A, 1221-1234.

[36] Vasudevan AK and Sadanada K. “Fatigue crack growth in advanced materials”. Fatigue’96: Proceedings of the 6th International Conference on Fatigue and Fracture Thresholds, Vol. I. edited by Lutjering G and Nowack H. Pergamon Press, Oxford, UK, 473-478.

[37] Sadanada K and Vasudevan AK. “Fatigue crack growth mechanisms in steels”. International Journal of Fatigue, 2003, 25, 899-914.

[38] Sadanada K and Vasudevan AK. “Analysis of high temperature fatigue crack growth behavior”. International Journal of Fatigue, 1997, 19, S183-S189.

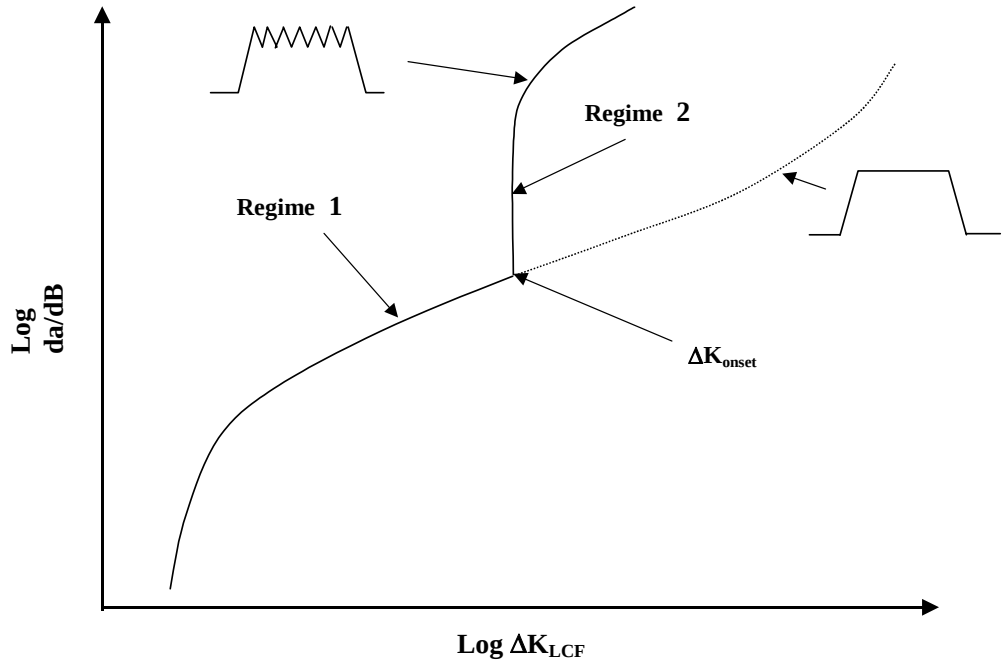

Fig 1. Fatigue crack growth rate regimes for HCF/LCF loadings

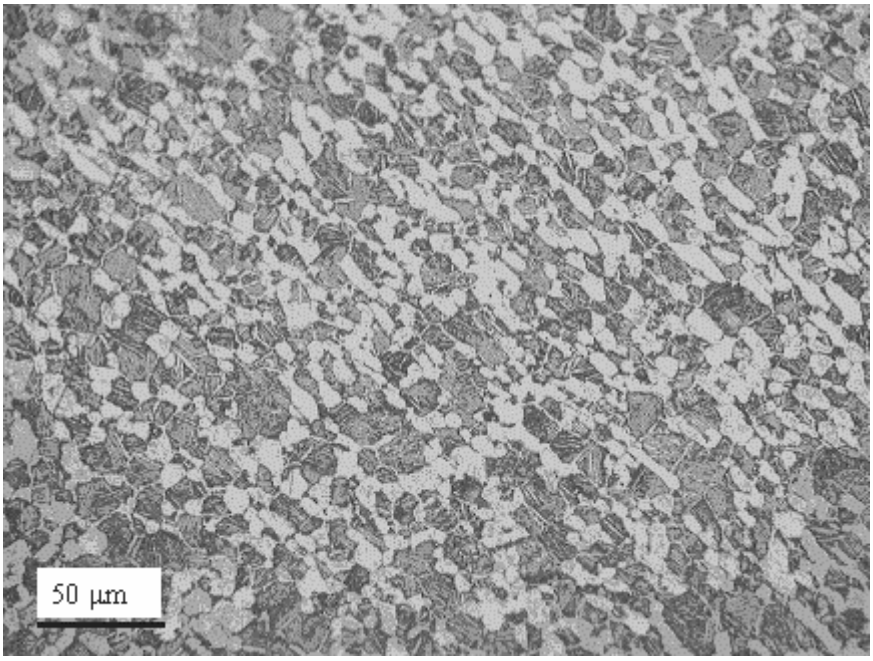

Fig. 2. Typical microstructure of the Ti-6Al-4V forged material

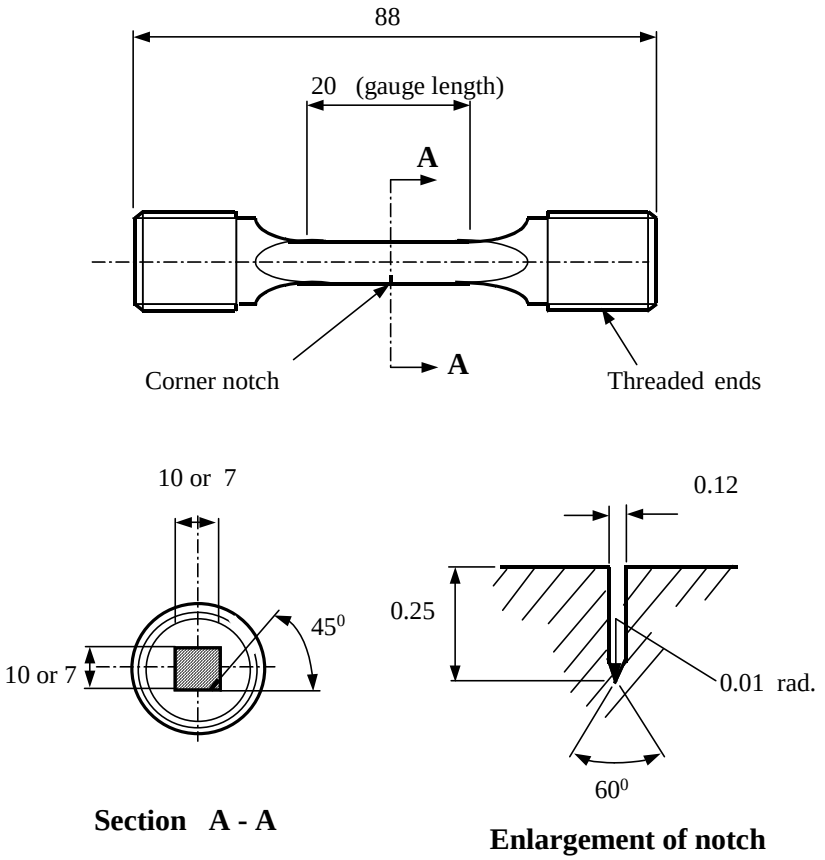

Fig. 3 Corner notch specimen

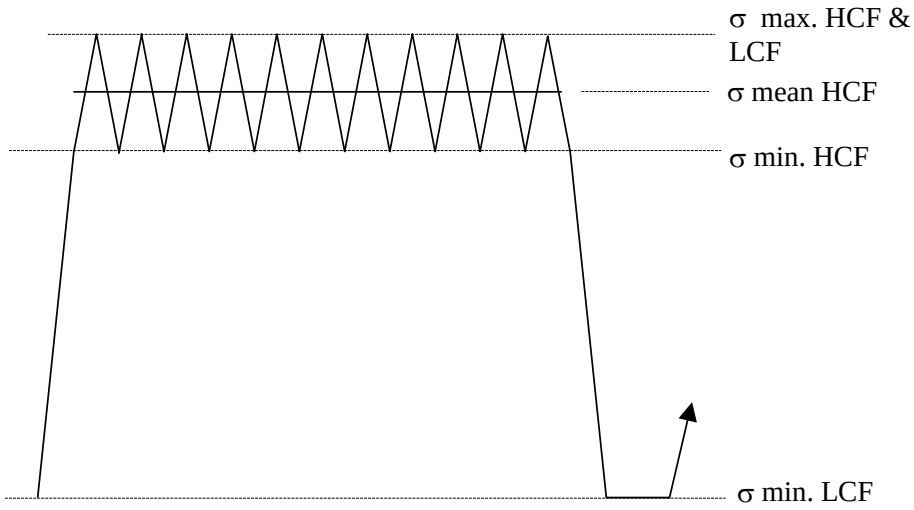

a) Without overload (T=1.0)

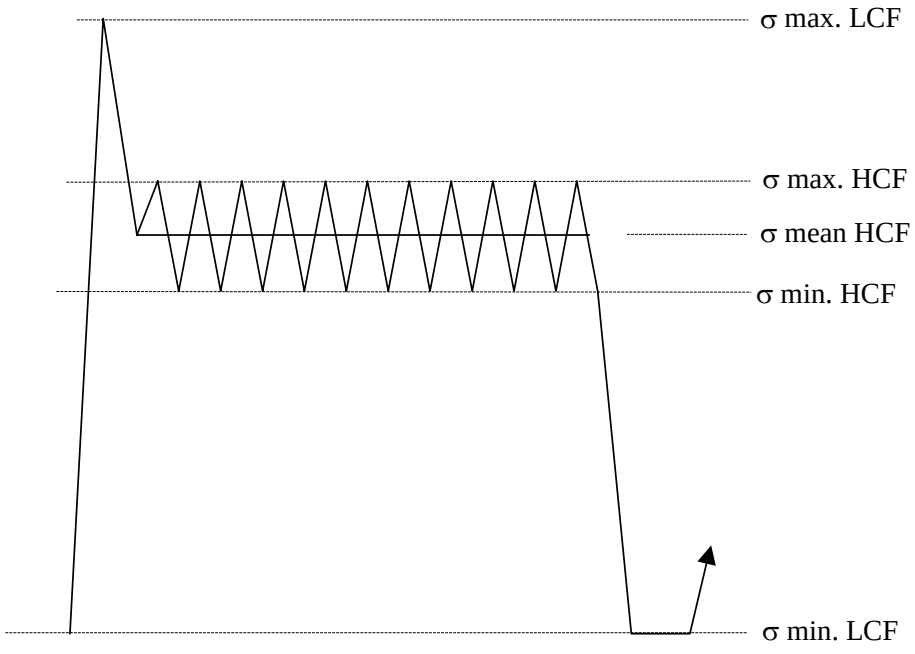

b) With overload (T>1.0)

Fig. 4 Schematic representations of the repeated stress – time sequences used in the tests. (a) without overload; (b) with overload

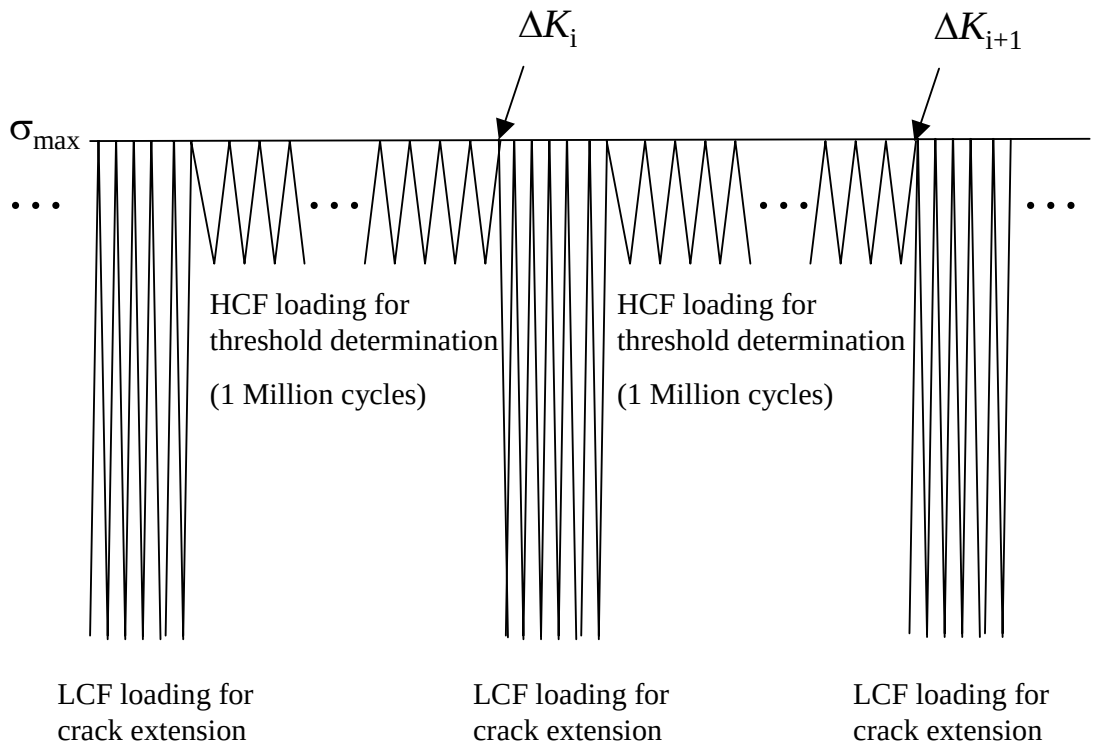

Fig. 5 A schematic loading pattern for fatigue threshold determination using the jump-in method

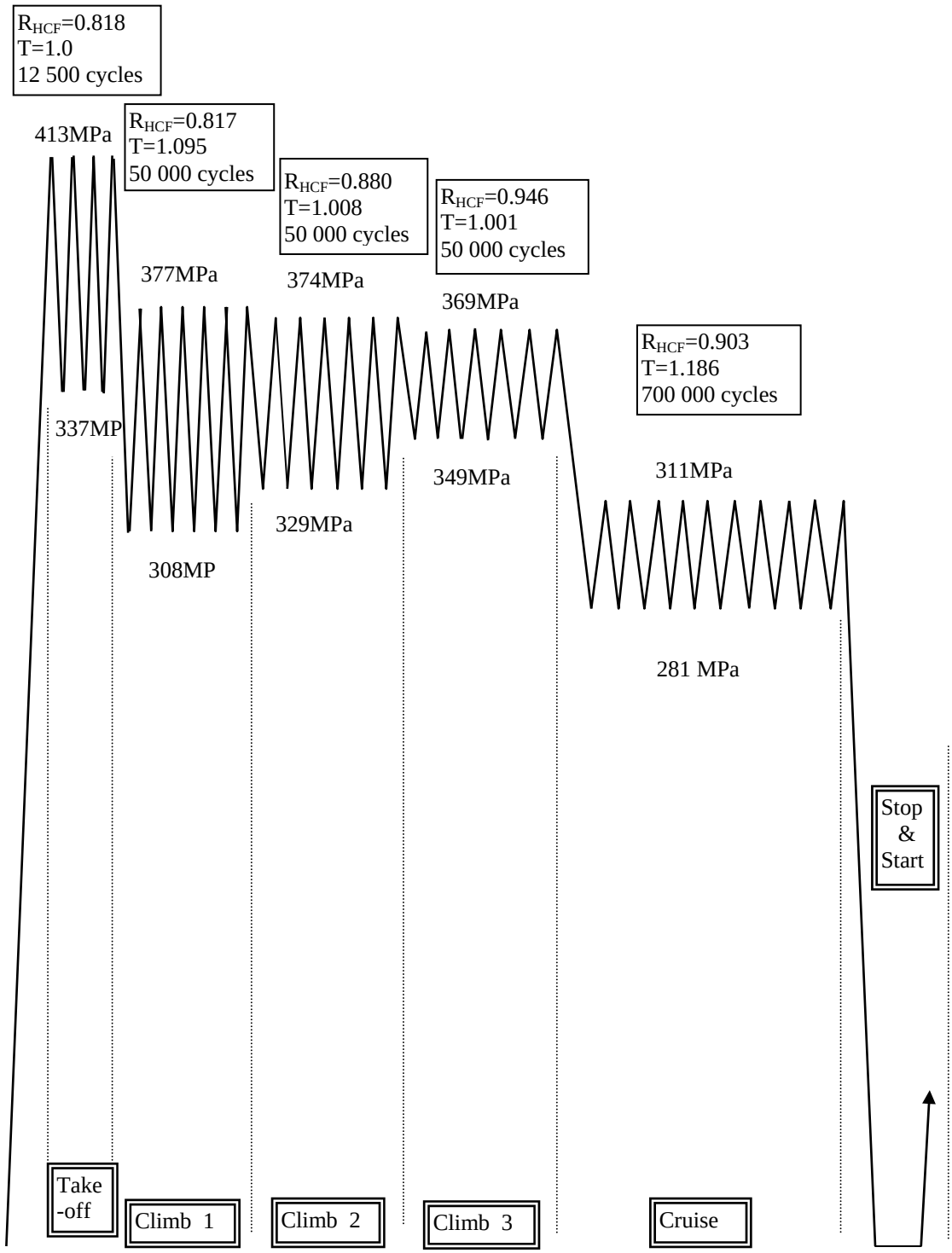

Fig. 6 Schematic diagram of the stresses used in the Flight Simulation experiments.

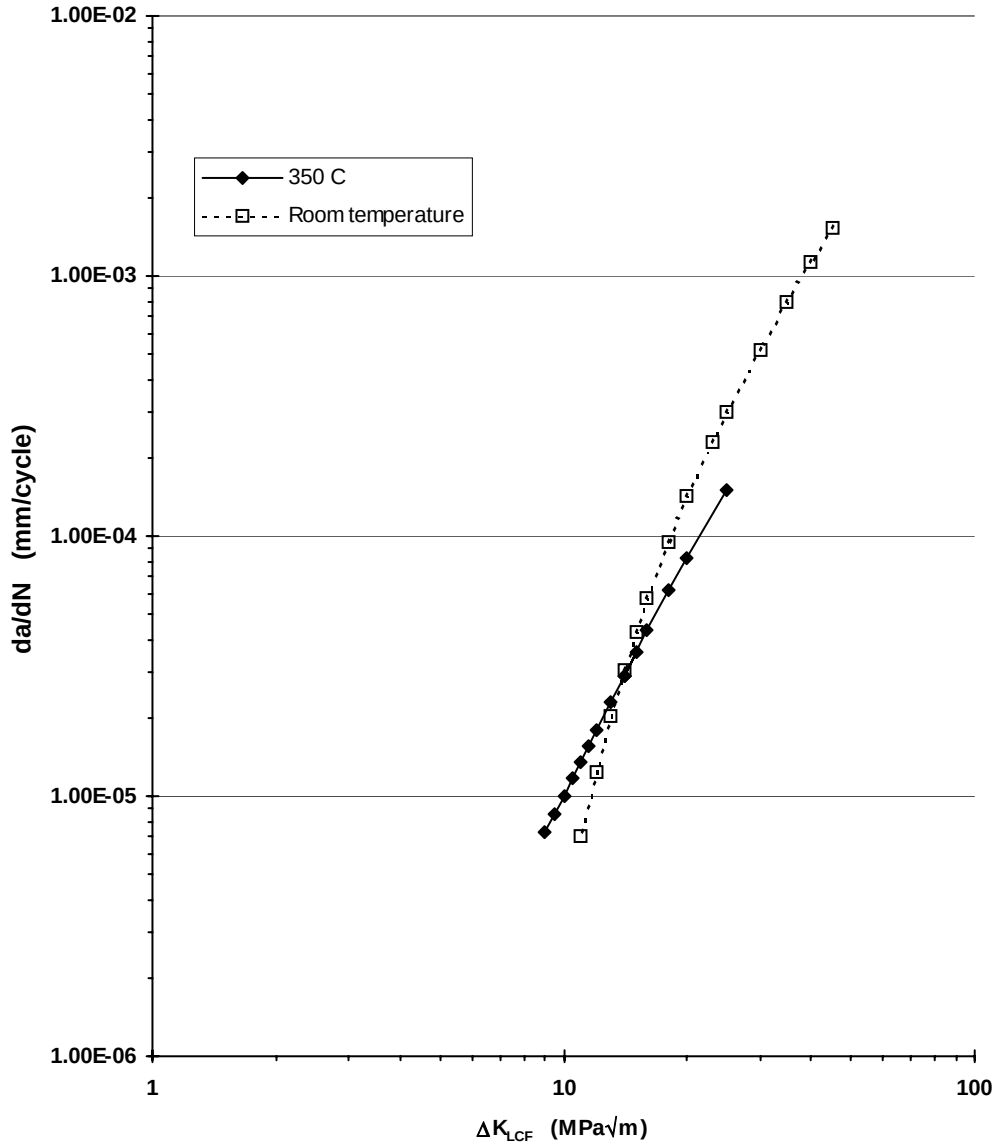

Fig. 7 Polynomial curves for FCG rates for LCF only cycles at 350^0C and room temperature

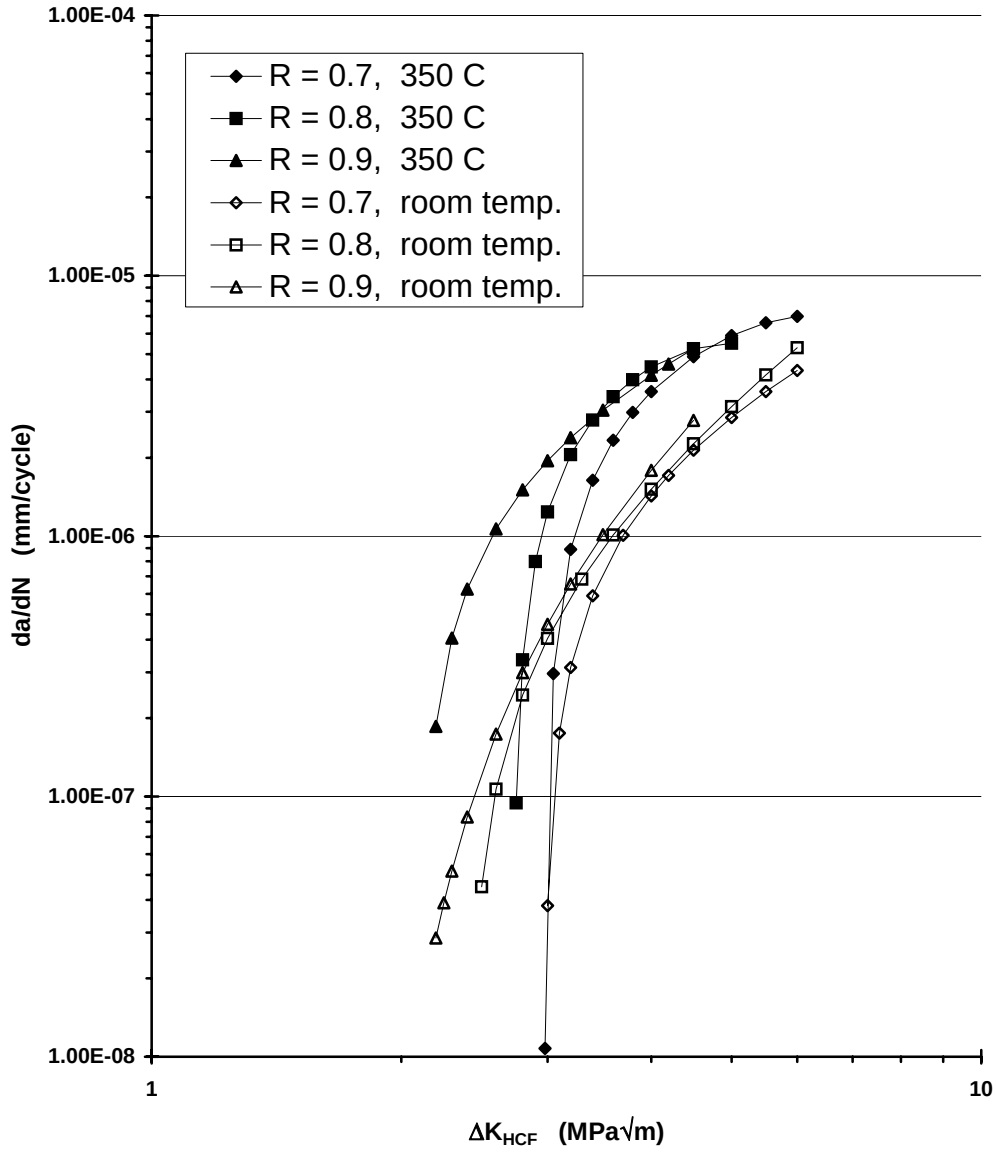

Fig. 8 Polynomial curves for FCG rates for HCF cycles only at 350^0C and room temperature

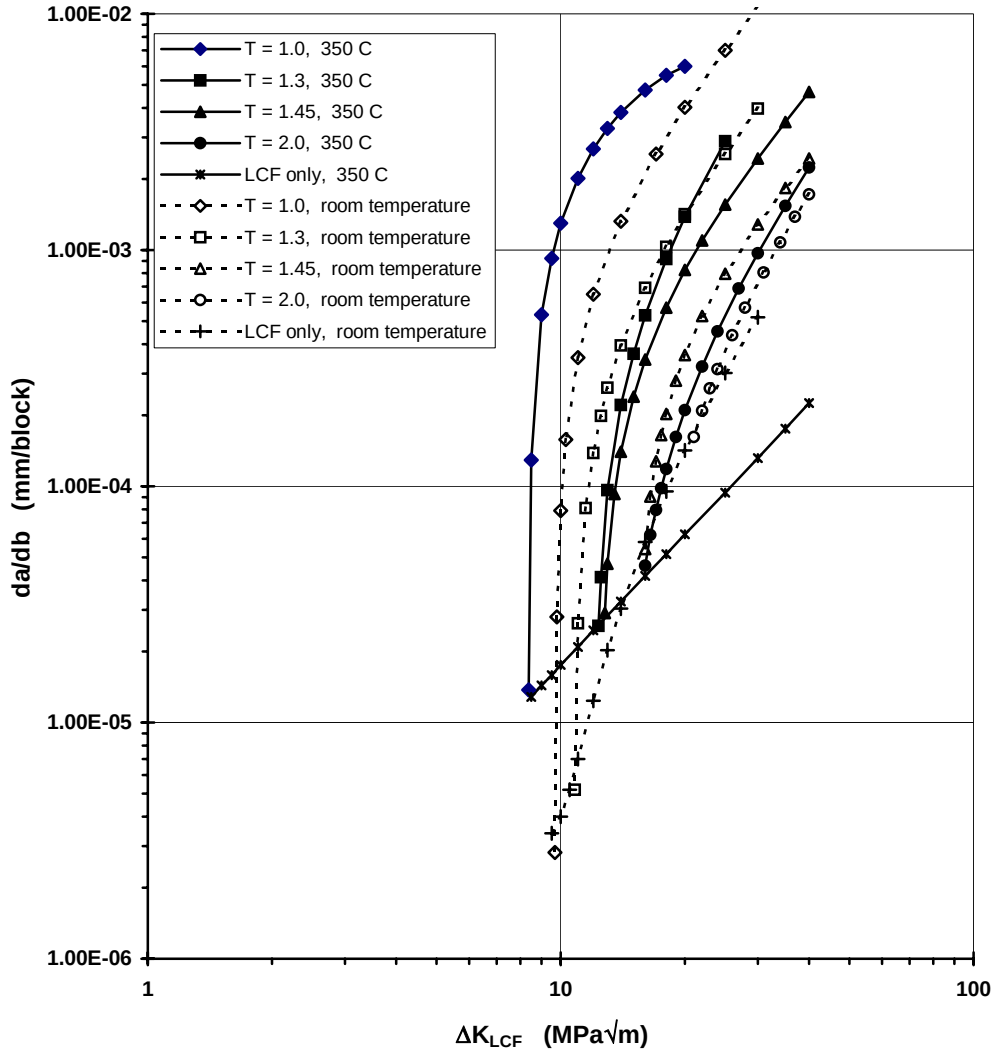

Fig. 9 Polynomial curves for FCG rates at 350^{0}C and room temperature
R_{HCF} = 0.7; n = 1000:1

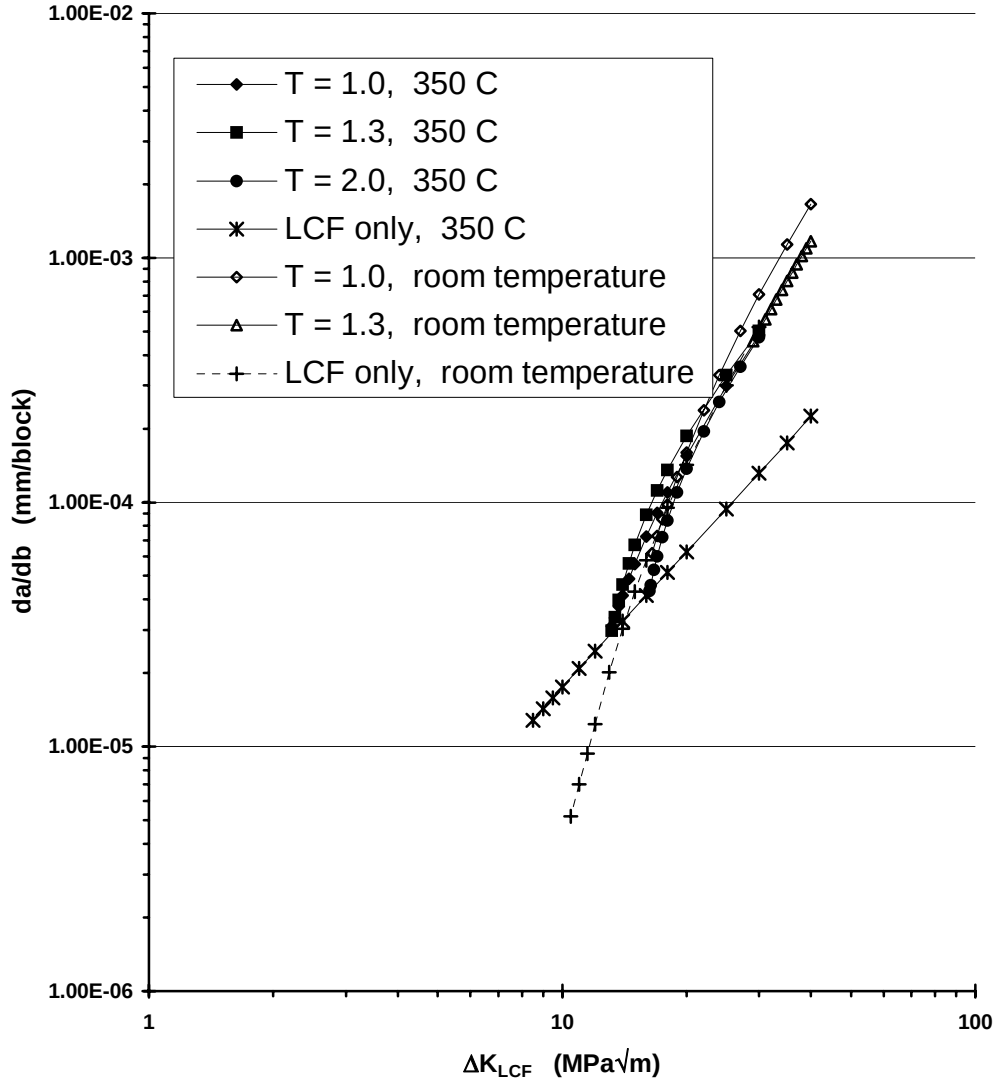

Fig. 10 Polynomial curves for FCG rates at 350^0C and room temperature
R_{HCF} = 0.9; n = 1000:1

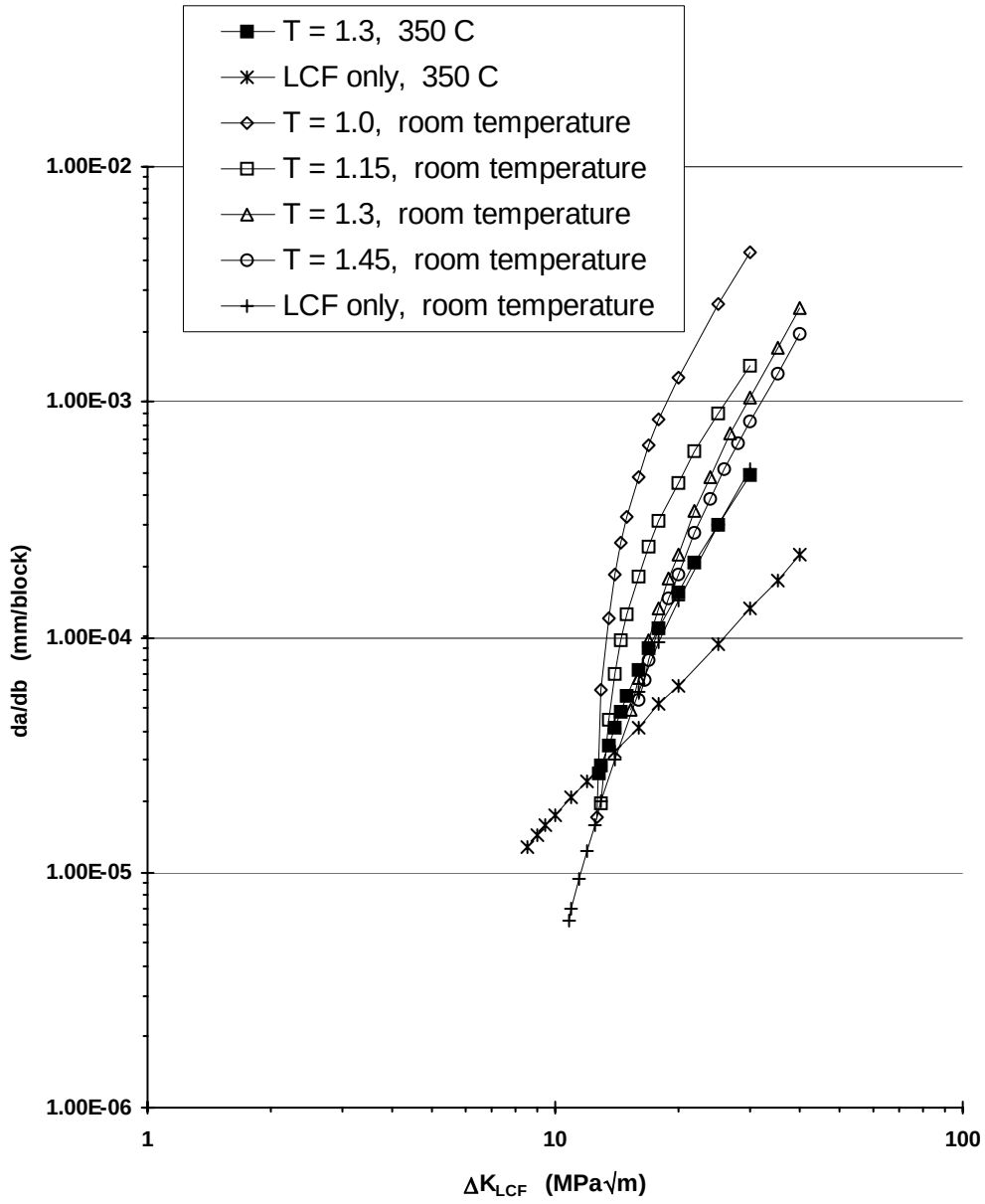

Fig 11 Polynomial curves for FCG rates at 350^{0}C and room temperature
R_{HCF} = 0.8; n = 1000:1

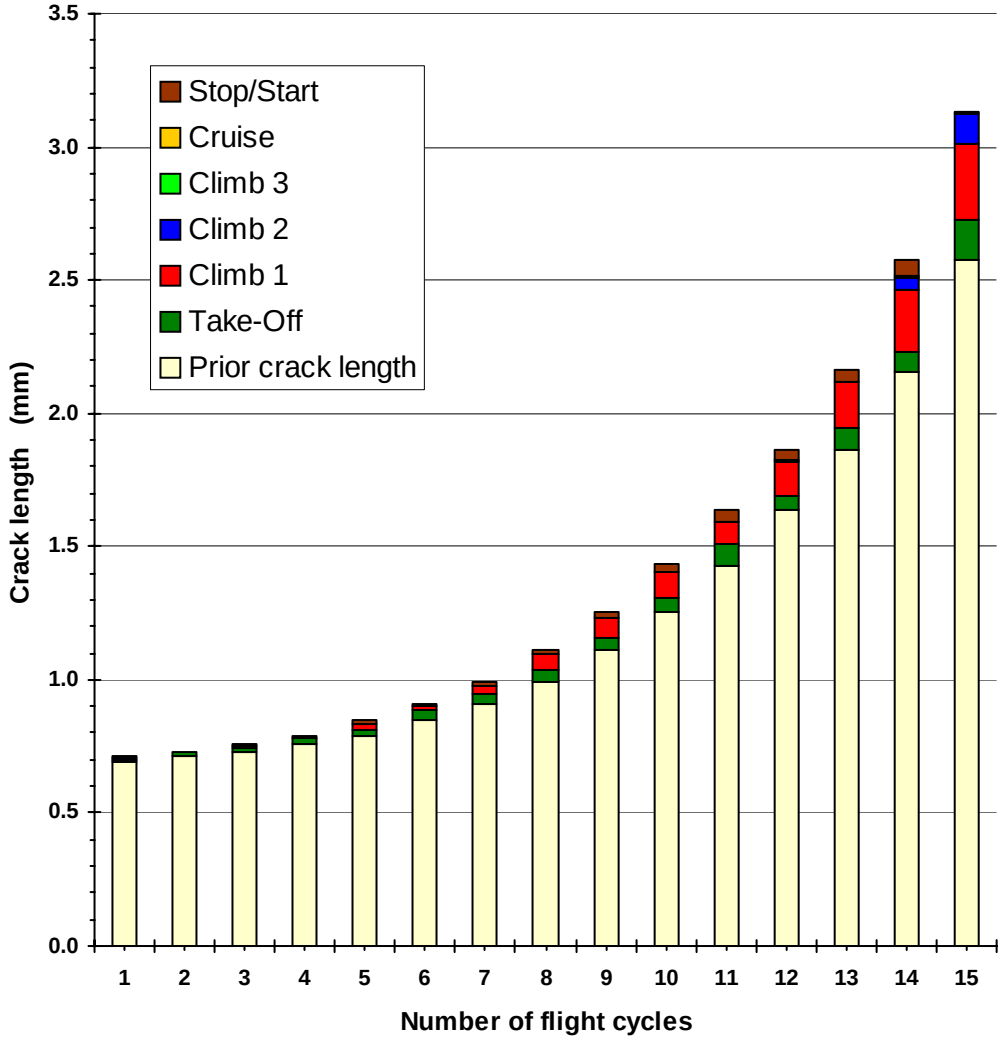

Fig. 12 Contribution to crack growth by each stage of flight simulation following the onset of combined loading effects at 350^{0}C

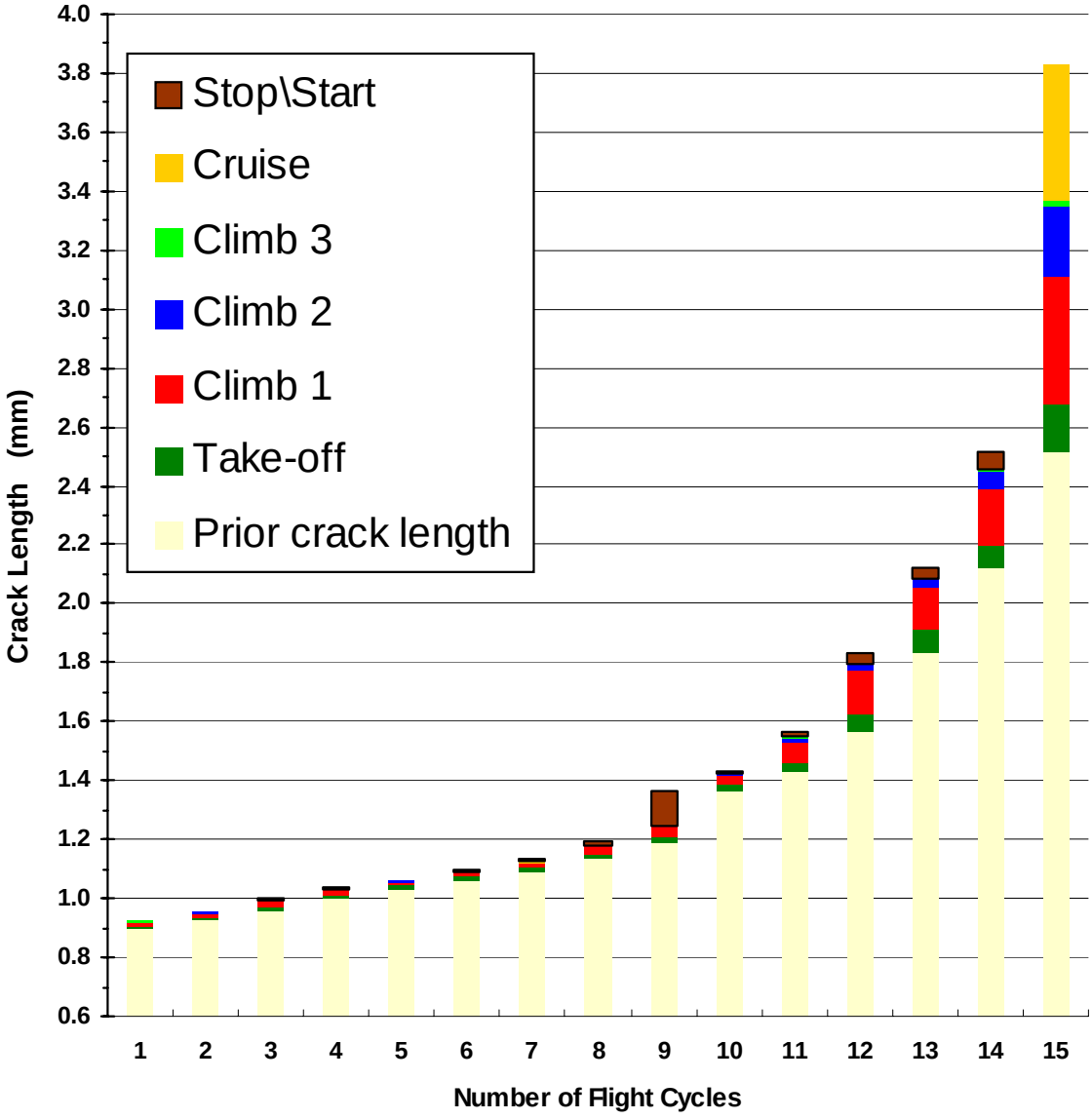

Fig. 13 Contribution to crack growth by each stage of the flight simulation following the onset of combined loading effects at room temperature.

Input

- Specimen geometry & α factor
- Material properties
- Initial crack length
- d*a*/d*N* vs. ΔK_{eff}
- $\Delta K_{eff,th}$ vs. *R*
- Combined HCF+LCF loading

Closure model

- Opening stress S_0'
- ΔK_{eff}

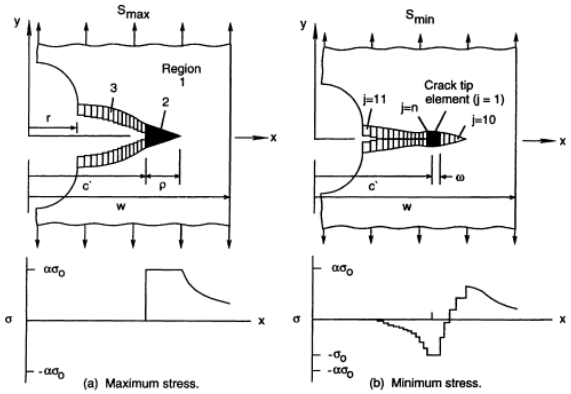

Crack growth Eq.

$$da/dN = C\left((\Delta K_p)_{eff}\right)^n G/H$$

where

$$G = 1 - (\Delta K_{eff,th} / \Delta K_{eff})^p$$

$$H = 1 - (K_{max} / C_5)^q$$

Life prediction

- *a* – *N*
- d*a*/d*N* - ΔK

Fig. 14 Flow chart of FASTRAN

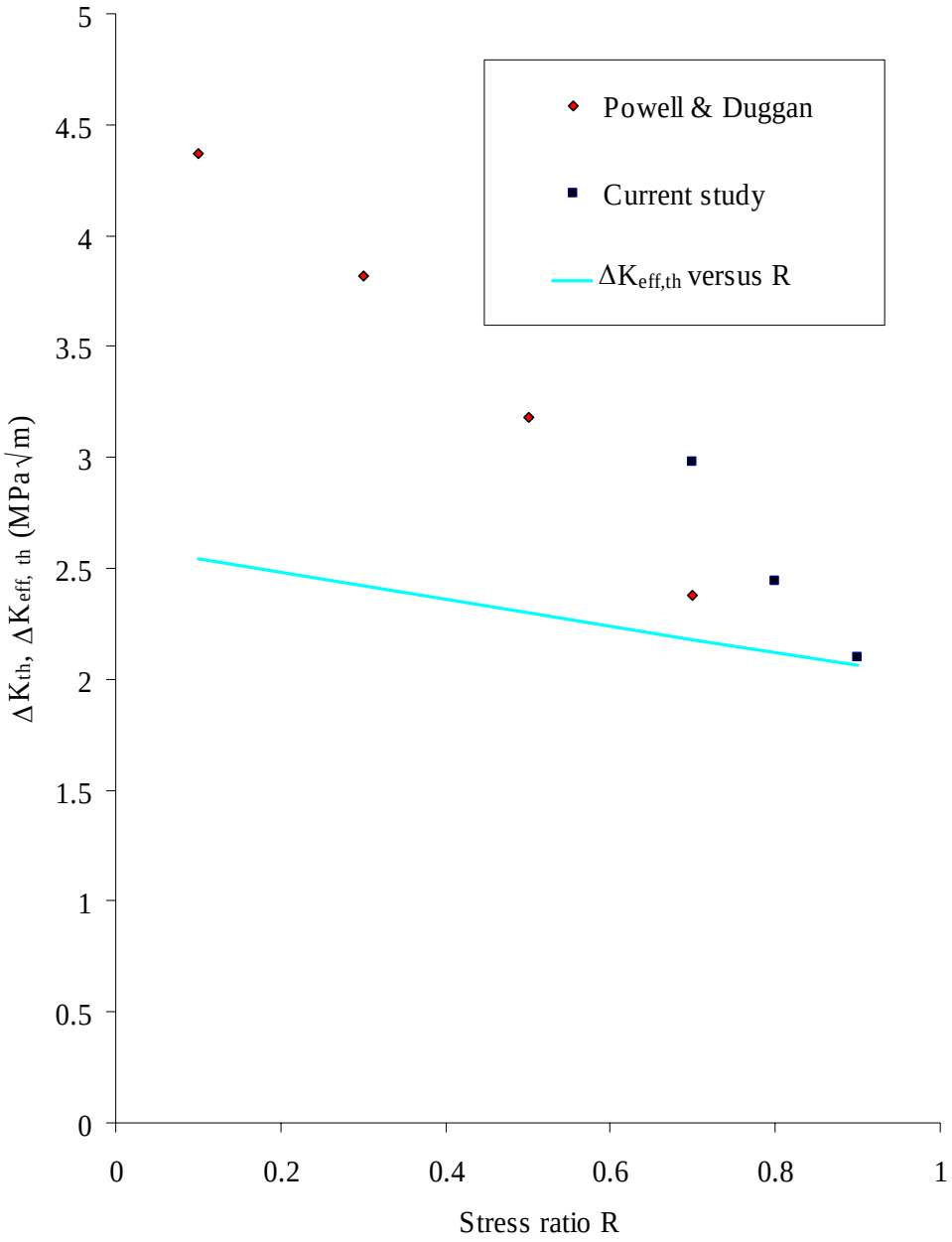

Fig. 15 Estimated effective threshold against stress ratio R, from experimental threshold data, at room temperature.

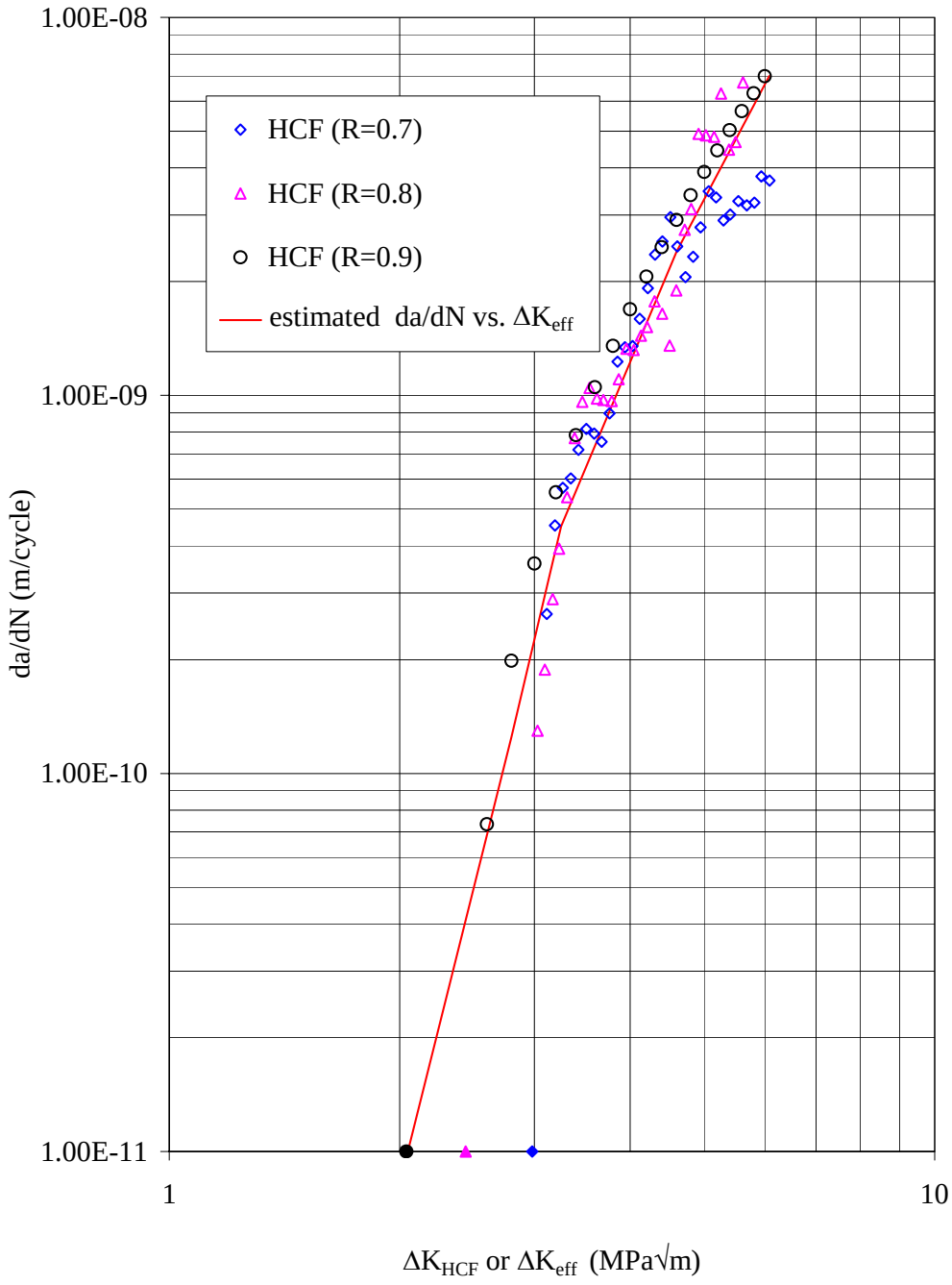

Fig. 16 FCG rates against effective stress intensity factor range curve, derived from experimental constant-amplitude HCF tests at room temperature.

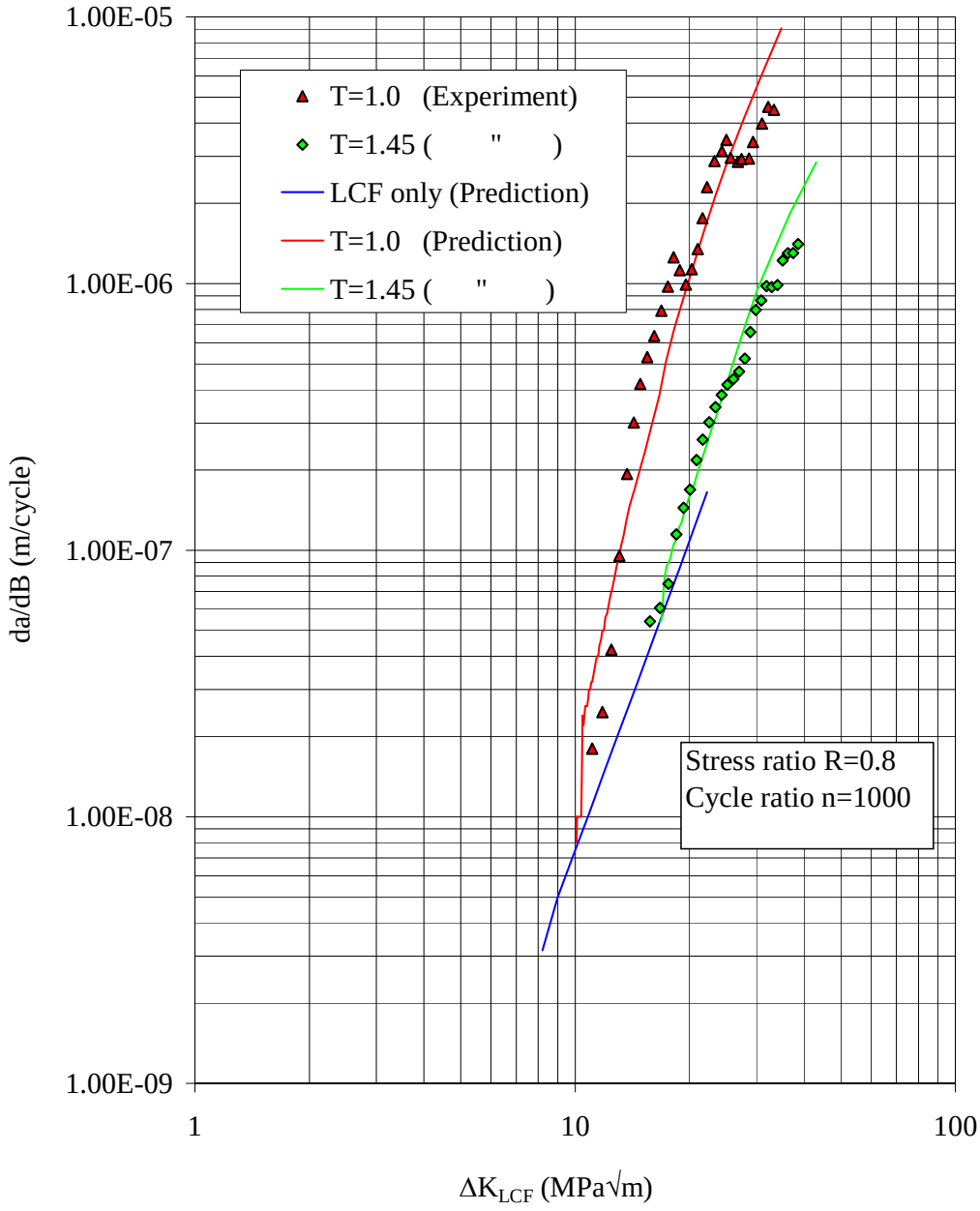

Fig. 17 Comparison of FASTRAN-predicted and experimental FCG rates without overload and with 45% overload, at room temperature. Stress ratio R_{HCF} = 0.8; cycle ratio = 1000 : 1.

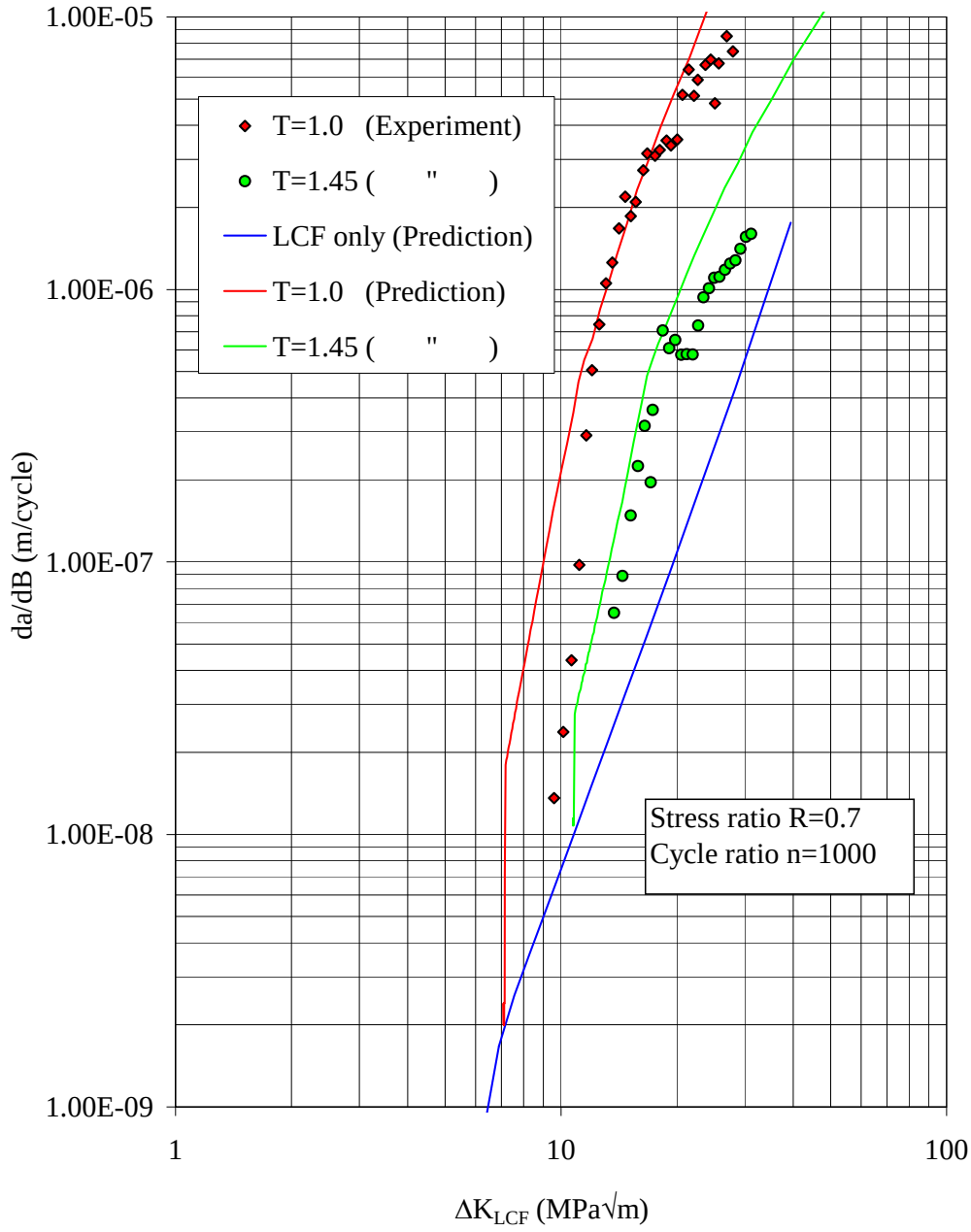

Fig. 18 Comparison of FASTRAN-predicted and experimental FCG rates without overload and with 45% overload, at room temperature. Stress ratio R_{HCF} = 0.7; cycle ratio = 1000 : 1.

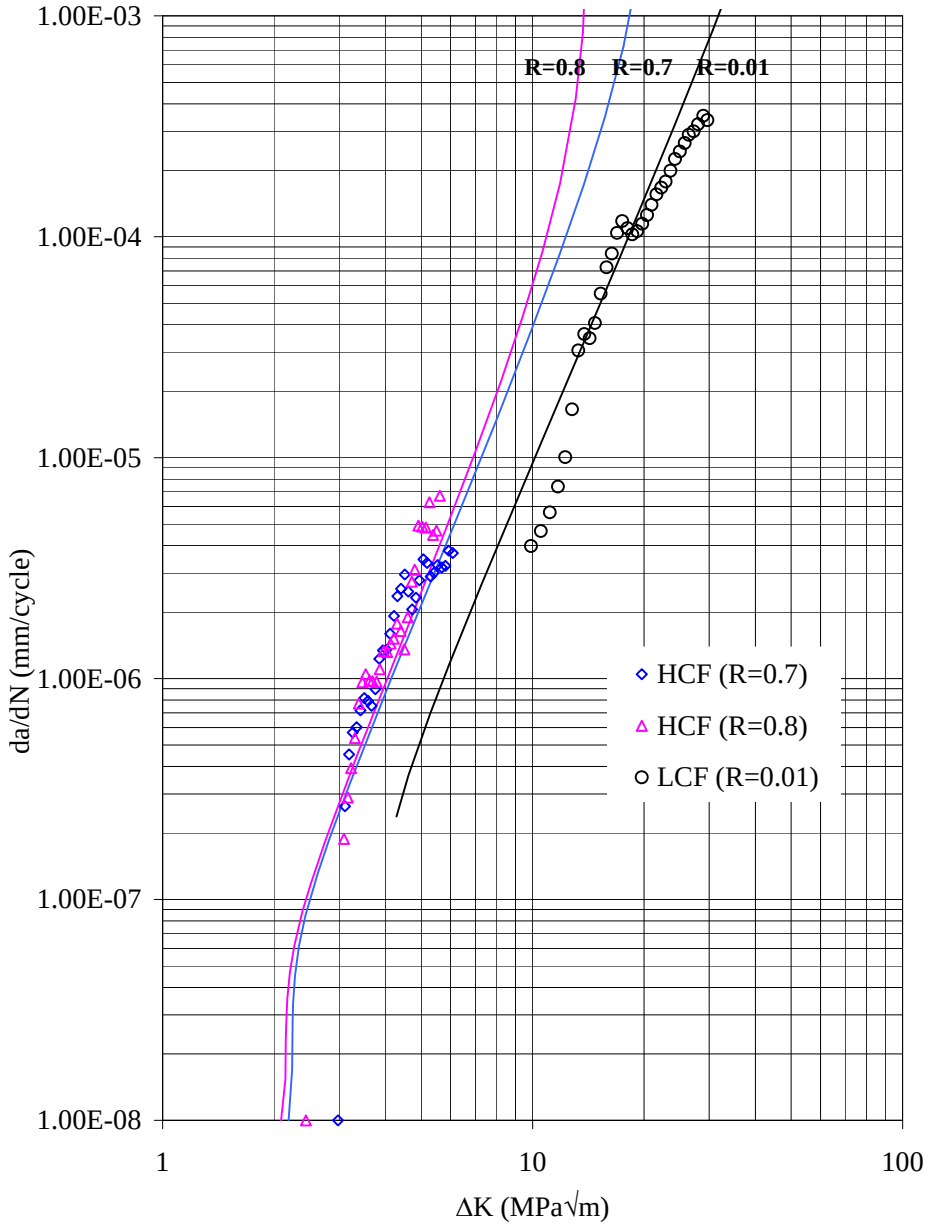

Fig. 19 Comparison of predicted HCF only FCG rates by the NASGRO equation (lines) and experimental data (points) for stress ratios of 0.01, 0.7 and 0.8 at room temperature.

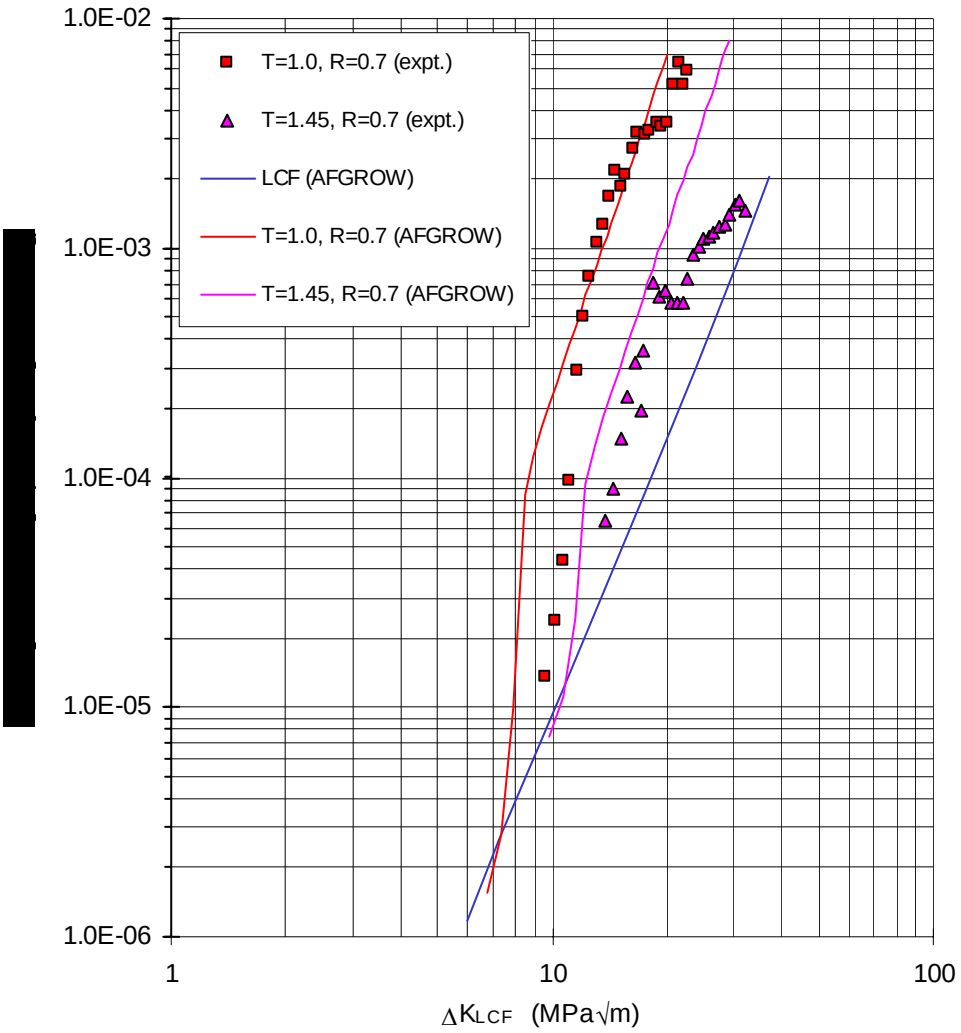

Fig. 20 Comparison of AFGROW-predicted and experimental FCG rates for different overload ratios. Stress ratio $R_{HCF} = 0.7$; cycle ratio = 1000 : 1 at room temperature.

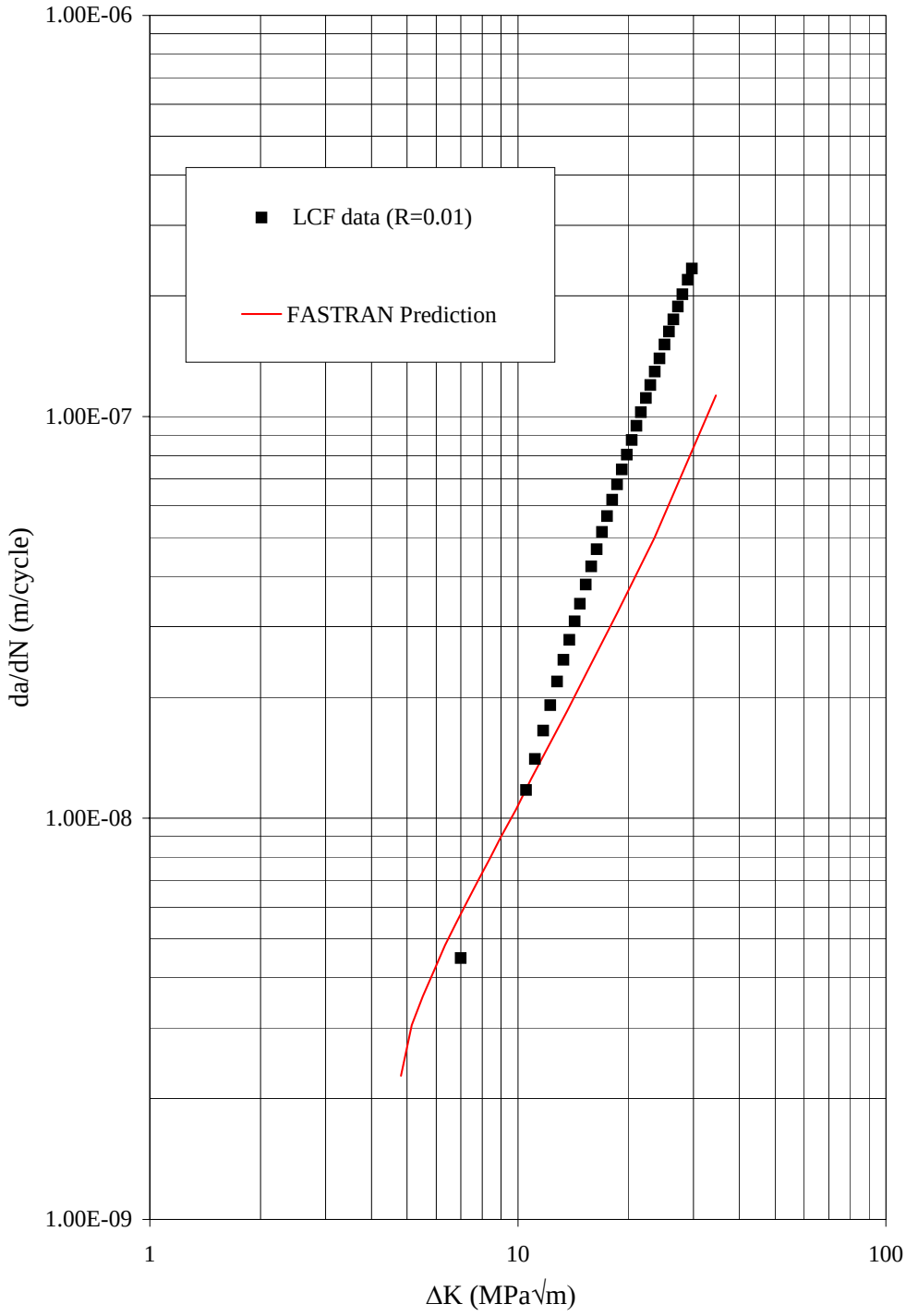

Fig. 21 Comparison of FASTRAN-predicted FCG rates and experimental results under LCF loading only at 350 °C.

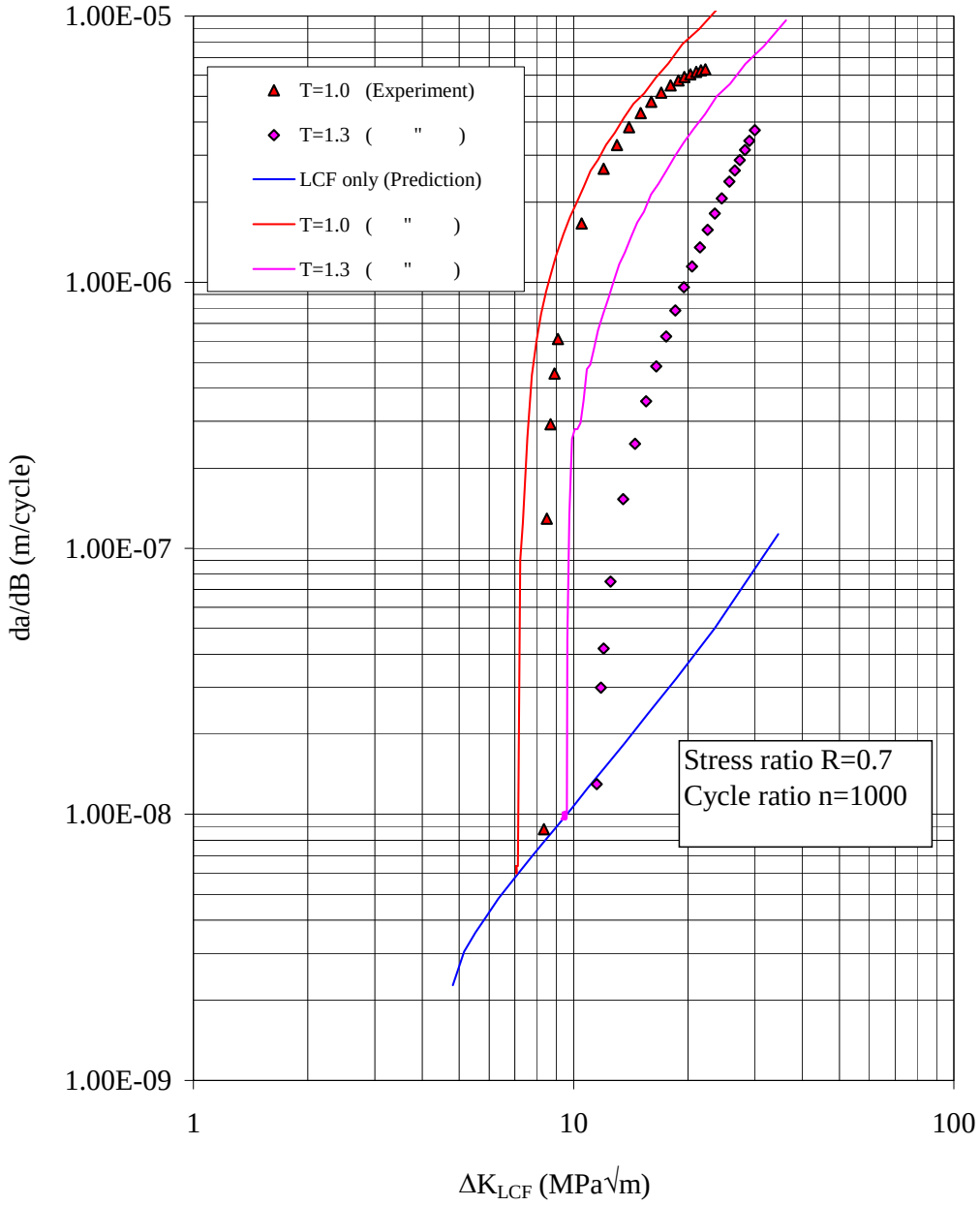

Fig. 22 Comparison of FASTRAN-predicted and experimental FCG rates without overload and with 30% overload at 350 °C. Stress ratio R_{HCF} = 0.7; cycle ratio = 1000 : 1.

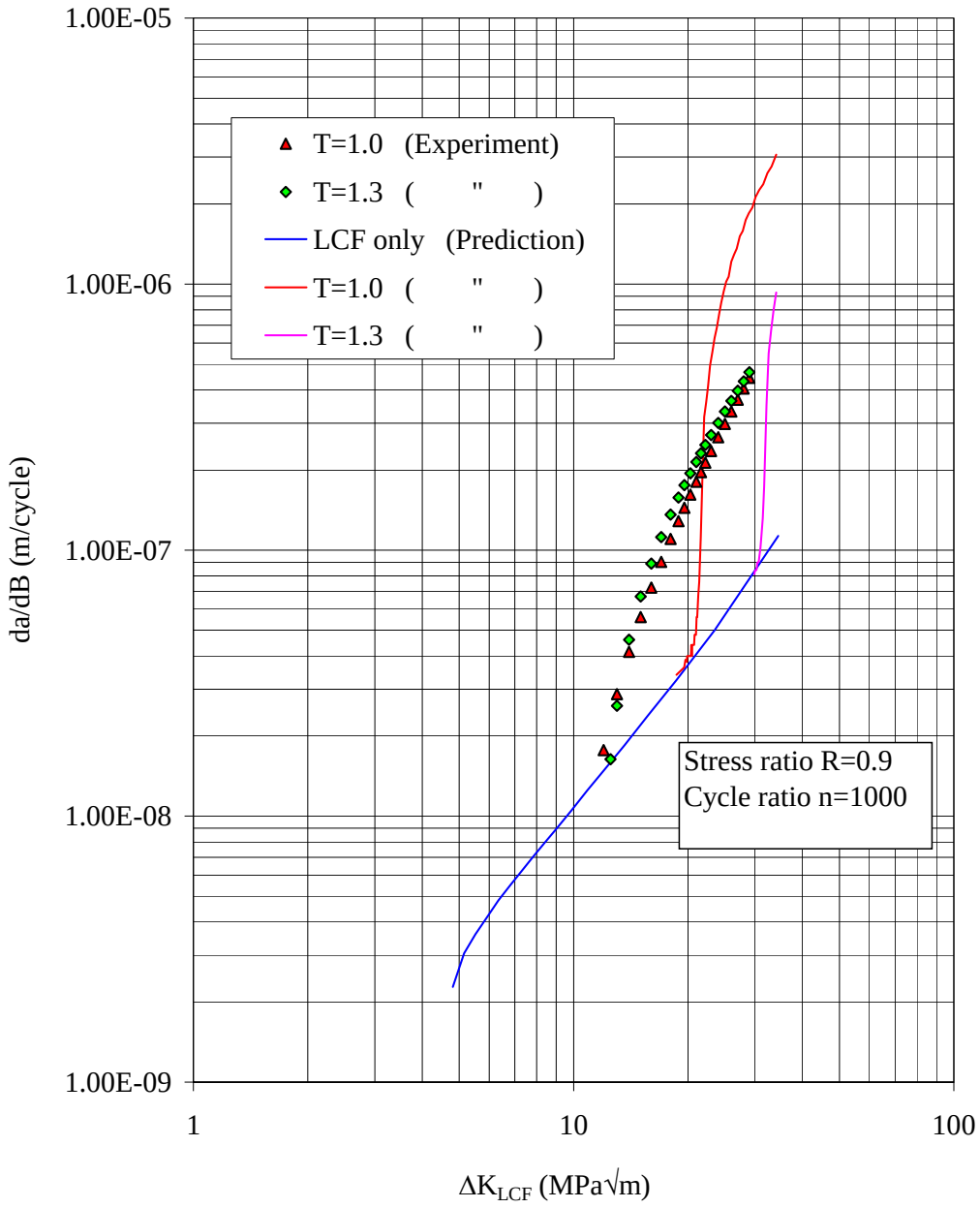

Fig. 23 Comparison of FASTRAN-predicted and experimental FCG rates without overload and with 30% overload at 350 °C. Stress ratio R_{HCF} = 0.9; cycle ratio = 1000 : 1.

UNIVERSITY OF PORTSMOUTH

HCF+LCF INTERACTIONS
at
ELEVATED TEMPERATURE

Final Report (F579)
January 2002 to December 2004

APPENDIX 1
Experimental Data

I.R.I. Research Report
Contract No. F61775-02-C4050

APPENDIX 1

Contents

Summary of experiments undertaken at 350^0C (maximum HCF stress = 187.5MPa).

Page number	Experiment type	Stress ratio, R	Overload ratio, T Max LCF/ Max HCF	Cycle ratio, n HCF cycles: LCF cycles	Number of experiments	Experiment Numbers
2	**LCF cycles only**	0.01			3	CN2106, CN2108 & CN2117
5	**HCF cycles only**	0.7			2	CN2107 & CN2111
7		0.8			2	CN2118 & CN2120
9		0.9			2	CN2082 & CN2084
11	**HCF+LCF cycles**	0.7	1.0	1000:1	2	CN2104 & CN2105
13		0.7	1.3	1000:1	2	CN2102 & CN2103
15		0.7	1.45	1000:1	1	CN2112
16		0.7	2.0	1000:1	2	CN2114 & CN2115
18		0.8	1.3	1000:1	2	CN2113 & CN2122
20		0.9	1.0	1000:1	2	CN2078 & CN2080
22		0.9	1.3	1000:1	1	CN2079
23		0.9	2.0	1000:1	2	CN2081 & CN2083
25	**HCF threshold**	0.7			3	CN2107, CN2109 & CN2111
		0.8			2	CN2118 & CN2120
		0.9			2	CN2082 & CN2084
27	**Flight simulation**				2	CN2119 & CN2121

LCF only FCG rates at 350^{0}C - CN2106
R_{LCF} = 0.01; T = 1.0

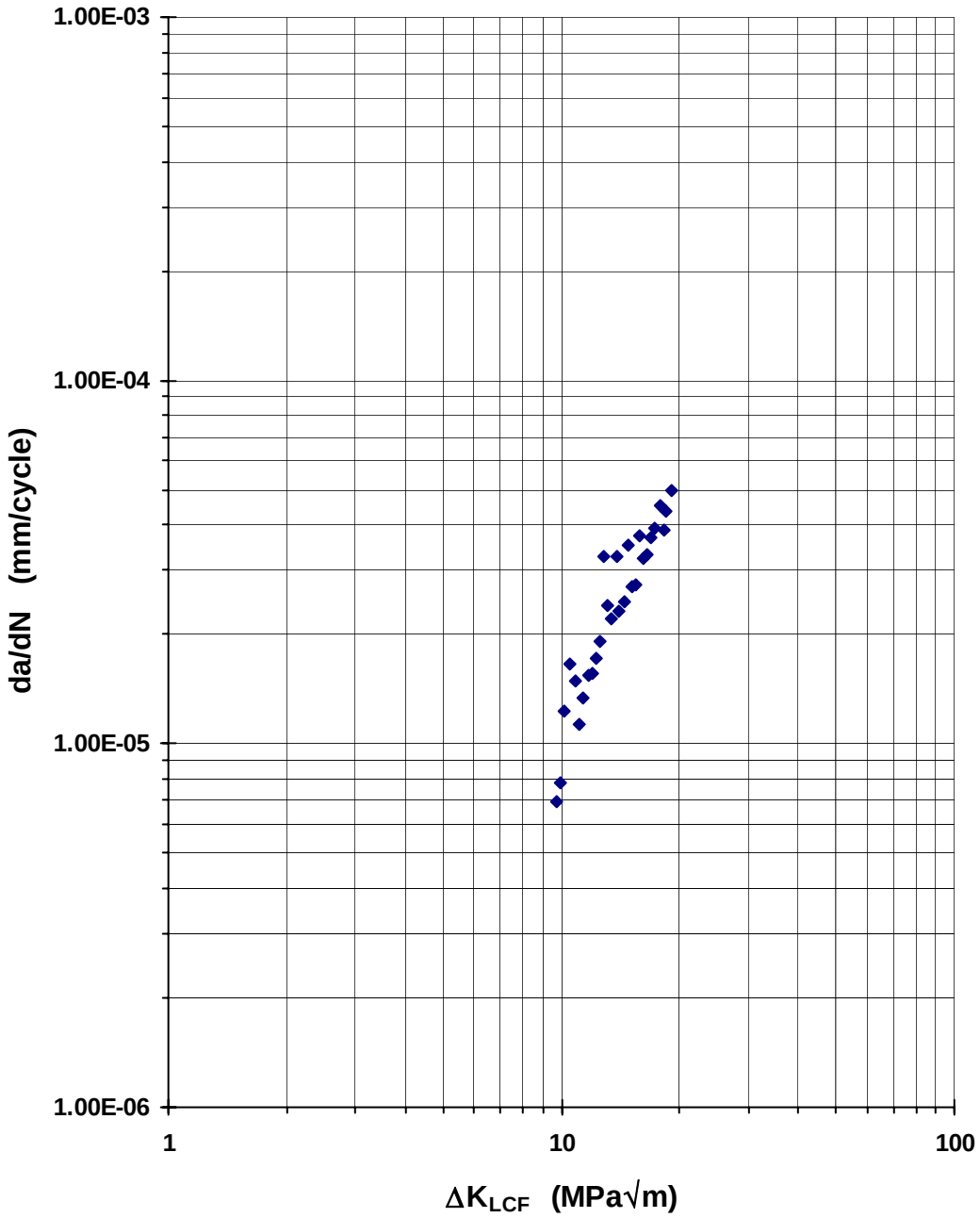

LCF only FCG rates at 350^{0}C - CN2108
R = 0.01; T = 1.0

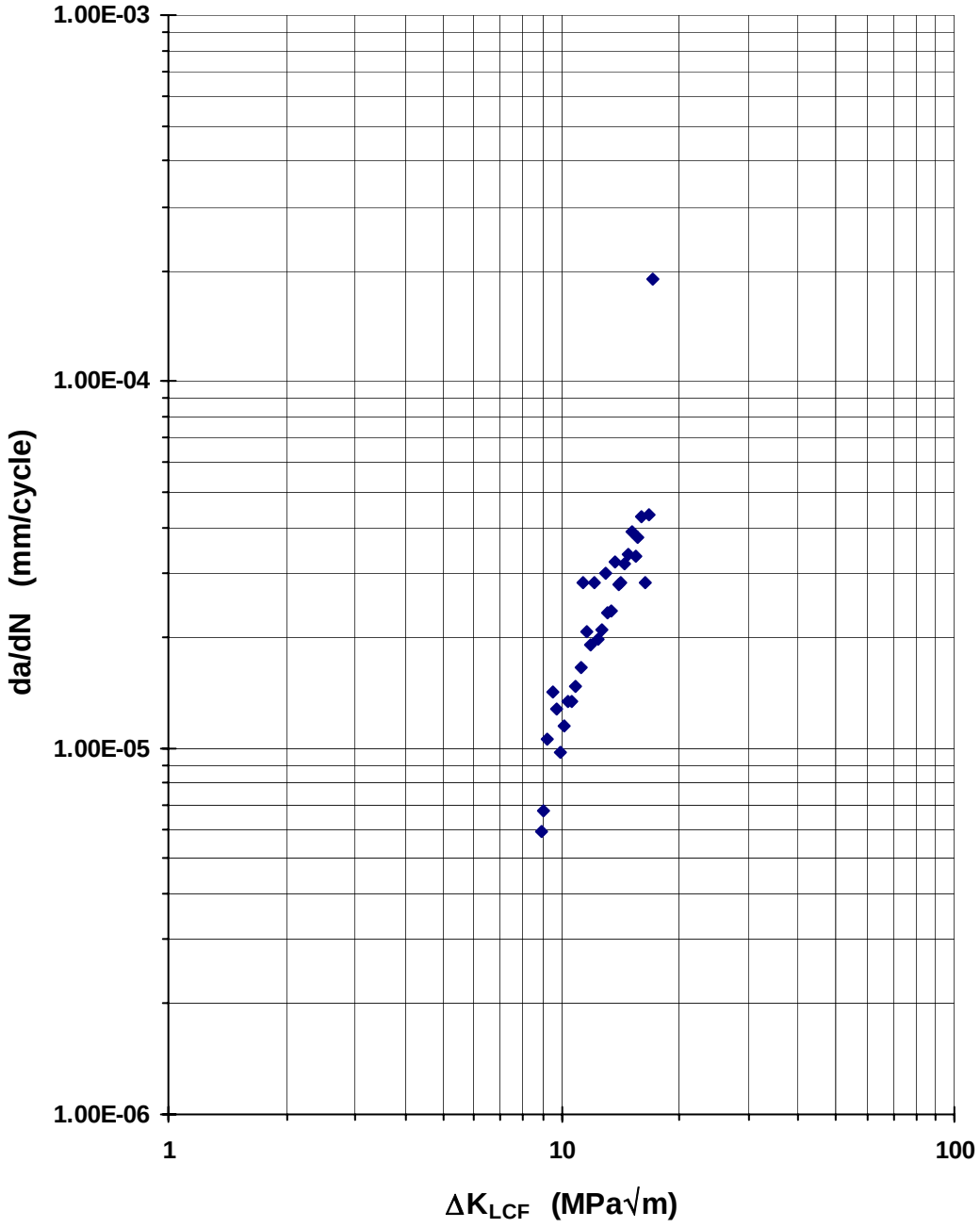

FCG rates for LCF only at 350^{0}C - CN2117
R_{LCF} = 0.01; T = 1.0

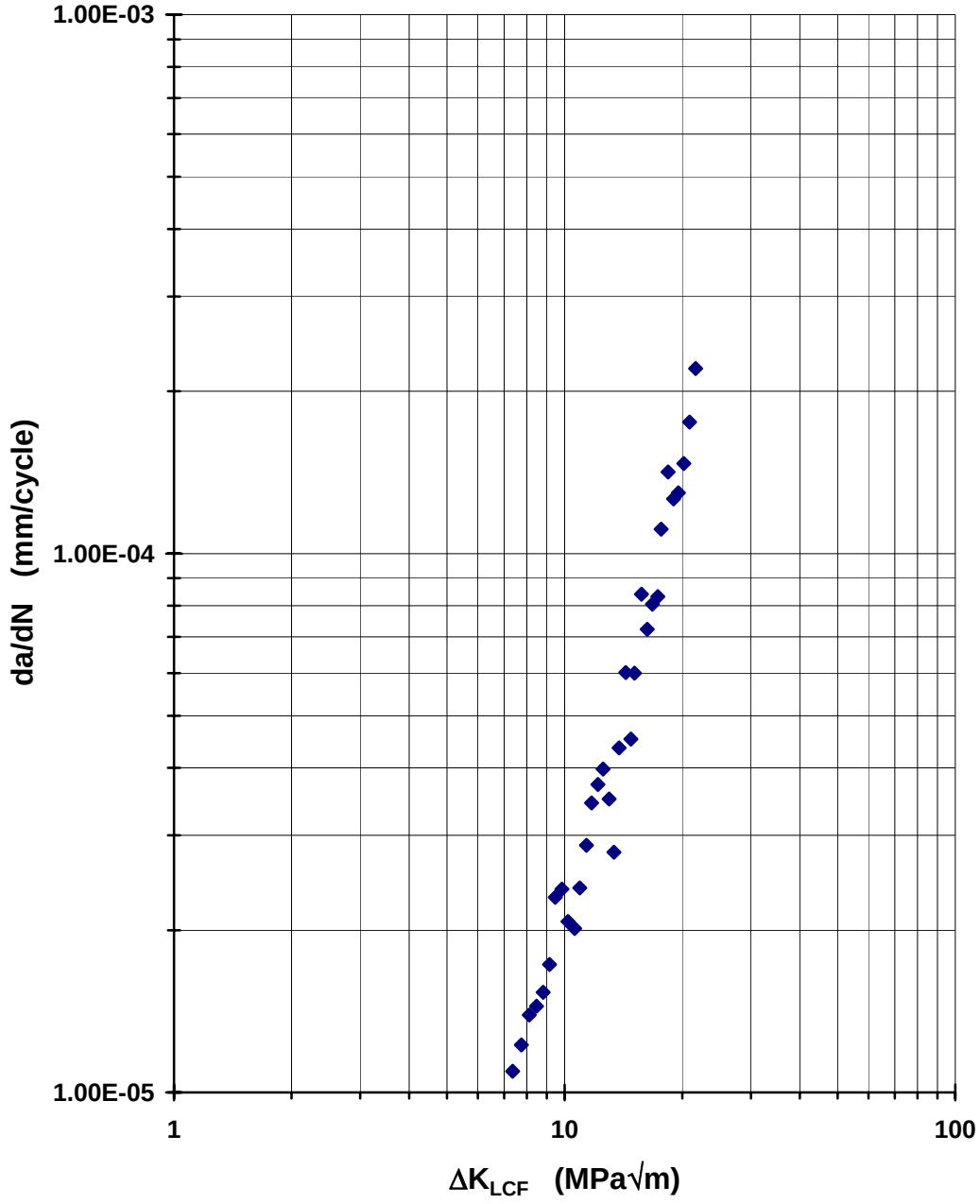

HCF only FCG ratesat 350^{0}C - CN2107
R_{HCF} = 0.7; T = 1.0

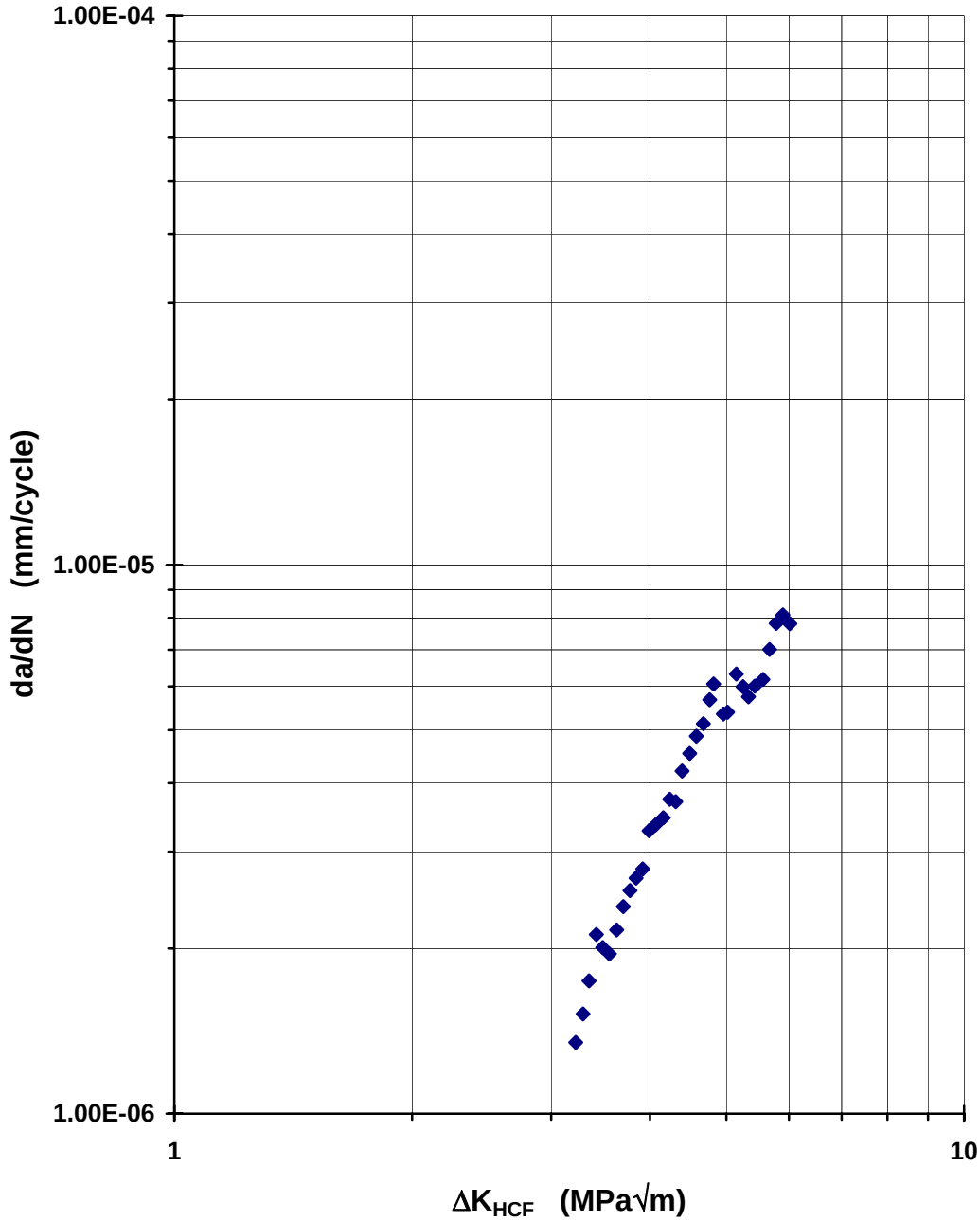

HCF only FCG rates at 350^{0}C - CN2111
R_{HCF} = 0.7; T = 1.0

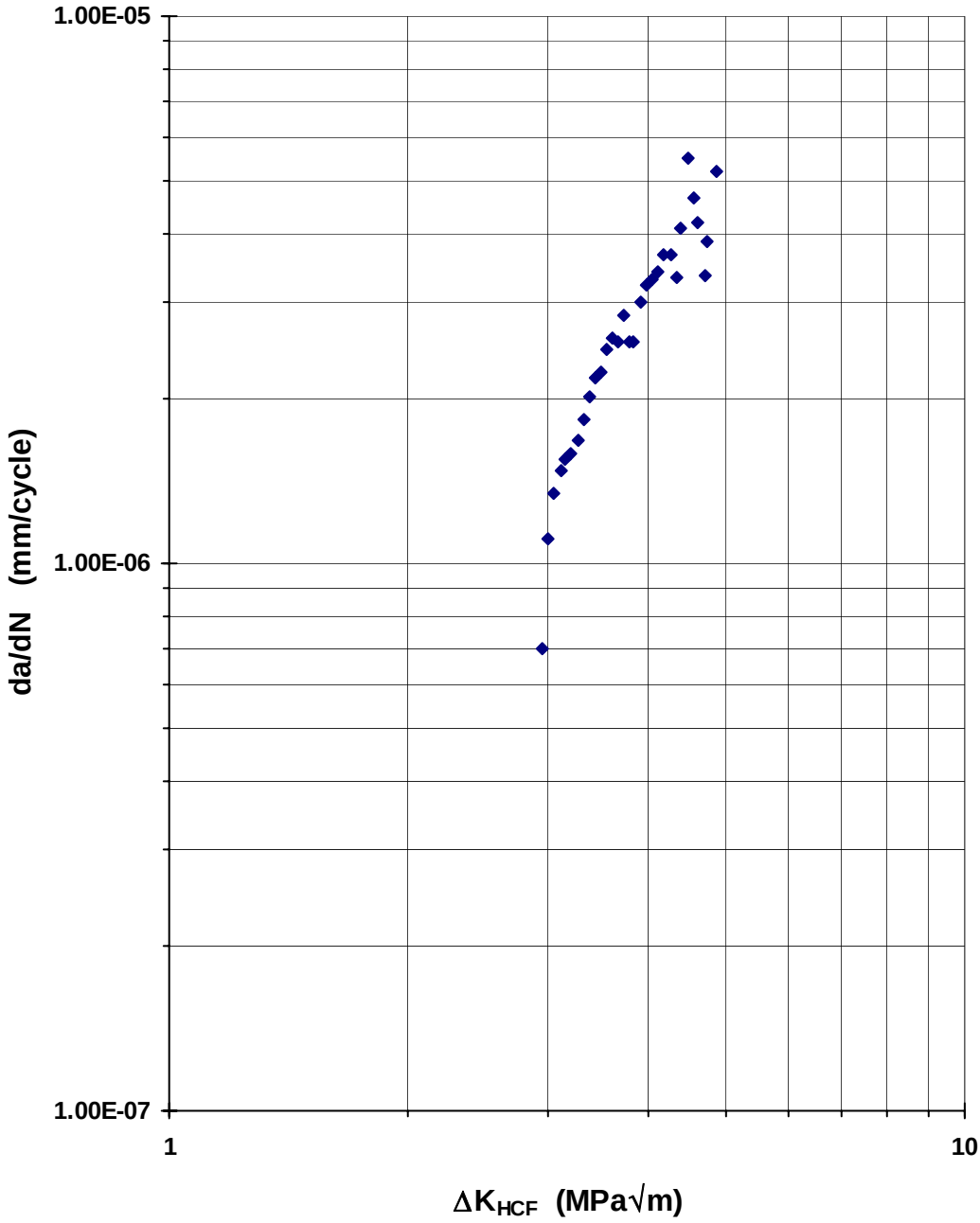

HCF only FCG rates at 350^{0}C - CN2118
R_{HCF} = 0.8 T = 1.0

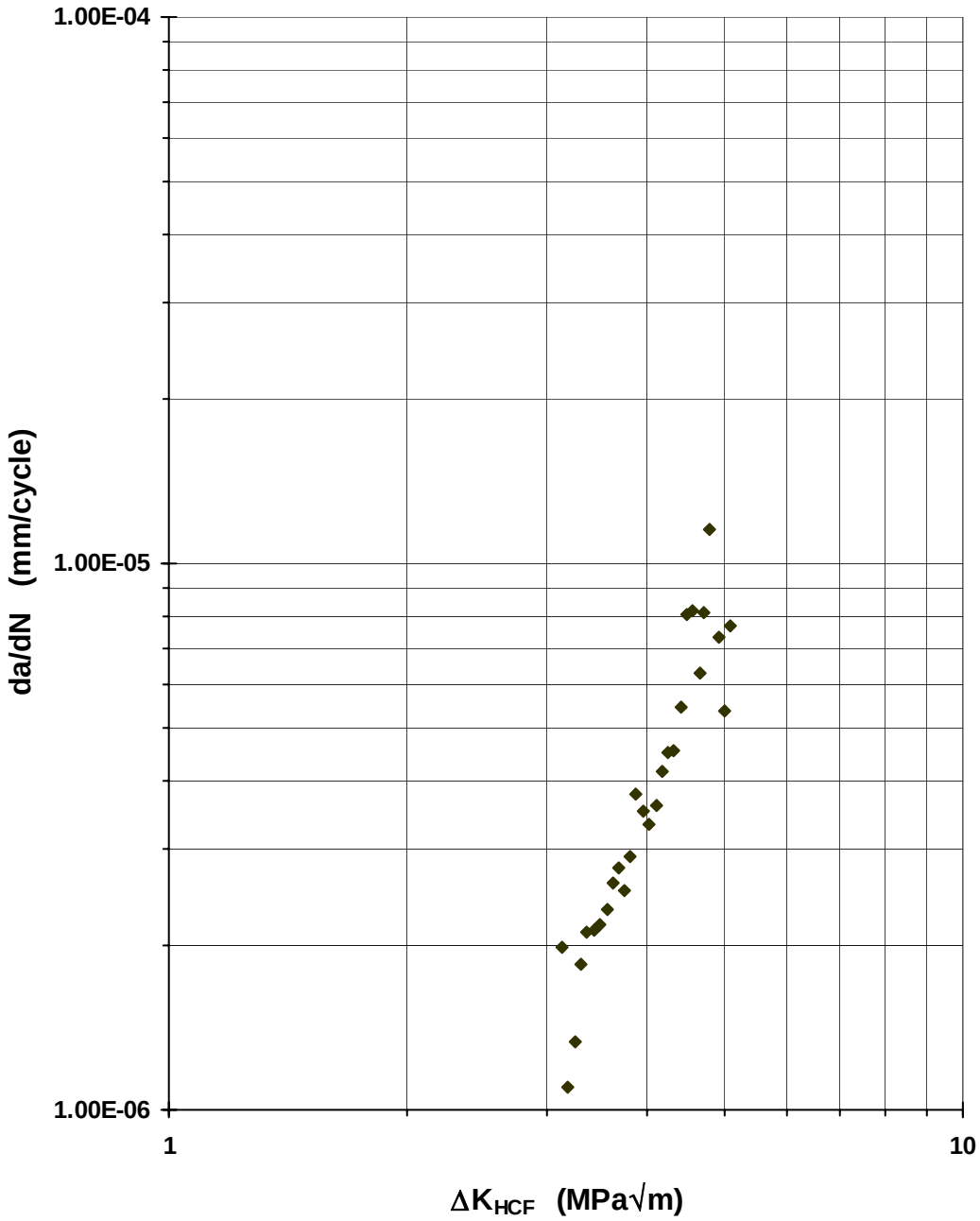

HCF only FCG rates at 350^{0}C - CN2120
R_{HCF} = 0.8; T = 1.0

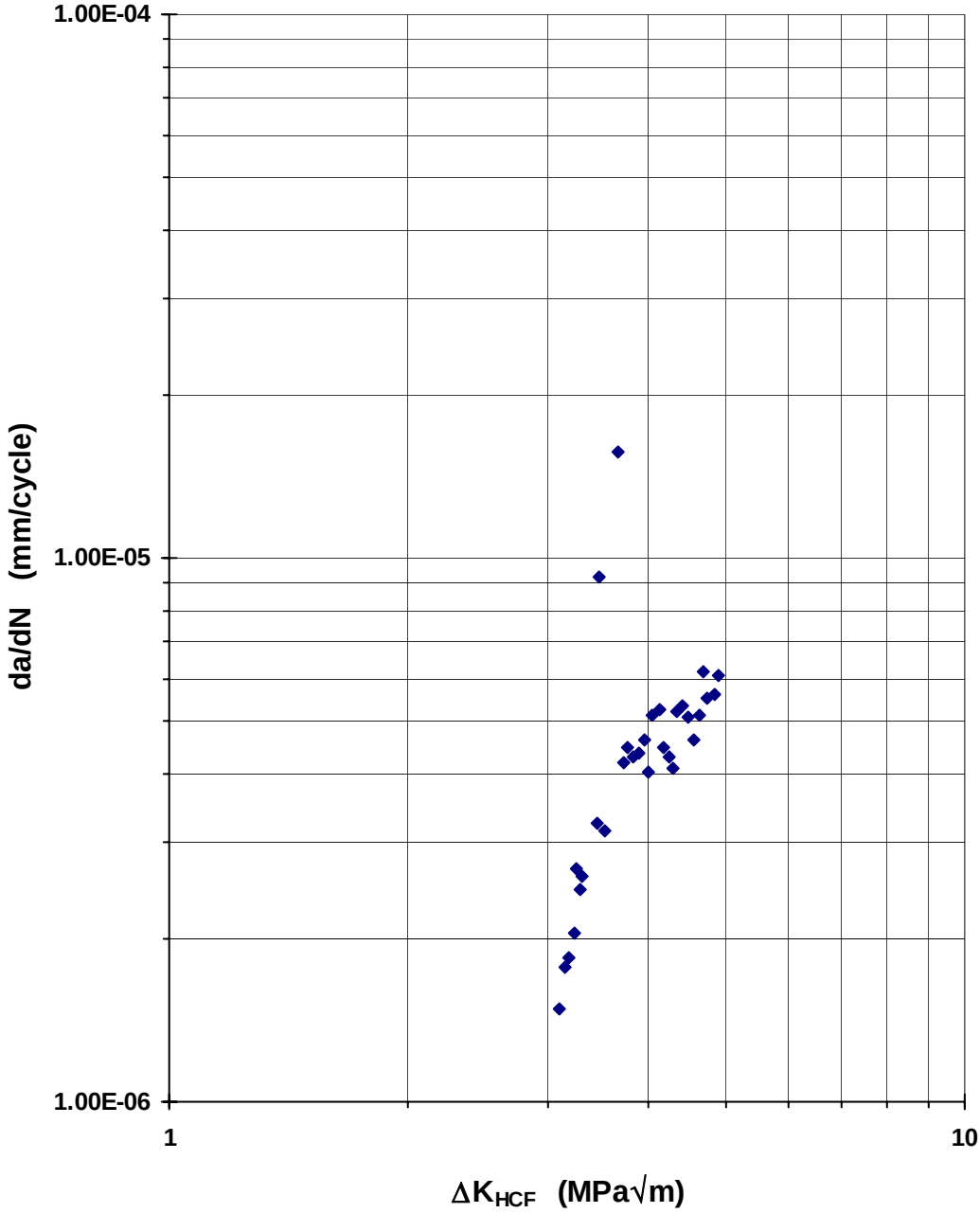

HCF only FCG rates at 350^{0}C - CN2082
R_{HCF} = 0.9

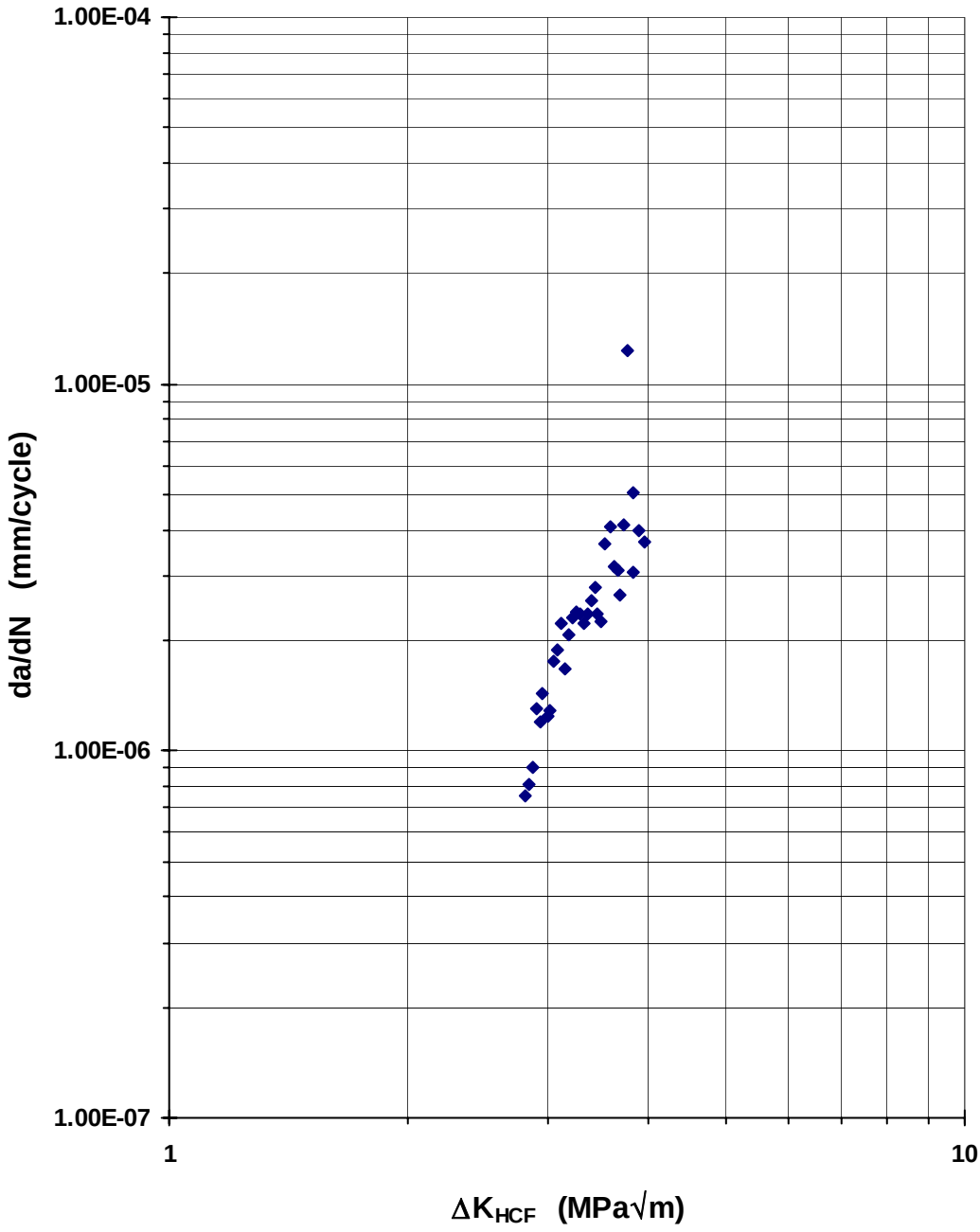

HCF only FCG rates at 350^{0}C - CN2084
R_{HCF} = 0.9; T = 1.0

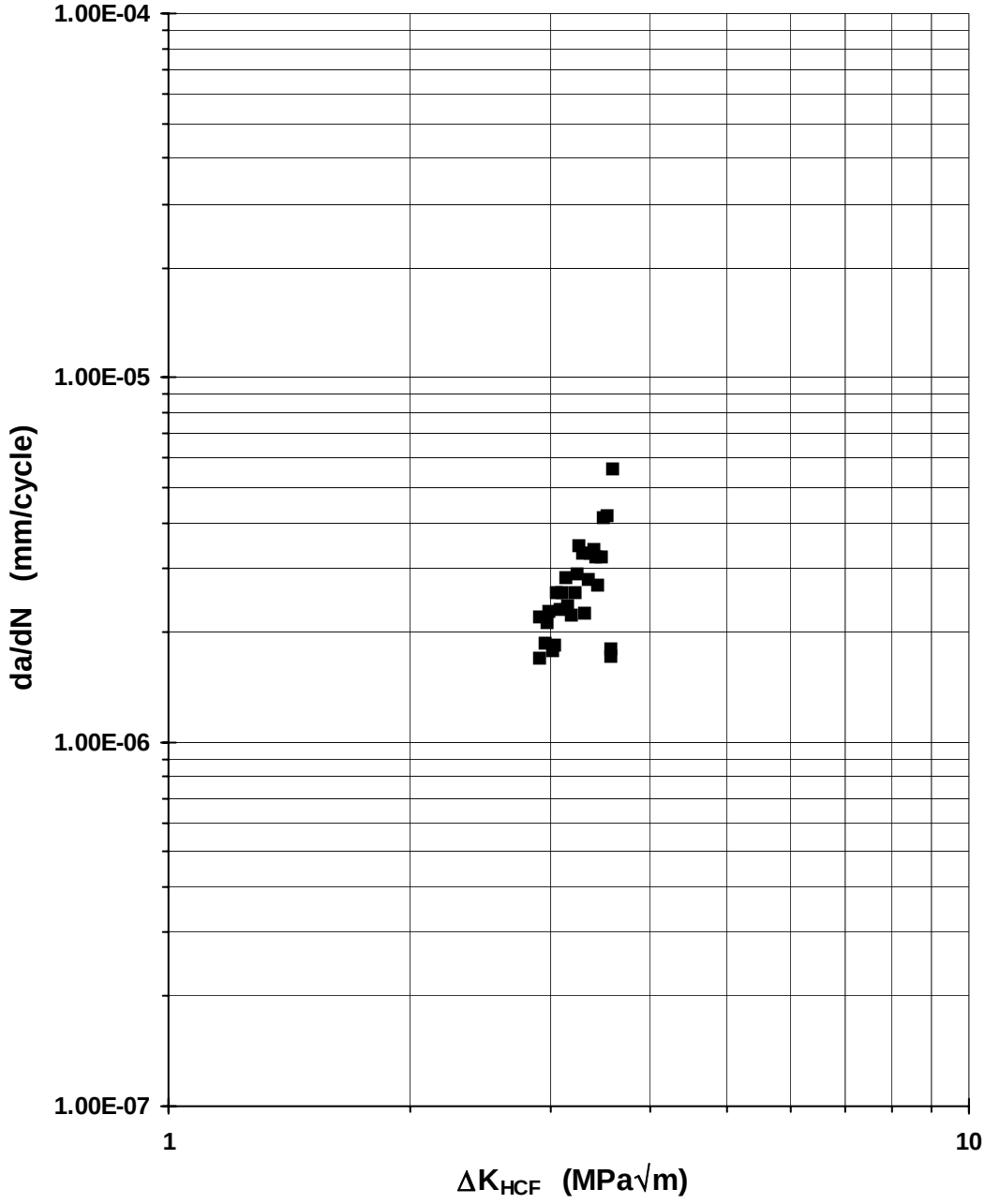

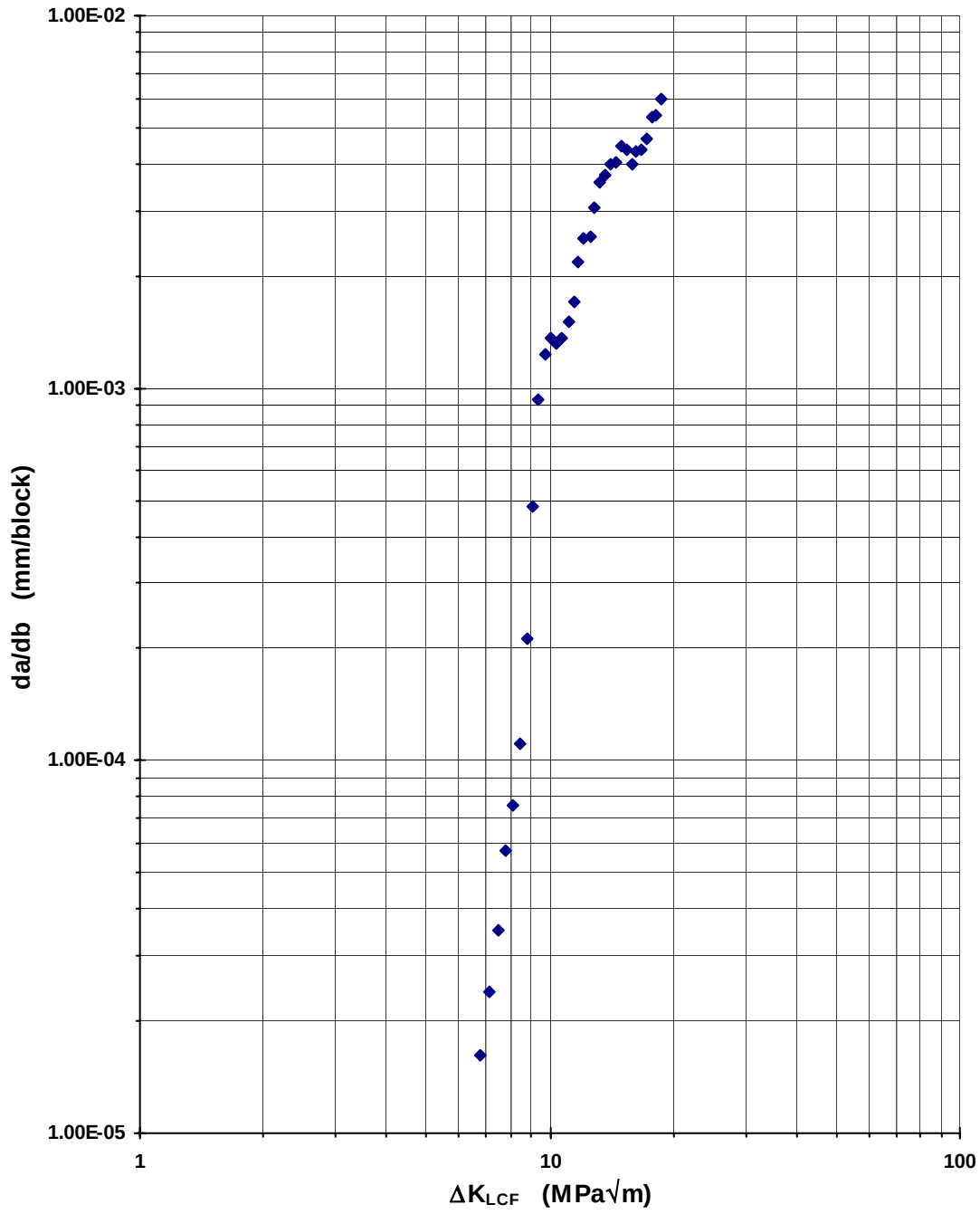
HCF+LCF FCG rates at 350^{0}C - CN2104
R_{HCF} = 0.7; T = 1.0; n = 1000:1
1.00E-02
1.00E-03
1.00E-04
1.00E-05
da/db (mm/block)
1
10
100
ΔK_{LCF} (MPa√m)

HCF+LCF FCG rates at 350^{0}C - CN2105
R_{HCF} = 0.7, T = 1.0; n = 1000:1

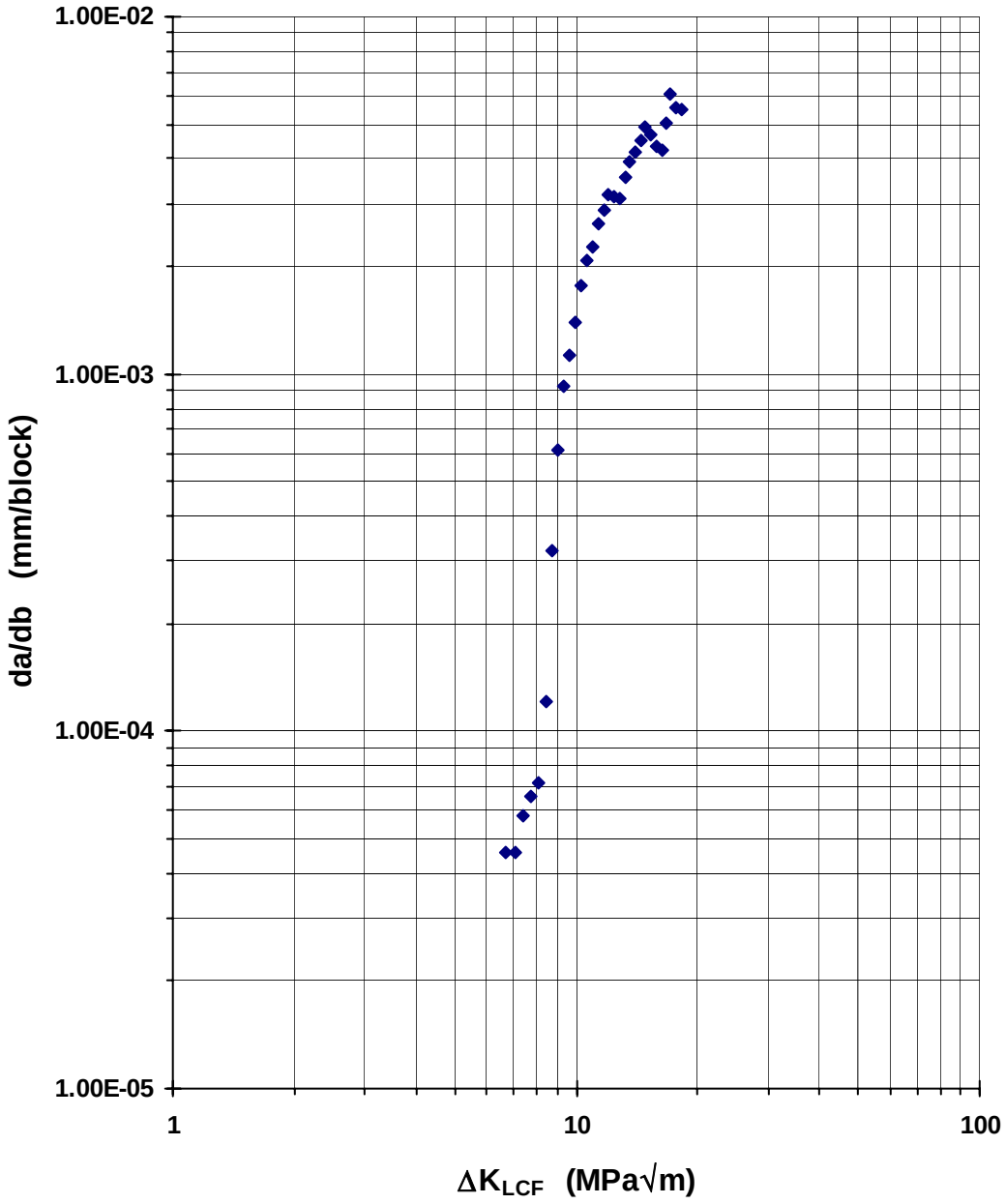

HCF+LCF with overload, FCG rates at 350^{0}C - CN2102. R_{HCF} = 0.7; T = 1.3; n = 1000:1

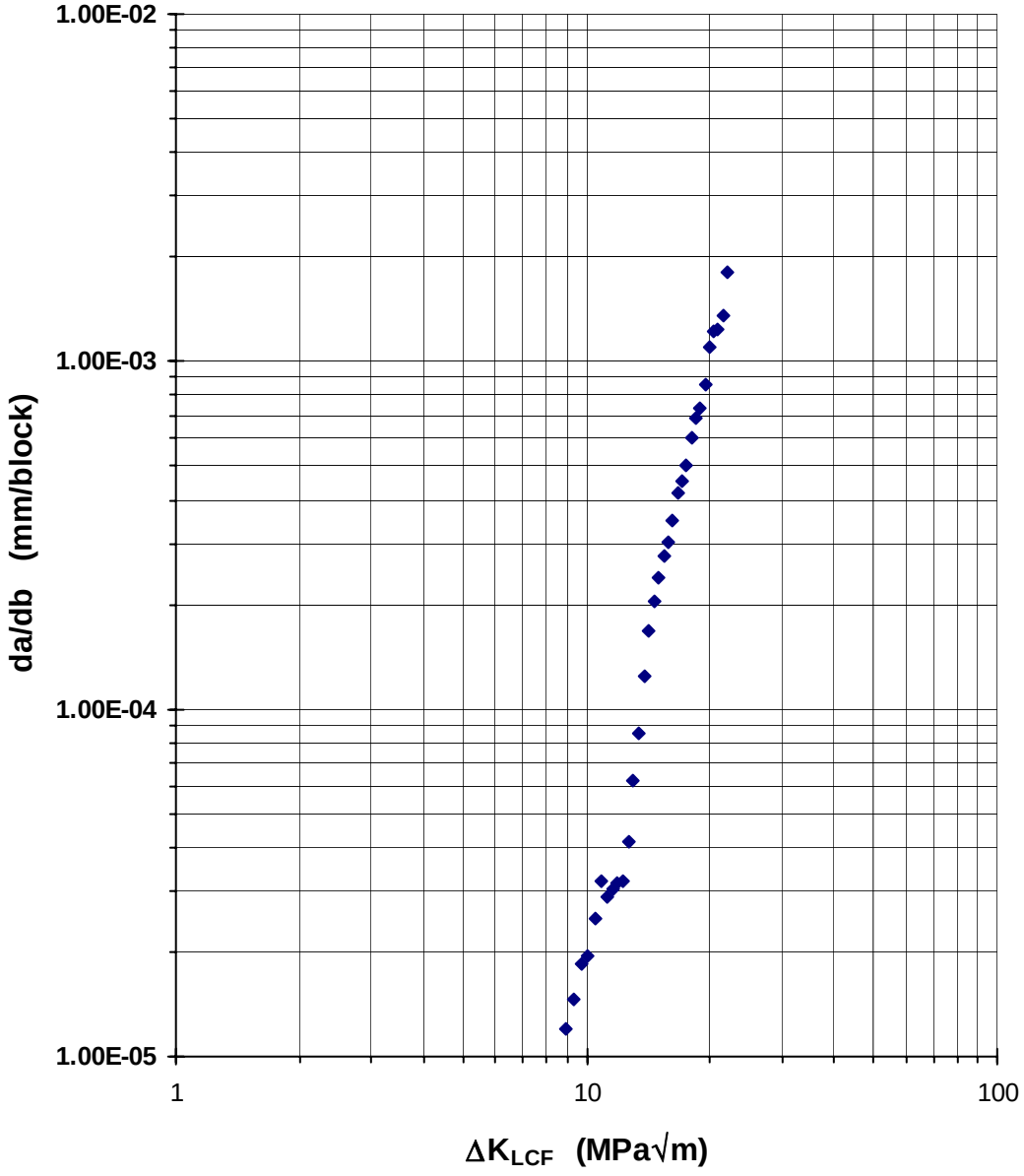

HCF+LCF with overload FCG rates at 350^{0}C - CN2103, R_{HCF} = 0.7; T = 1.3; n = 1000:1

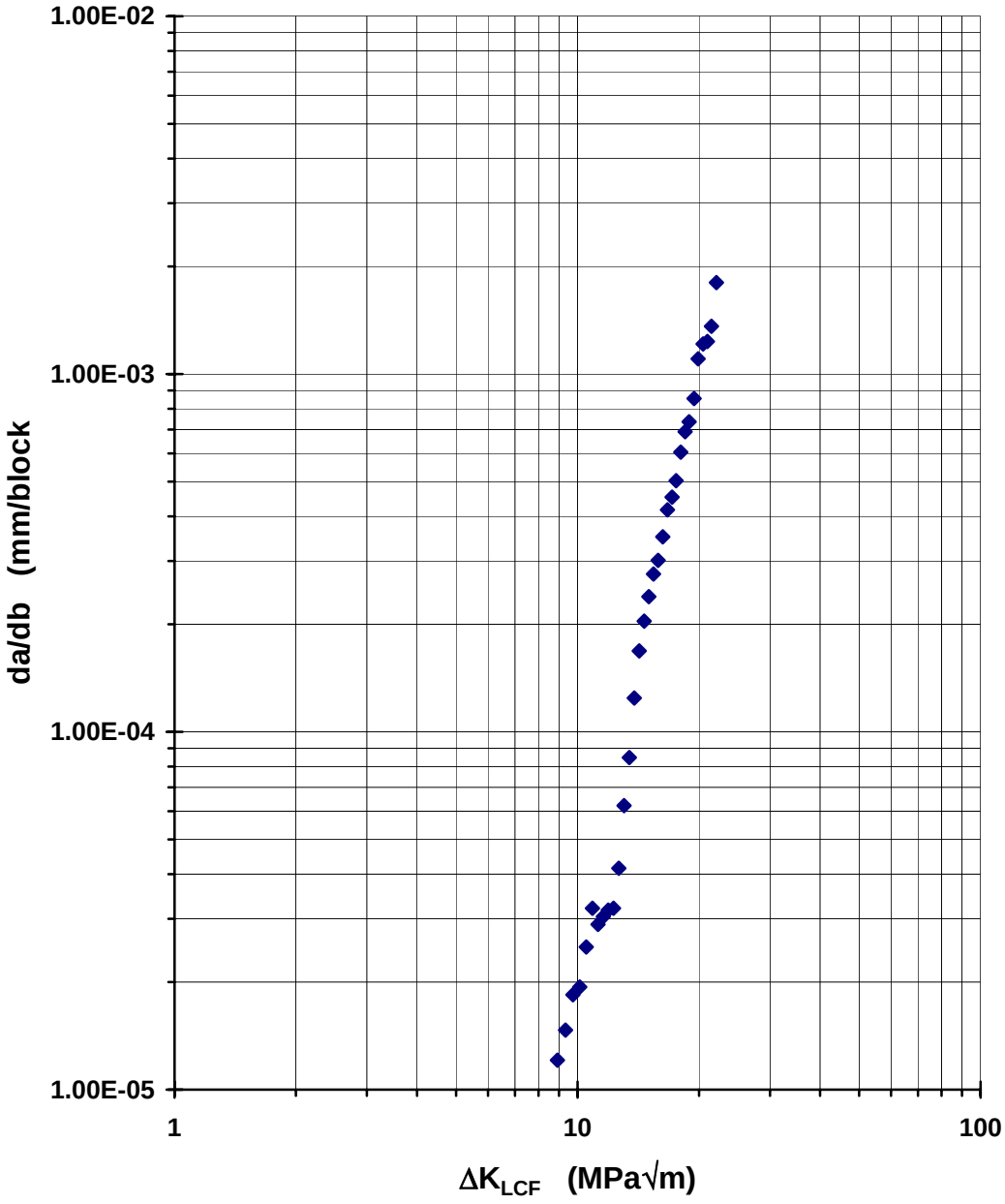

HCF+LCF with overloads, FCG rates at 350^{0}C - CN2112, R_{HCF} = 0.7; T = 1.45; n = 1000:1

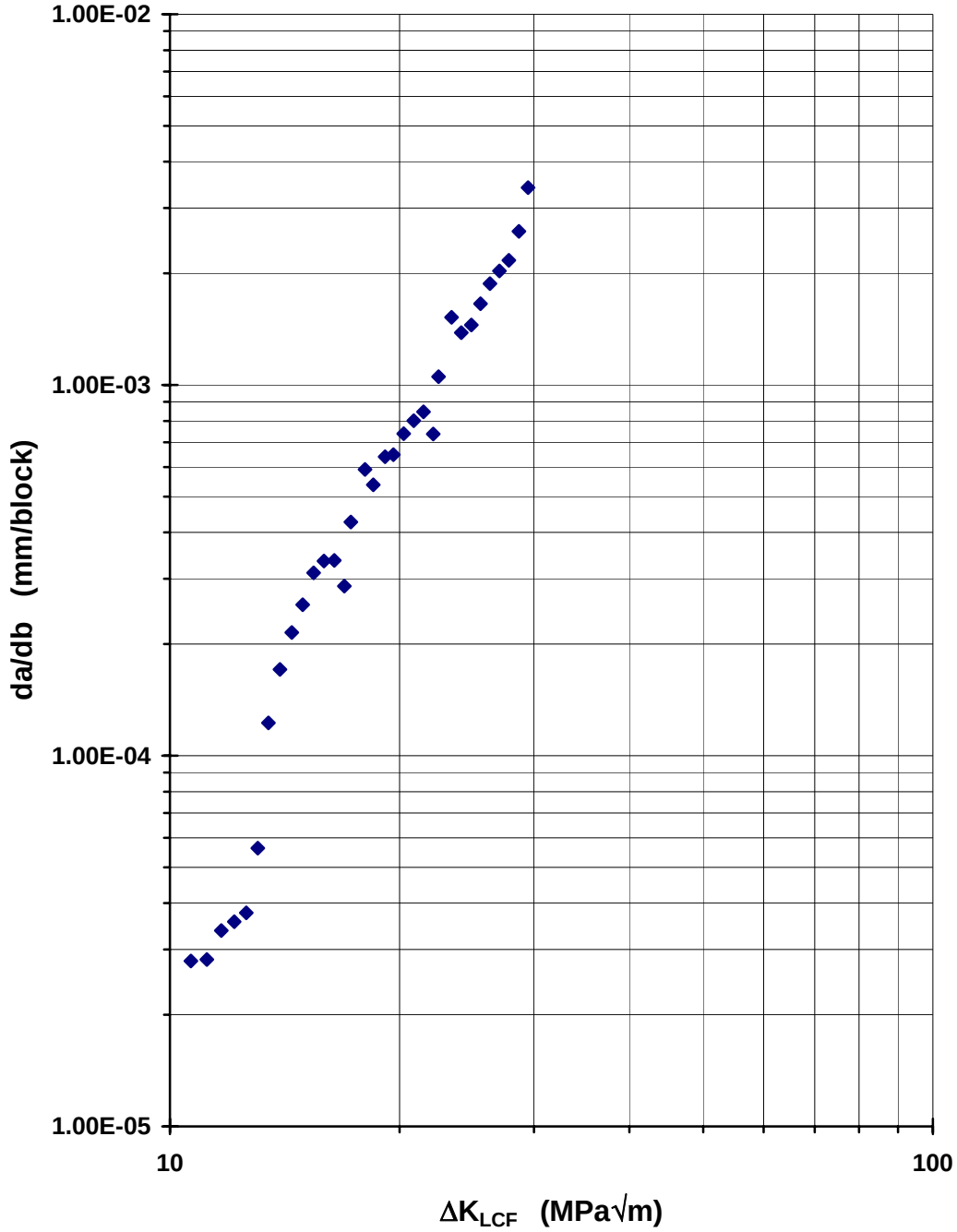

HCF+LCF with overload, FCG rates at 350^{0}C - CN2114, R_{HCF} = 0.7; T = 2.0; n = 1000:1

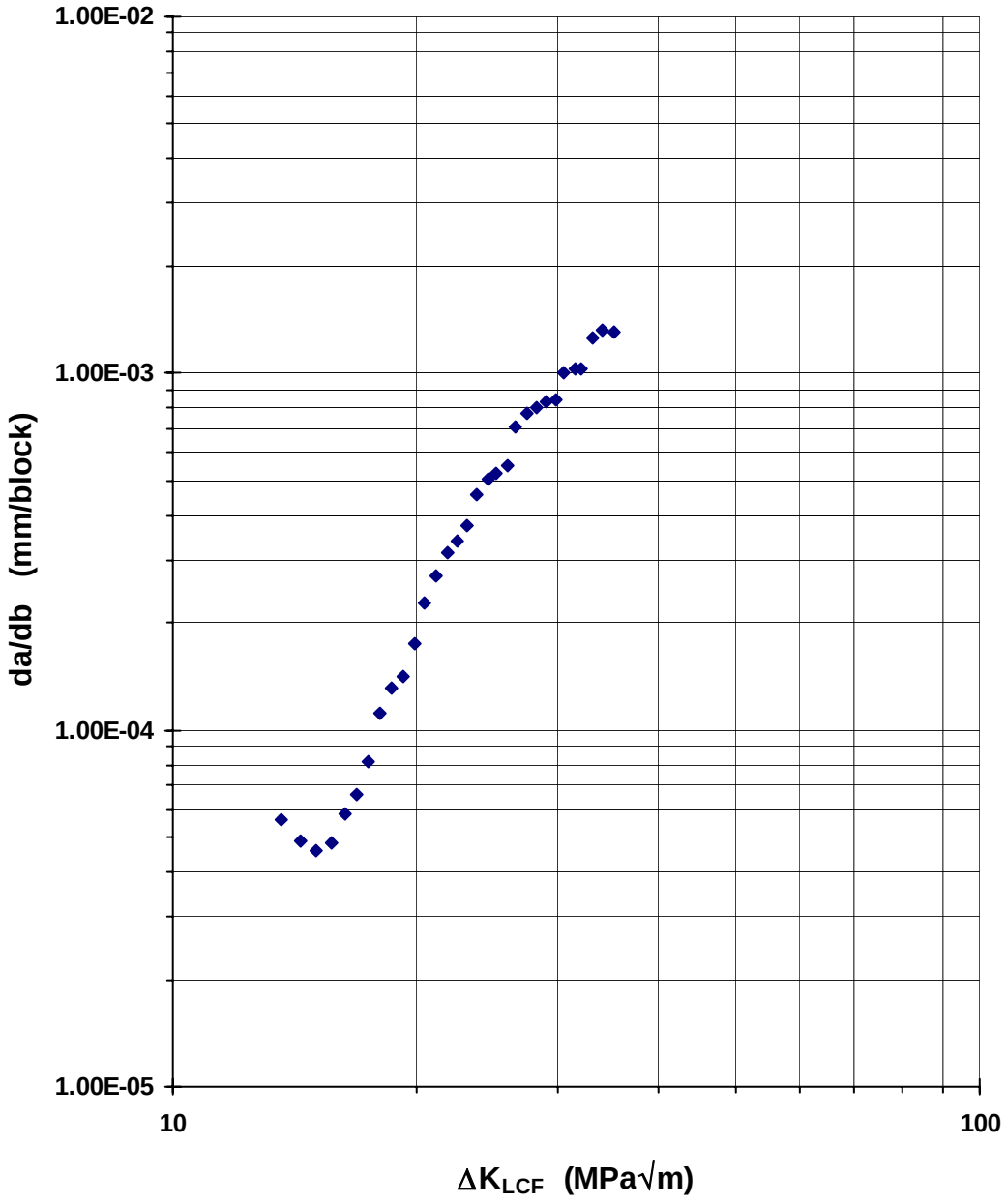

HCF+LCF with overload, FCG rates at 350^0C - CN2115, R_{HCF} = 0.7; T = 2.0; n = 1000:1

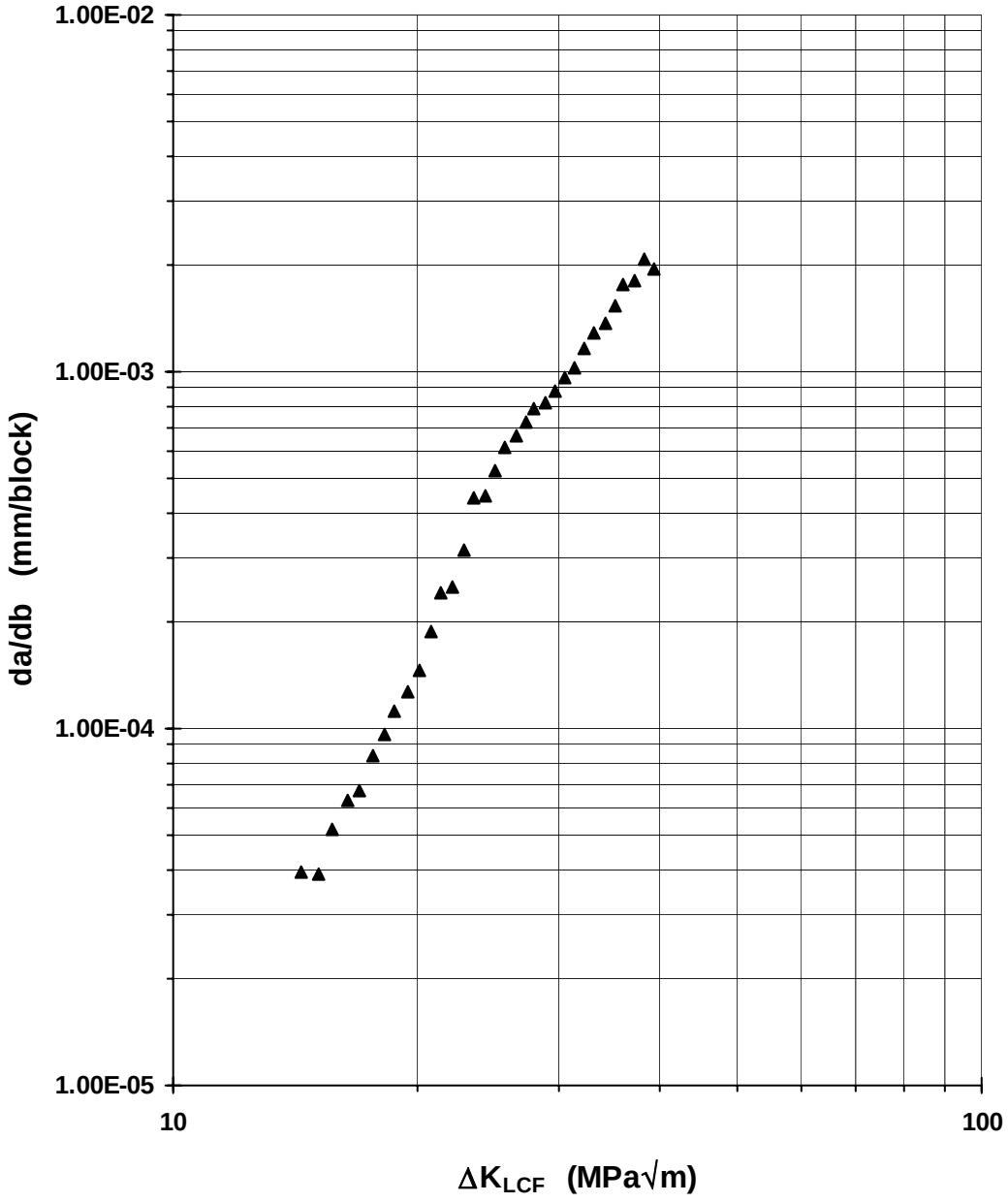

HCF+LCF with overloads, FCG rates at 350^{0}C - CN2113, R_{HCF} = 0.8; T = 1.3; n = 1000:1

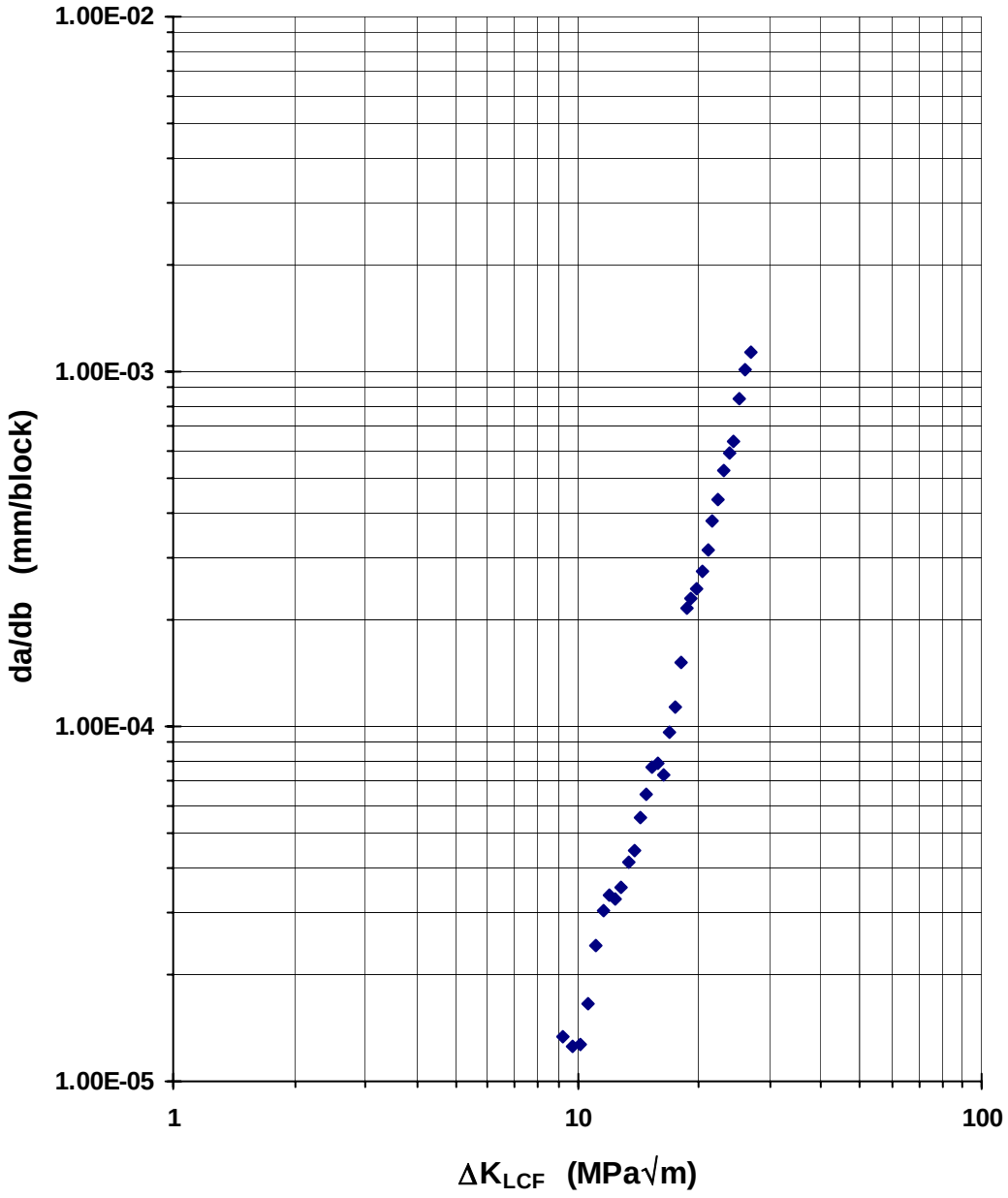

HCF+LCF with overloads, FCG rates at 350^{0}C - CN2122, R_{HCF} = 0.8; T = 1.3; n = 1000:1

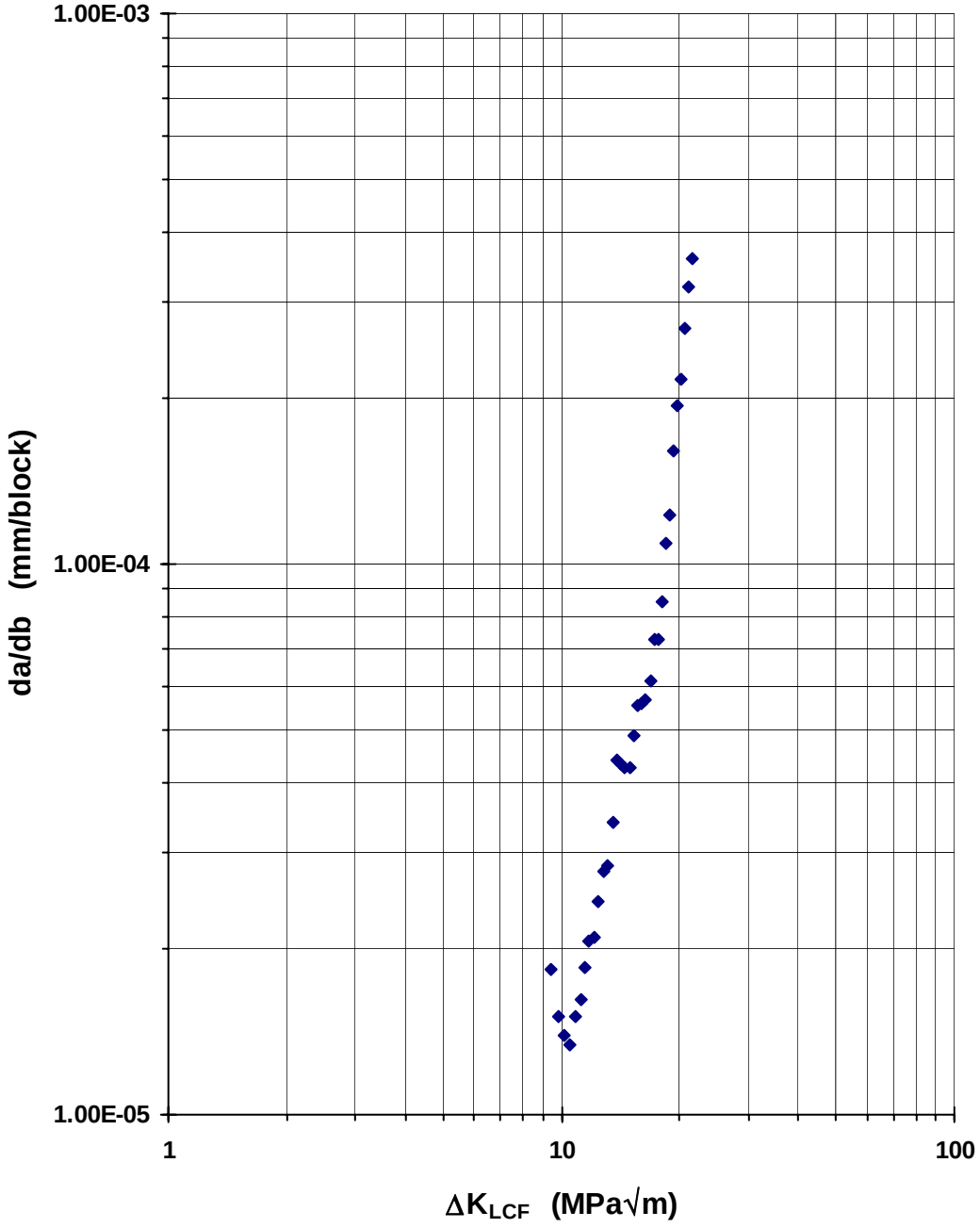

HCF+LCF FCG rates at 350^{0}C - CN2078
R_{HCF} = 0.9; T = 1.0; n = 1000:1

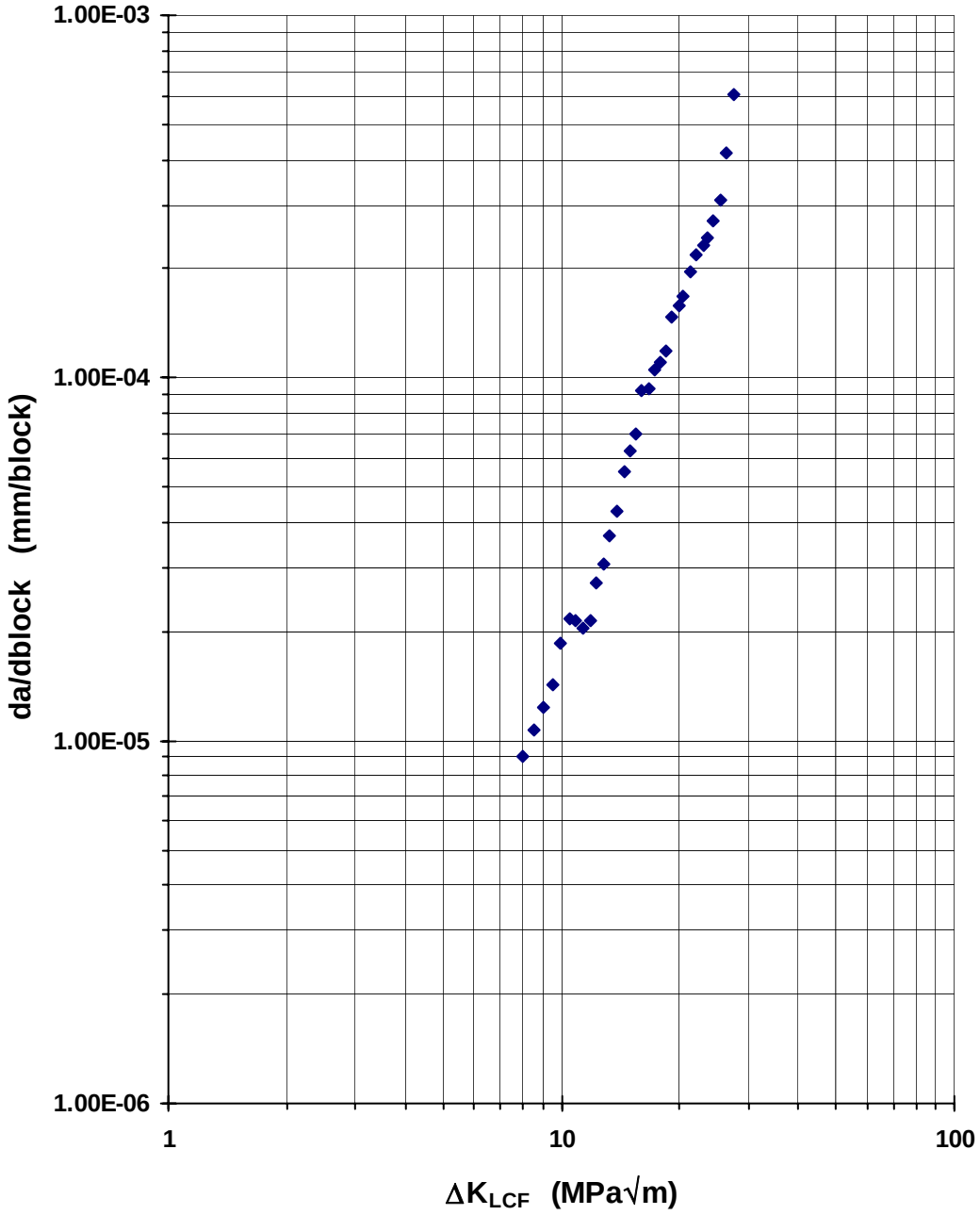

HCF+LCF FCG rates at 350^{0}C - CN2080
R_{HCF} = 0.9; T = 1.0; n = 1000:1

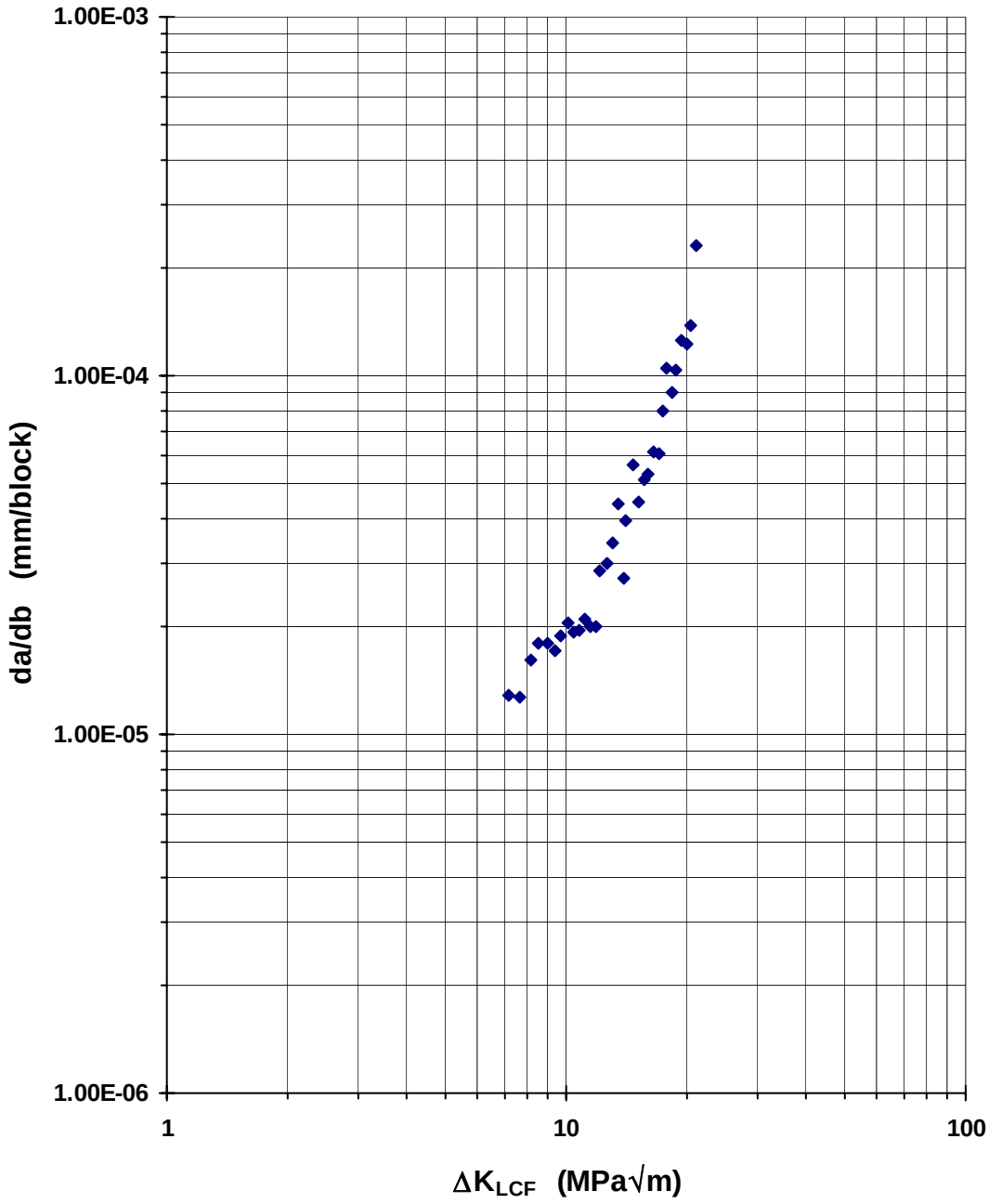

HCF+LCF with overload, FCG rates at 350^{0}C - CN2079, R_{HCF} = 0.9; T = 1.3; n = 1000:1

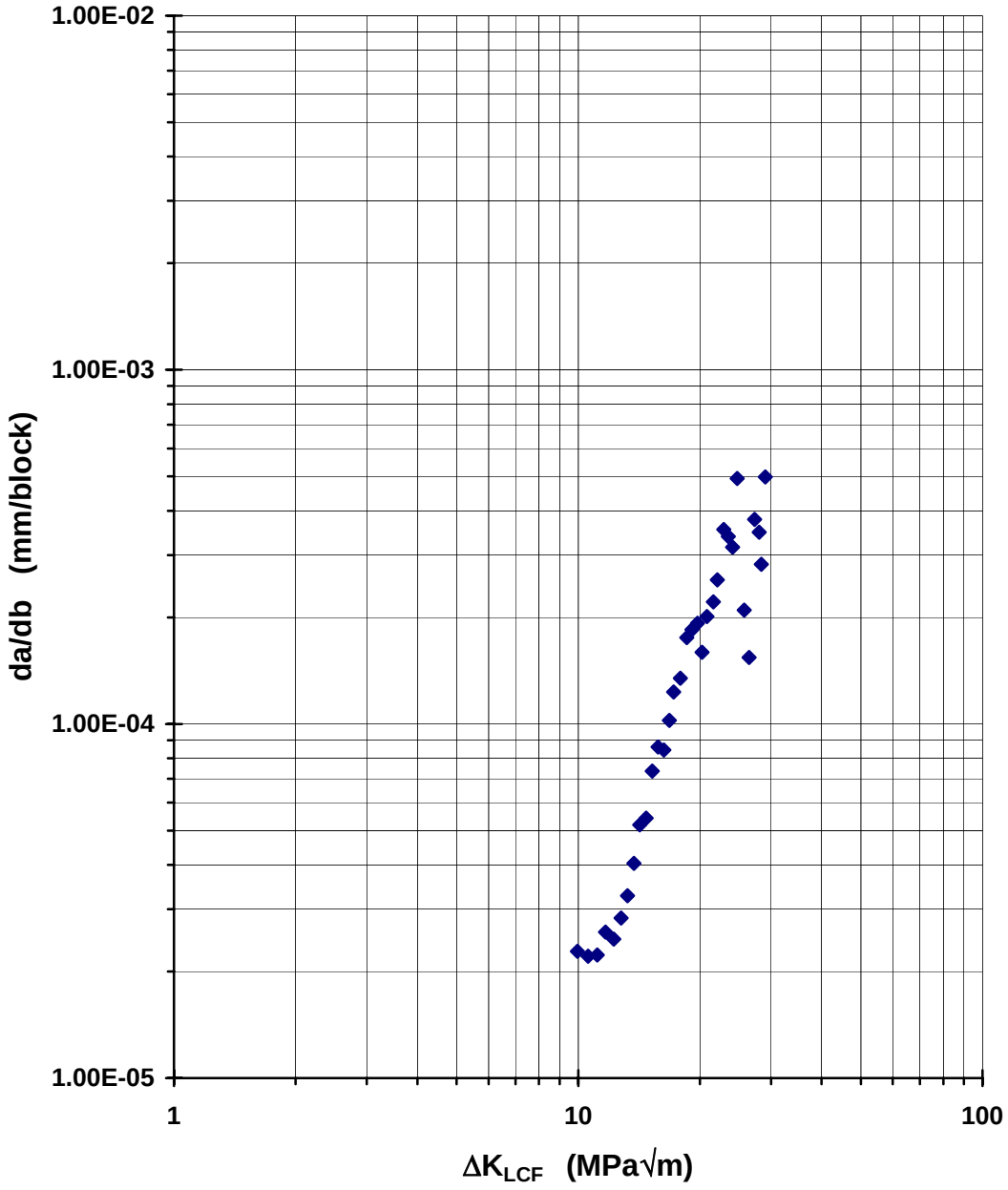

HCF+LCF with overload, FCG rates at 350^{0}C - CN2081, R_{HCF} = 0.9; T = 2.0; n = 1000:1

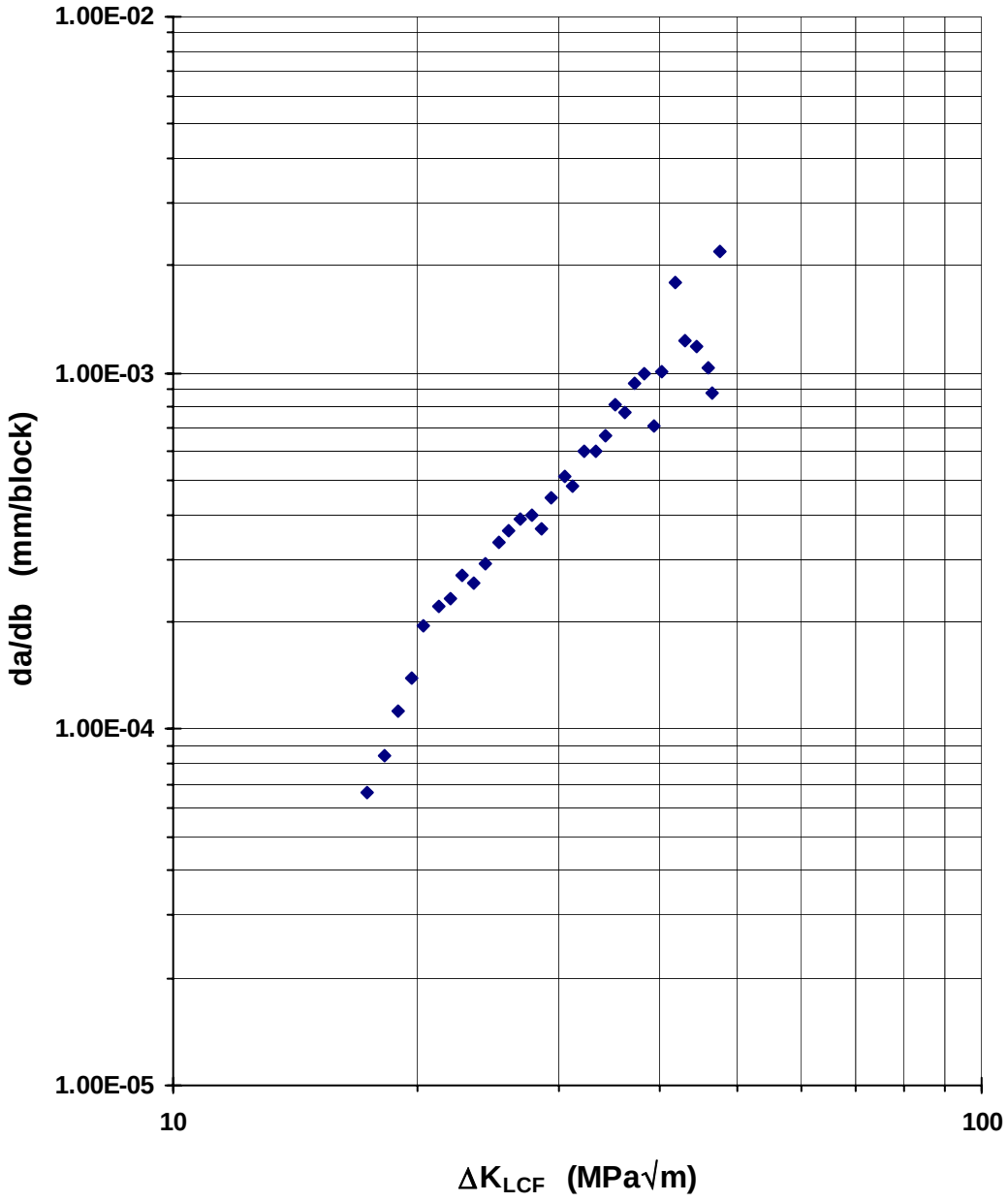

HCF+LCF with overload, FCG rates at 350^{0}C - CN2083, R_{HCF} = 0.9; T = 2.0; n = 1000:1

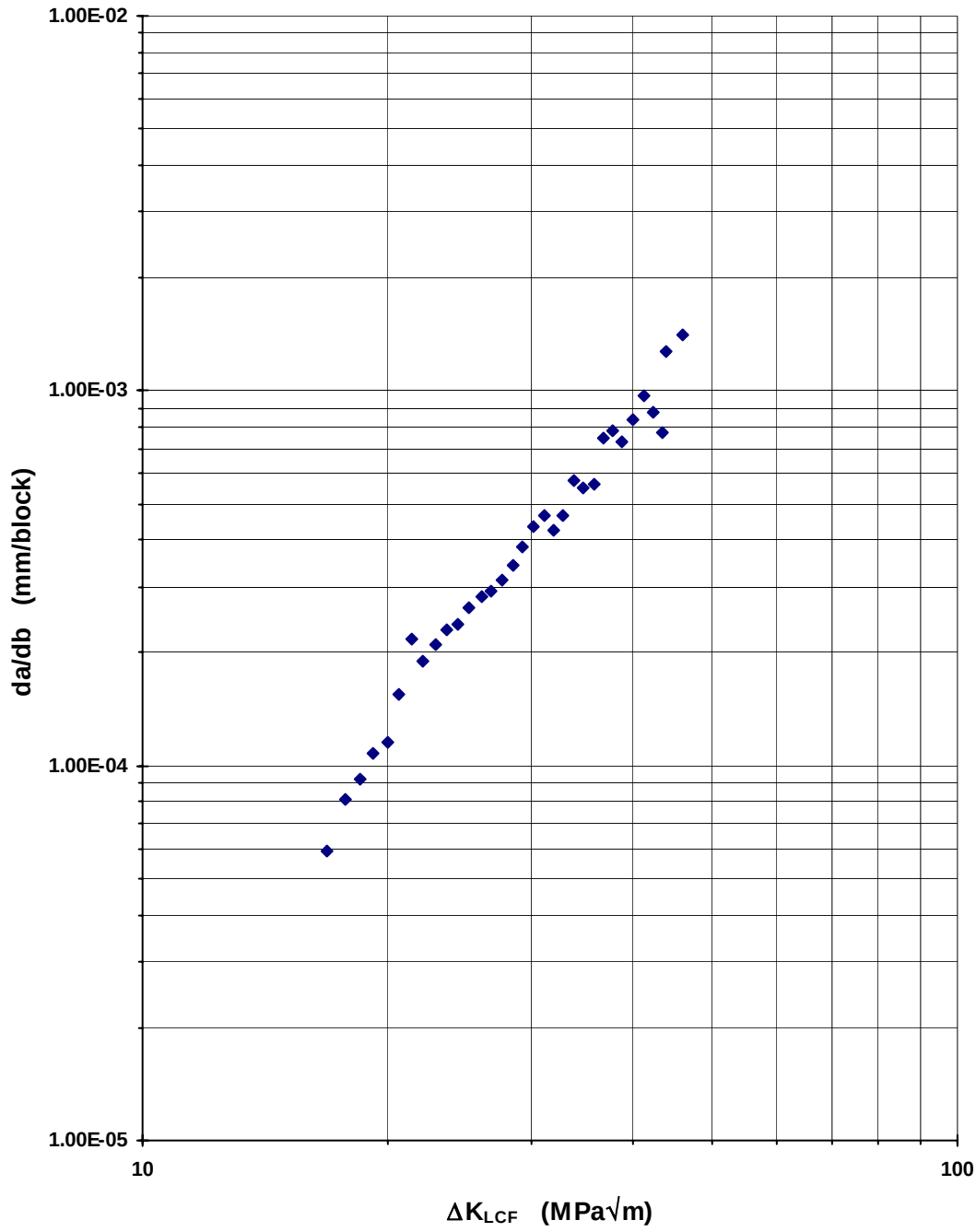

Results of jump-in threshold experiments at 350^0C

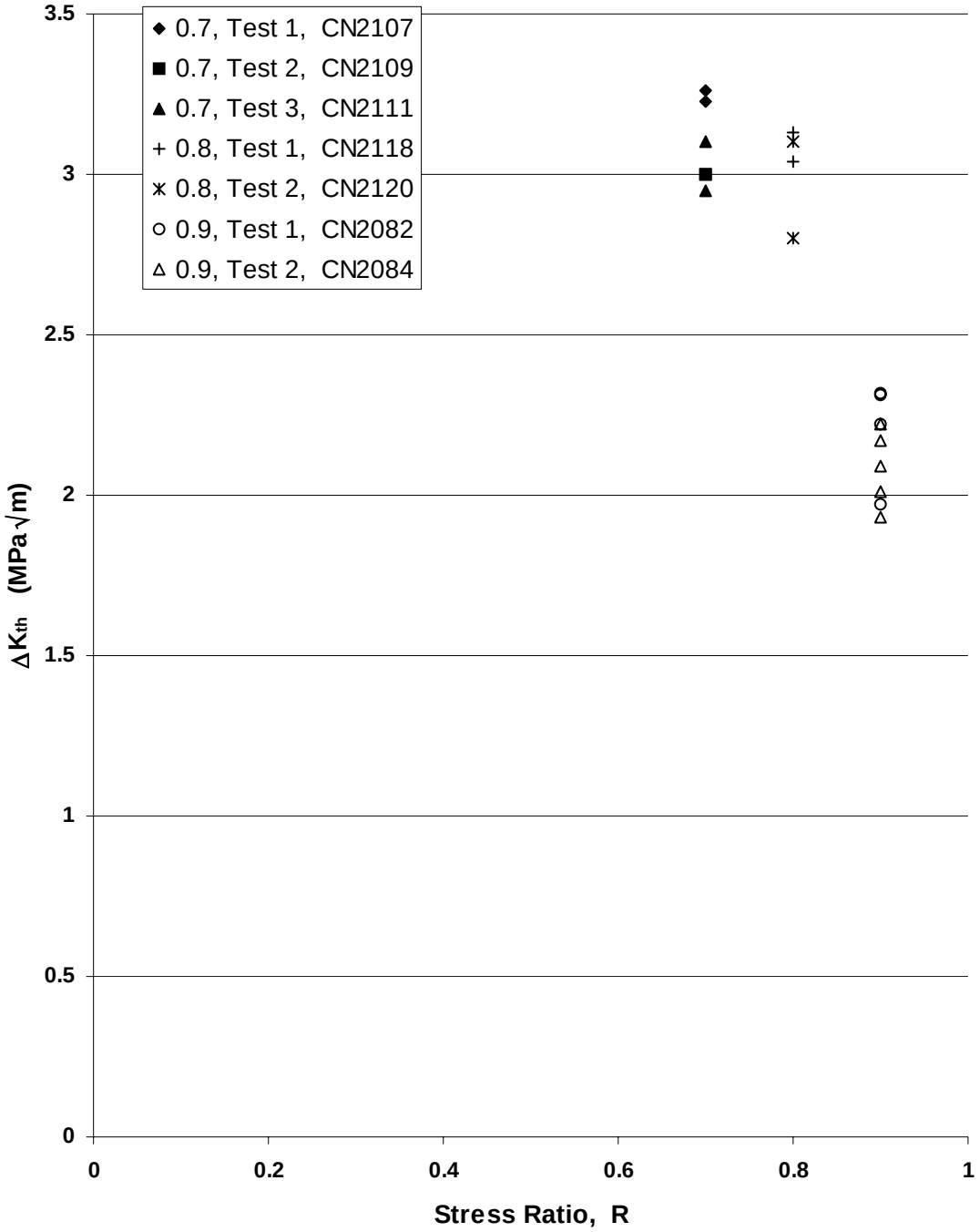

Average values of jump-in threshold at 350^0C

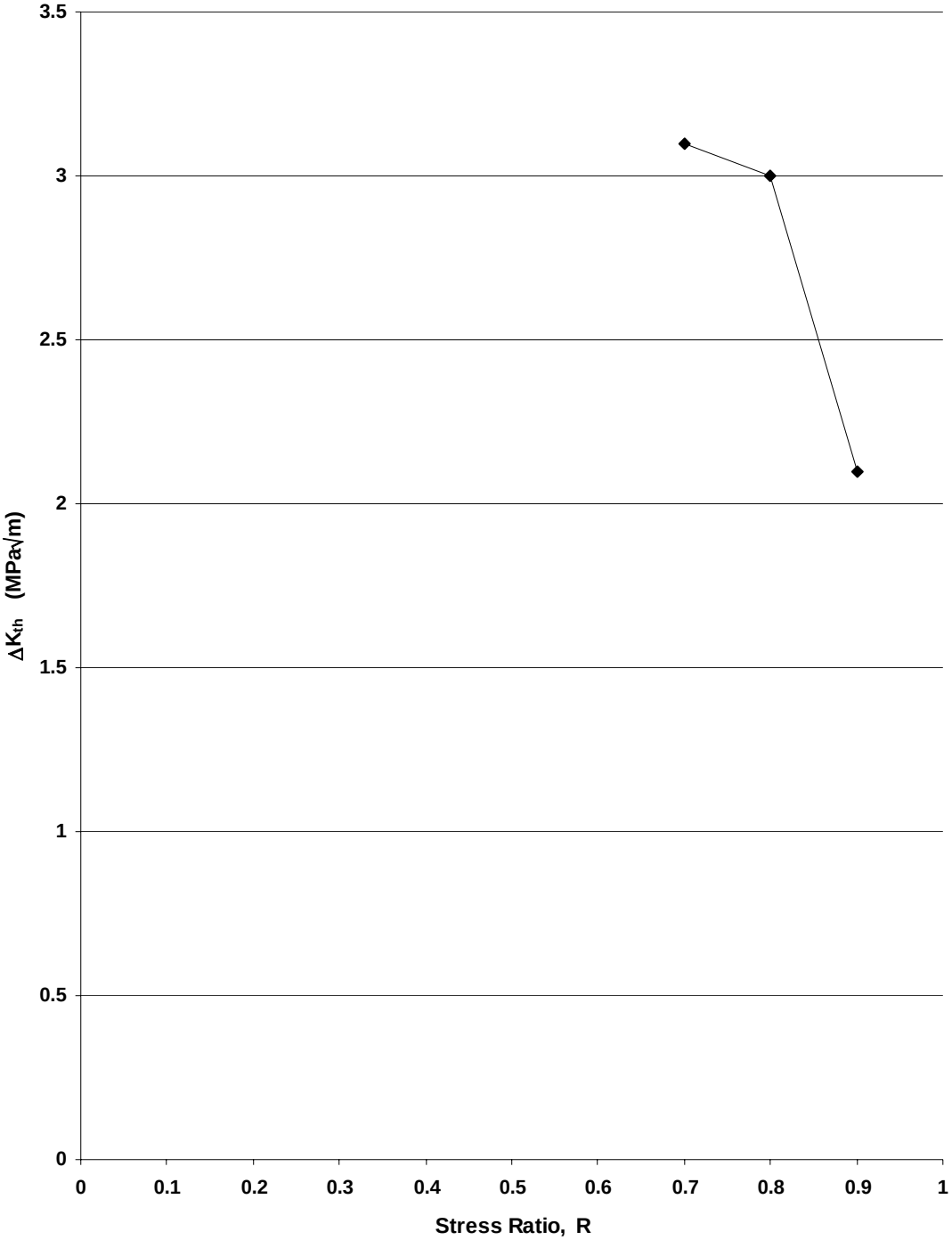

Contribution to crack growth by each stage of flight simulation following the onset of combined loading effects at 350^0C

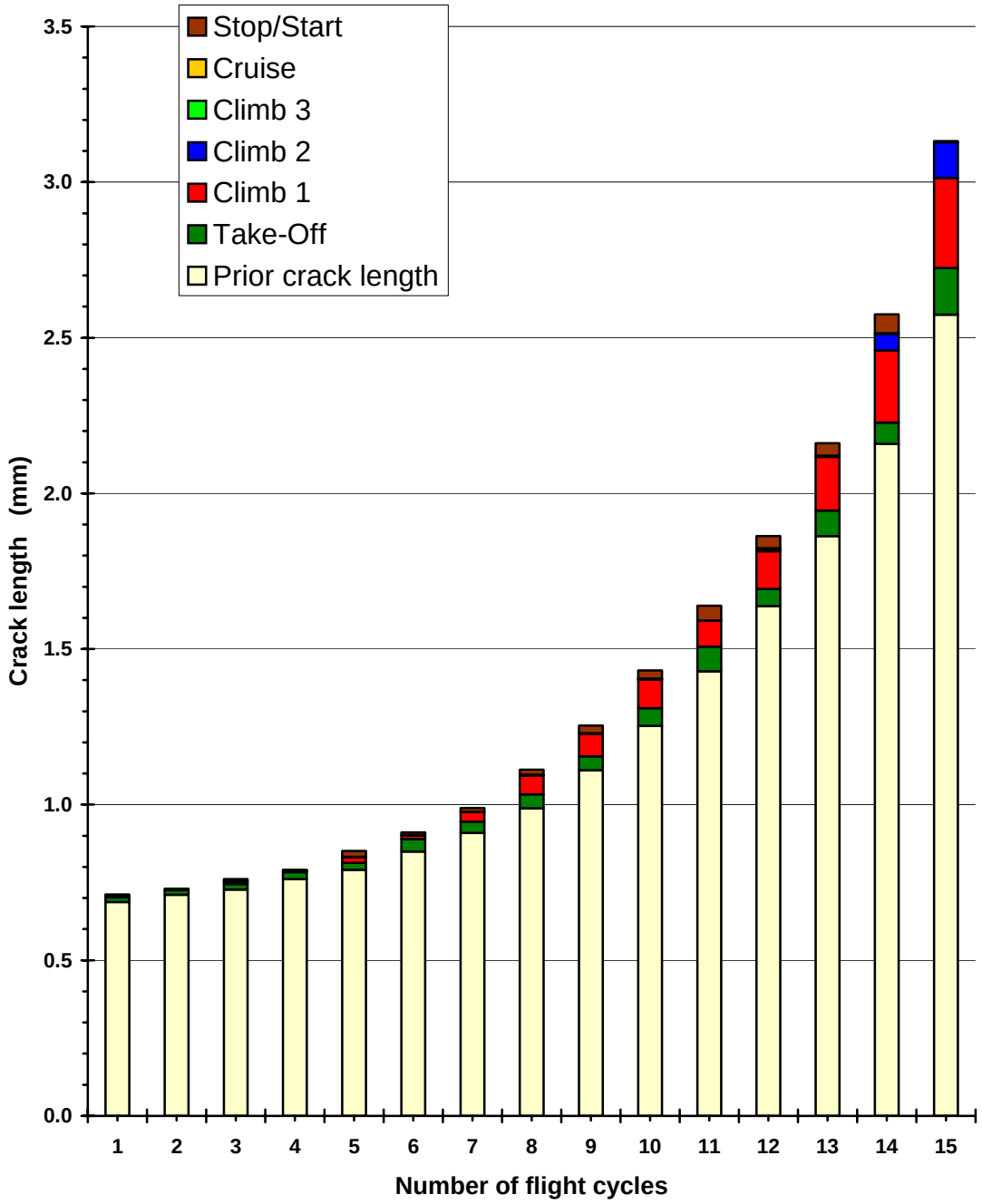

Contribution to crack growth by each stage of flight simulation following the onset of combined loading effects at 350^{0}C